

BIASED ELECTRODE EXPERIMENTS IN ADITYA TOKAMAK

By

PRAVESH DHYANI

PHYS06200704016

Institute for Plasma Research, Gandhinagar

*A thesis submitted to the
Board of Studies in Physical Sciences*

*In partial fulfillment of requirements
for the Degree of*

DOCTOR OF PHILOSOPHY

of

HOMI BHABHA NATIONAL INSTITUTE

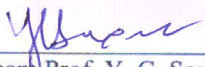


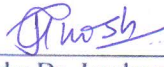
August, 2014

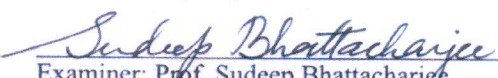
Homi Bhabha National Institute

Recommendations of the Viva Voce Committee

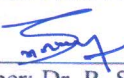
As members of the Viva Voce Committee, we certify that we have read the dissertation prepared by **Pravesh Dhyani** entitled "**Biased Electrode Experiments in ADITYA Tokamak**" and recommend that it may be accepted as fulfilling the thesis requirement for the award of Degree of Doctor of Philosophy.


Chairman: Prof. Y. C. Saxena **Date:** 09/04/2015


Guide: Dr. Joydeep Ghosh **Date:** 09/04/2015


Examiner: Prof. Sudeep Bhattacharjee **Date:** 09/04/2015


Member: Prof. P. K. Chattopadhyay **Date:** 09/04/2015


Member: Dr. R. Srinivasan **Date:** 09/04/2015

Final approval and acceptance of this dissertation is contingent upon the candidate's submission of the final copies of the thesis to HBNI.

I hereby certify that I have read this thesis prepared under my direction and recommend that it may be accepted as fulfilling the thesis requirement.

Date: 9/04/2015

Place: IPR, Gandhinagar


Guide: Dr. Joydeep Ghosh

STATEMENT BY AUTHOR

This dissertation has been submitted in partial fulfillment of requirements for an advanced degree at Homi Bhabha National Institute (HBNI) and is deposited in the Library to be made available to borrowers under rules of the HBNI.

Brief quotations from this dissertation are allowable without special permission, provided that accurate acknowledgement of source is made. Requests for permission for extended quotation from or reproduction of this manuscript in whole or in part may be granted by the Competent Authority of HBNI when in his or her judgment the proposed use of the material is in the interests of scholarship. In all other instances, however, permission must be obtained from the author.


Pravesh Dhyani

DECLARATION

I, hereby declare that the investigation presented in the thesis has been carried out by me. The work is original and has not been submitted earlier as a whole or in part for a degree/diploma at this or any other Institution/University.



Pravesh Dhyani

List of Publications arising from the thesis

Peer Reviewed Journals:

1. **A novel approach for mitigating disruptions using biased electrode in ADITYA tokamak,**

Pravesh Dhyani, J. Ghosh, P.K. Chattopadhyay, R.L. Tanna, D. Raju, S. Joisa, Asim Kumar Chattopadhyay, Debjyoti Basu, N. Ramaiya, S. Kumar, K. Sathyanarayana, S.B. Bhatt, P.K. Atrey, C.N. Gupta, C.V.S. Rao, Ratneshwar Jha, Y.C. Saxena, and R. Pal,

Nuclear Fusion **54** 083023 (2014)

2. **A Set up for Biased Electrode Experiment in ADITYA Tokamak,**

Pravesh Dhyani, Joydeep Ghosh, Sathyanarayana, Praveenlal V E, Pramila, Minsha Shah, R.L. Tanna, Pintu Kumar, C. Chavda, N.C. Patel, V. Panchal, C.N. Gupta, K.A. Jadeja, S.B. Bhatt, S. Kumar, D. Raju, P.K. Atrey, S. Joisa, P.K. Chattopadhyay, Y. C. Saxena and ADITYA team,

Measurement Science and Technology **25** 105903 (2014)

3. **Effect on electrostatic and magnetic fluctuations due to biased electrode in ADITYA tokamak**

Pravesh Dhyani, et al. (*To be submitted to Physics of Plasmas*)

4. **Suppression of Drift - Alfvén waves due to biased electrode in ADITYA tokamak**

Pravesh Dhyani, et al. (*To be submitted to Physics of Plasmas*)

Articles Accepted for Publication in International Conference Proceedings

1. **Disruption Control Using Biased Electrode in ADITYA Tokamak (EX/P7-17),**

Pravesh Dhyani, J. Ghosh, P.K. Chattopadhyay, R.L. Tanna, D. Raju, S. Joisa, Asim Kumar Chattopadhyay, Debjyoti Basu, N. Ramaiya, S. Kumar, K. Sathyanarayana, S.B. Bhatt, P.K. Atrey, C.N. Gupta, C.V.S. Rao, Ratneshwar Jha, Y.C. Saxena, and R. Pal,

25th IAEA Fusion Energy Conference (FEC-2014), 13–18 October 2014, St. Petersburg, Russian Federation.

2. **Novel approaches for mitigating runaway electrons and plasma disruptions in ADITYA tokamak,**
R.L. Tanna, J. Ghosh, P.K. Chattopadhyay, **Pravesh Dhyani**, Shishir Purohit, S. Joisa, C.V.S. Rao, V.K. Panchal, D. Raju, K.A. Jadeja, S.B. Bhatt, C.N. Gupta, Chhaya Chavda, S.V. Kulkarni, B.K. Shukla, Praveenlal E.V, Jayesh Raval, A. Amardas, P.K. Atrey, U. Dhobi, R. Manchanda, N. Ramaiya, N. Patel, M. B. Chowdhuri, S. K. Jha, R. Jha, A. Sen, Y. C. Saxena, D. Bora and the ADITYA Team,
25th IAEA Fusion Energy Conference (FEC-2014), 13–18 October 2014, St. Petersburg, Russian Federation.

Contributions in Conferences/ Workshops/ Schools

International

1. Floating potential fluctuations study in GOLEM tokamak
Under the supervision of Dr. Jan Stockel, Institute of Plasma Physics, Czech Republic
GOlem re**M**ote **TR**Aining Course (GOMTRAIC-2012) from March, 2012 to May, 2012 (Note: GOMTRAIC is a remote training course)
2. Biased Electrode Experiment in ADITYA Tokamak: Confinement Improvement and Disruption Control (Poster)
Pravesh Dhyani, Joydeep Ghosh, P.K. Chattopadhyay, K. Sathyanarayana, K.A. Jadeja, R.L. Tanna, S.B. Bhatt, D.S. Varia, M.B. Kalal, Pintu Kumar, V.K. Panchal, JayeshRaval, Shankar Joisa, Nilam Ramaiya, M.B. Chowdhuri, Aniruddh Mali, Umesh Dhobi, P.K. Atrey, Kumudni Tahiliani, C.N. Gupta, Y.C. Saxena and ADITYA Team
International Conference on Complex Processes in Plasmas and Nonlinear Dynamical Systems (ICPPNDS-2012), Institute for Plasma Research, 06-09 November 2012, Gandhinagar, INDIA

3. Biased Electrode Experiment in ADITYA Tokamak (Poster)

Pravesh Dhyani, Joydeep Ghosh, P.K. Chattopadhyay, K. Sathyanarayana, K.A. Jadeja, R.L. Tanna, S.B. Bhatt, D.S. Varia, M.B. Kalal, Pintu Kumar, V.K. Panchal, Jayesh Raval, Shankar Joisa, Nilam Ramaiya, M.B. Chowdhuri, Aniruddh Mali, Umesh Dhobi, P.K. Atrey, Kumudni Tahiliani, C.N. Gupta, Y.C. Saxena and ADITYA Team

ITER International School (IIS-2012), Institute for Plasma Research, 02-06
December 2012, Gandhinagar, INDIA

4. Disruption Control Using Biased Electrode in ADITYA Tokamak,

Pravesh Dhyani, J. Ghosh, P.K. Chattopadhyay, R.L. Tanna, D. Raju, S. Joisa, Asim Kumar Chattopadhyay, Debjyoti Basu, N. Ramaiya, S. Kumar, K. Sathyanarayana, S.B. Bhatt, P.K. Atrey, C.N. Gupta, C.V.S. Rao, Ratneshwar Jha, Y.C. Saxena, and R. Pal,

25th IAEA Fusion Energy Conference (FEC-2014), 13–18 October 2014, St. Petersburg, Russian Federation.

5. Novel approaches for mitigating runaway electrons and plasma disruptions in ADITYA tokamak,

R.L. Tanna, J. Ghosh, P.K. Chattopadhyay, **Pravesh Dhyani**, Shishir Purohit, S. Joisa, C.V.S. Rao, V.K. Panchal, D. Raju, K.A. Jadeja, S.B. Bhatt, C.N. Gupta, Chhaya Chavda, S.V. Kulkarni, B.K. Shukla, Praveenlal E.V, Jayesh Raval, A. Amardas, P.K. Atrey, U. Dhobi, R. Manchanda, N. Ramaiya, N. Patel, M. B. Chowdhuri, S. K. Jha, R. Jha, A. Sen, Y. C. Saxena, D. Bora and the ADITYA Team, 25th IAEA Fusion Energy Conference (FEC-2014), 13–18 October 2014, St. Petersburg, Russian Federation.

National

1. Biased Electrode Experiment in ADITYA Tokamak: Confinement Improvement (Oral)

Pravesh Dhyani, J. Ghosh, P.K. Chattopadhyay, K. Sathyanarayana, K.A. Jadeja, Debjyoti Basu, R.L. Tanna, Amit Prajapati, S.B. Bhatt, D.S. Varia, M.B. Kalal, Jayesh Raval, Shankar Joisa, Nilam Ramaiya, M.B. Chowdhuri, Aniruddh Mali,

Umesh Dhobi, P.K. Atrey, Kumudni Tahiliani, C.N. Gupta, Y.C. Saxena and ADITYA Team

First PSSI- Plasma scholars' colloquium, 3-4 July 2012, Institute for Plasma Research, Gandhinagar, INDIA.

2. DST-SERC school on Plasma Diagnostics
Institute for Plasma Research, 20-31 July, 2009, Gandhinagar, INDIA.
3. Conceptual design of electrode assembly and pulsed power supply for electrode biasing experiment in ADITYA Tokamak. (Poster)
Pravesh Dhyani, Joydeep Ghosh, P.K. Chattopadhyay, Deepak Sangwan, K.A. Jadeja, S.B. Bhatt
24th National Symposium on Plasma Science & Technology, 8 – 11 Dec, 2009, Hamirpur, INDIA.
4. Experimental Studies with Newly Installed S.B.1 Power Supply in Capacitor Bank Discharges of ADITYA Tokamak (Poster)
R.L. Tanna, M.B. Kalal, D.S. Varia, Deepak Sangwan, **Pravesh Dhyani**, K. Satyanarayana, M.N. Makawana, S.B. Bhatt, J. Ghosh, P.K. Chattopadhyay, Y.C. Saxena and ADITYA Team
24th National symposium on Plasma Science & Technology (Plasma-2009), Dec. 8-11, 2009, National Institute of technology, Hamirpur, India.
5. Electrode Biasing Experiment In ADITYA Tokamak: Preliminary results of biasing experiments (Poster)
Pravesh Dhyani, J. Ghosh, P.K. Chattopadhyay, K. Sathyanarayana, K.A. Jadeja, Debjyoti Basu, R.L. Tanna, Amit Prajapati, S.B. Bhatt, D.S. Varia, M.B. Kalal, Jayesh Raval, Shankar Joisa, Nilam Ramaiya, M.B. Chowdhuri, Aniruddh Mali, Umesh Dhobi, P.K. Atrey, Kumudni Tahiliani, C.N. Gupta, Y.C. Saxena and ADITYA Team
26th National Symposium on Plasma Science & Technology, 20 – 23 Dec, 2011, Patna, INDIA.

6. Overview of Plasma Operations in ADITYA Tokamak (Poster)
R.L. Tanna, S.B. Bhatt, C.N. Gupta, Chhaya Chavda, V.K. Panchal, K.A. Jadeja, Kunal Shah, Y.S. Joisa, P.K. Atrey, Kishore Mishra, S.V. Kulkarni, Kumar Ajay, J. Govind Rajan, Deepak Sangwan, R. Jha, **Pravesh Dhyani**, D. Raju, J. Ghosh, P.K. Chattopadhyay and ADITYA team
26th National Symposium on Plasma Science & Technology, 20 – 23 Dec, 2011, Patna, INDIA.

7. Generation of nonthermal electrons at the Sawtooth crash and their radial transport in ADITYA tokamak
J. Ghosh, D. Raju, P.K. Chattopadhyay, R.L. Tanna, Sankar Joisa, **P. Dhyani**, D. Sangwan, S.B. Bhatt, C.V.S. Rao, R. Jha, C.N. Gupta, P.K. Atrey, M.B. Chowdhuri, Y.C. Saxena and the ADITYA Team
26th National symposium on Plasma Science & Technology (Plasma-2011), Dec. 20 – 23, 2011, BIT Mesra, Patna, Bihar, India.

8. Biased Electrode Experiment in ADITYA Tokamak: Confinement Improvement and Disruption stretch (Poster)
Pravesh Dhyani, Joydeep Ghosh, P.K. Chattopadhyay, D. Raju, K.A. Jadeja, R.L. Tanna, S.B. Bhatt, Pintu Kumar, D.S. Varia, M.B. Kalal, V.K. Panchal, Jayesh Raval, Shankar Joisa, Aniruddh Mali, Nilam Ramaiya, M.B. Chowdhuri, Umesh Dhobi, P.K. Atrey, Kumudni Tahiliani, C.N. Gupta, Y.C. Saxena and ADITYA Team
27th National Symposium on Plasma Science & Technology, PLASMA - 2012, Pondicherry, 10-13 December 2012

9. Spectroscopic studies of ADITYA Tokamak Discharges During Electrode Biasing Experiments (Poster)
Nilam Ramiaya, **Pravesh Dhyani**, Niral Chanchpara, Aniruddh Mali, Ranjana Manchanda, M. B. Choudhari, J. Ghosh, R. Tanna, P. K. Chattopadhyay, S. B. Bhatt and ADITYA team
27th National Symposium on Plasma Science & Technology, PLASMA - 2012, Pondicherry, 10-13 December 2012

10. Timing control circuit for real time control of events in ADITYA tokamak (Poster)
Praveenlal E.V., Prakash Naicker, Rachna Rajpal, **Pravesh Dhyani**, Joydeep Ghosh,
R. Tanna, P.K. Chattopadhyay and ADITYA team
28th National Symposium on Plasma Science & Technology, PLASMA - 2013,
Bhubaneswar, 10-13 December 2013

11. Effect on Electrostatic and Magnetic Fluctuations Due to Biased Electrode in
ADITYA Tokamak (Poster)
Pravesh Dhyani, J. Ghosh, Y.C. Saxena, P.K. Chattopadhyay, R.L. Tanna, D. Raju,
S. Joisa, S.B. Bhatt, P.K. Atrey, C.N. Gupta, C.V.S. Rao, R. Jha and ADITYA team
29th National Symposium on Plasma Science & Technology, PLASMA - 2014,
Kottayam, 8-11 December 2014

ईशावास्यमिदम् सर्वं यत्किञ्च जगत्यां जगत्।

I dedicate this study to my late parents Shrimati Jashoda Dhyani and Shri Pyarelal Dhyani. They ensured that their children would receive much more education, although they were not much educated. They could not witness this day, but they are still with me and will always be.

Acknowledgements

I would like to start by expressing my sincere gratitude to my thesis supervisor Dr. Joydeep Ghosh for the continuous support of my PhD study and research, for his patience, motivation, enthusiasm, and immense knowledge. I am also thankful to him for many hours of help and discussion he gave. I humbly appreciate his motivating ideas and fruitful discussions with him. His guidance helped me in all the time of research and writing of this thesis.

My deepest gratitude is to Prof. Y.C. Saxena. I have been amazingly fortunate to have a teacher like Prof. Saxena, whose patience and support helped me overcome many crisis situations and finish this thesis. Prof. Saxena is one of the best teachers that I have had in my life. I am deeply grateful to him for the discussions that helped me sort out the technical details of my work.

I would like to extend my thanks to Prof. P.K. Chattopadhyay. He has been always there to listen and give advice. His insightful comments and constructive criticisms at different stages of my research were thought-provoking and they helped me focus my ideas.

I specially thank to Dr. A.K. Chattopadhyay and Dr. D. Raju, for their kind help in data analysis. I would also like to thank Dr. R. Srinivasan and Prof. R. Jha for their encouragement, insightful comments, and hard questions. I am also thankful to Prof. P.K. Kaw, Prof. Abhijeet Sen, Prof. R. Pal, Prof. R. Singh, Dr. D. Chandra, Prof. R. Ganesh, Prof. Amita Das, Prof. S. Sengupta, RNDr. Jan Stöckel, Dr. Manoj Warior, Dr. S.K. Pathak, Dr. D. Sharma, Dr. Ramsubramanian, Dr. S.V. Kulkarni, and Prof S. Mukherjee for numerous discussions and lectures on related topics that helped me improve my knowledge in the plasma physics.

Many thanks belong also to Mr. S.B. Bhatt, Mr. K. Sathyanarayana, Mr. P.K. Atrey, Mr. Shankar Joisa, Mrs. R. Manchanda, Ms. Jana Brotankova, Dr. M. B. Choudhary, Dr. S. Bannerjee, Mrs. K. Tahiliyani, Dr. L.K. Awasti, Mr. P.K. Srivastava for valuable discussions. I have been lucky to be part of the ADITYA tokamak group. I am also thankful to Mr. R.L. Tanna, Pintu, Mr. M.B. Kalal, Mr. D.S. Varia, Sameer ji, Gopal ji, Mrs. C. Chavda, Mr. C.N. Gupta, Jadeja ji, Prakash ji, Amit, Pradhuman, Tarkik, Aniruddh, Acharya ji, Panchal ji, Vaibhav, Mr. R.K. Sinha, Varsha ji, Jayesh, Umesh and other members of ADITYA tokamak group for helping me in experiments. I am also grateful to the staff members from workshop, drafting section, computer centre, library, stores, purchase section and administration at Institute for Plasma Research for their co-operation and help during my entire duration of PhD.

I also thank my classmate friends – Rameswar, Sanat, Sushil, Nishant and Imran for providing me unforgettable cool ambience during first year course work and throughout my Ph.D. Thanks go to Rameswar, Sanat, Sushil, Rana, Veda and Ravinder. Without their help and humour our hostel would have been a very dull place.

I also thank my senior research scholars- Kishor bhaiya, Maya di, Pintu da, Ritu di, Vikrant bhai, Sharad bhai, Satya da, Shekhar anna, Jugal da, Sunita, Vikram bhai, Ashwin, Prabal bhai, Sita, Deepak, Kshitish, Gurudatt, Ujjwal, Linthish, and junior research scholars- Sayak, Manjit, Soumen, Aditya, Vikram, Sandeep, Dushyant, Vara, Vibhu, Neeraj, Rupendra, Akanksha, Deepa, Mangilal, Vidhi, Harish and all other junior research scholars for providing me a friendly ambience in the hostel as well as in scholar hall.

I would like to thank my brothers- Prasant bhaiya and Pramod bhaiya for being an emotional strength and supporting me spiritually throughout my life. I also thank my sister Pratibha for being a constant source of love, concern, support and strength all these years. I have to give a special mention for the support given by my wife Taruna, who encouraged me during this endeavour. Her support helped me overcome setbacks and stay focused on my study. I deeply appreciate her belief in me.

Lastly and most importantly, I would like to thank my late parents. No words are sufficient to describe their contribution to my life. I owe every bit of my existence to them. None of this would have been possible without their blessings, love, unconditional support and patience. Their memories have been a source of inspiration to me.

I would like to express my heart-felt gratitude to my family.

Pravesh Dhyani

August, 2014

ADITYA Tokamak Group

Institute for Plasma Research

Gandhinagar

Contents

Synopsis.....	iv
List of Figures.....	xii
List of Tables	xvii
Chapter 1	1
Introduction.....	1
1.1 A quest towards Controlled Thermonuclear Fusion	1
1.1.1 Lawson criterion	1
1.1.2. Development of fusion research based on tokamaks	2
1.2 Confinement regimes in Ohmic discharges	2
1.3 Confinement regimes with auxiliary heating	3
1.3.1 L- mode discharge.....	4
1.3.2 The H- mode	5
1.4 Biasing experiments in tokamaks	6
1.5 Different models to explain L- H transition.....	12
1.6 Recent results and renewed interest in electrode-biasing experiments.....	14
1.7 Interplay between radial electric fields and MHD activity	15
1.8 Motivation of the thesis work	16
1.9 Thesis Outline	16
1.10 References.....	17
Chapter 2	22
Tokamaks and ADITYA Tokamak.....	22
2.1 Tokamaks.....	22
2.1.1 Equilibrium of tokamak plasma.....	24
2.1.2 Grad- Shafranov equation and the Shafranov shift.....	25
2.1.3 Tokamak confinement	27
2.1.4 Heating.....	28
2.1.5 Instabilities.....	31
2.2 Resistive tearing instability.....	35
2.2.1 Ideal and resistive instabilities	36
2.2.2 Tearing modes.....	37
2.2.3 Growth of tearing modes	38
2.2.4 Linear and non-linear tearing mode growth.....	38
2.2.5 Effect of sheared flows on growth of tearing modes	39

2.3 Disruptions in tokamak	40
2.3.1 Causes of disruptions	40
2.4 ADITYA Tokamak	42
2.4.1 ADITYA tokamak subsystems	43
2.4.1.1 Magnetic coils in ADITYA	43
2.4.1.2 Vacuum vessel and associated systems	45
2.4.1.3 Wall conditioning.....	46
2.4.1.4 Gas puff system.....	47
2.4.1.5 Limiter.....	47
2.4.1.6 ADITYA Pulsed Power System (APPS)	47
2.4.1.7 ADITYA Data acquisition system and control system	49
2.4.2 Typical ADITYA tokamak discharge	49
2.4.3 Operational diagnostics in ADITYA tokamak	51
2.4.3.1 Magnetic measurements.....	51
2.4.3.1.1 Loop voltage measurement	52
2.4.3.1.2 Rogowski coil	52
2.4.3.1.3 Mirnov coil.....	52
2.4.3.1.4 Diamagnetic loop	52
2.4.3.2 Microwave interferometry	53
2.4.3.3 Soft X-ray measurements.....	54
2.4.3.4 Hard X-ray measurements	55
2.4.3.5 Spectroscopy	55
2.5 References.....	55
Chapter 3	57
Experimental Set-up	57
3.1 Electrode and its holding assembly.....	57
3.1.1 Design criteria	57
3.1.2 Electrode Material.....	58
3.1.3 Electrode holding assembly	58
3.2 Biasing Pulsed Power Supply	61
3.2.1 Criteria and philosophy	61
3.2.2 Power Supply	61
3.2.2.1 Capacitor Bank.....	62
3.2.2.2 Trigger circuits.....	63
3.2.2.2.1 Loop voltage generated trigger (T1)	63
3.2.2.2.2 MHD signal generated trigger (T2)	65
3.2.2.3 Performance of the pulsed power supply	67

3.3. Experimental Diagnostics	67
3.3.1 Radial array of Langmuir probe.....	67
3.3.1.1 Theory	68
3.3.1.2 Probe construction and installation.....	70
3.3.1.3 Measurements	72
3.3.2 Radial array of radial and poloidal magnetic probes	74
3.3.2.1 Theory	74
3.3.2.2 Probe construction and installation.....	74
3.3.2.3 Calibration of probes.....	75
3.3.2.4 Measurements	78
3.4 Techniques for MHD island identification and island width calculations.....	78
3.4.1 Singular Value Decomposition (SVD) method	78
3.4.2 Soft X-ray tomographic reconstruction	79
3.5 References.....	81
Chapter 4	82
Disruption Mitigation Using Biased Electrode in ADITYA Tokamak.....	82
4.1 Introduction.....	82
4.2 Observations of suppression of MHD fluctuations with bias	83
4.3 Control of MHD triggered disruption	88
4.4 Discussion	94
4.5 Summary	102
4.6 References.....	103
Chapter 5	106
Effect on Electrostatic and Magnetic Fluctuations Due to Biased Electrode in ADITYA Tokamak	106
5.1 Introduction.....	106
5.2 Experimental parameters	107
5.3 Time evolution of biasing voltage and electrode current.....	107
5.4 Electrostatic and magnetic fluctuation behaviour during electrode biasing	111
5.5 Discussion.....	120
5.6 Summary	122
5.7 References.....	123
Chapter 6	125
Conclusions and Future Outlook.....	125
6.1 Summary and conclusions	125
6.2 An outlook for future studies	127

Synopsis

The underlying physics of low to high confinement (L – H) transition discovered in ASDEX tokamak [1] with Neutral beam heating (NBI) still remains an open question that engages the interest of fusion physicists all over the world. For ITER to be operated in the H-modes, it is very important to understand the physics of (L – H) transition, which are regularly observed in many tokamaks with different heating schemes such as NBI, ECRH, ICRH etc. Observations of modifications in poloidal rotations generated due to the setting up of radial electric field during L – H transition are thought to be one of causes of this transition. Although, there is substantial support for the paradigm of sheared radial electric field (E_r) suppression of electrostatic turbulence as an element of the L–H transition, no single theory accounts for all the observations [2]. Different mechanisms of shear generation, e.g., ion-orbit loss, neutral particle effects, Reynolds stress and pressure gradients lead to bifurcation in different situations in tokamaks [2–5]. On the other hand, experiments [6–10] and theories [11–13] have also been put forward establishing the significant role of toroidal current density (j_ϕ) profile modification in the L–H transition. The importance of an increased $E_r \times B_\phi$ shear in confinement improvement during the H-mode has been further strengthened by the edge plasma biasing experiments [14, 15], where E_r -profile modification is created by a biased electrode. Electrode biasing experiments have been carried out in many tokamaks [14-20] with different magnetic configurations for decades after it was first demonstrated in CCT tokamak [14] to understand improved energy confinement in tokamaks. Majority of the high confinement mode features observed in L - H transition with auxiliary heating such as sharp transport barrier formation, reduction of H_α emission (656.2 nm) intensity, substantial reduction in electrostatic fluctuations are reproduced with placing a biased electrode inside the last closed flux surface of many tokamaks. But, the effect of sheared rotation generated due to induced radial electric field by biased electrode on magnetohydrodynamic (MHD) fluctuations have been overlooked till very recently and have generated renewed interest in electrode biasing experiments through observations of substantial modifications in magnetic fluctuations as well as in toroidal current density (j_ϕ) profiles due to biasing. In very low q_a (VLQ) and normal q_a discharges of SINP- tokamak improved confinement with extension of plasma current duration are observed with inserting biased electrode and the results are attributed to the observed edge toroidal current profile modification due to the biased

electrode [21, 22]. They have shown that radial electric field profile modification comes much later in time than the toroidal current profile modification. In TCABR tokamak, both suppression and excitation of MHD activity has been observed using voltage polarised electrode placed in the edge region [23]. Very recent experiments in SINP tokamak, spontaneous disruptions are successfully mitigated with biased electrodes placed in the edge region of this tokamak [14]. However, the physical mechanisms of interplay between induced electric fields generated rotations and MHD activities are not well understood.

The primary objective of the work described in this thesis is to investigate the effect of biased electrode on the MHD modes present in tokamaks. Further, controlling these MHD modes using biased electrode, we aim to control plasma disruptions initiated by growth in MHD instabilities, as the success of ITER and big tokamaks as fusion systems depend heavily on avoidance of disruptions. In this thesis we present the description of a novel approach towards controlling the tokamak disruptions by electrode biasing which is demonstrated for the first time. As suppression of both the electrostatic and magnetic fluctuations is observed in different tokamaks, we further seek to answer the temporal chronology of events, i.e., which event is the cause and which one is the effect. Furthermore, there exists no definite criterion for achieving L – H transitions using biased electrode in different tokamaks, which have used different electrode dimensions, have drawn different electrode currents using different biasing voltages to achieve transition. In this thesis we intend to find most effective parameter responsible for the transition by designing a special electrode-holding assembly by which we can change the electrode dimension by changing its exposed length (L_{exp}) in-situ along with its position (r_{elec}) movement inside the ADITYA tokamak.

This thesis consists of six chapters. The first chapter is an introduction to biased electrode experiments carried out in different tokamaks and also includes the motivation and objective of the thesis. The second chapter describes tokamaks, especially Aditya tokamak its parameters, operational regimes and diagnostics. The third chapter includes experimental set up, design and fabrication of electrode holding assembly, design and fabrication of biasing power supply and its sub-systems along with various diagnostics especially developed for biasing experiments. The fourth chapter describes the novel approach of mitigating tokamak plasma disruption using biased electrode and its physical mechanism. The fifth chapter discusses the effect of biased electrode on electrostatic and magnetic fluctuations leading to better confined state. Conclusions and future scopes are presented in the last chapter.

After describing the importance of biased electrode experiments carried out in different tokamaks and renewed interest in this kind of experiments from the point of view of their capability to avoid tokamak plasma disruptions in Chapter 1, a brief introduction of tokamaks and ADITYA tokamak along with its operational regimes and diagnostics is presented in Chapter 2. It includes description on working principle of tokamak, its equilibrium, instabilities, and disruptions. The subsystems of Aditya tokamak, such as magnetic coil systems, vacuum systems, data acquisition systems and power supply systems, are described. Operational diagnostics in ADITYA tokamak and typical ADITYA tokamak discharge is also presented in this chapter. ADITYA [25] is a medium-size, air-core, limiter tokamak, which has a major radius $R = 0.75$ m and minor or plasma radius $a = 0.25$ m. For results presented in this thesis, Aditya is operated with following typical central parameters: toroidal magnetic field, $B_\phi = 0.7$ to 0.8 T, plasma current $I_p \approx 60 - 80$ kA, electron density $n_{eo} \approx 1.0 - 1.5 \times 10^{19} m^{-3}$, electron temperature $T_{eo} \approx 0.25 - 0.45$ keV, ion temperature $T_{io} \sim 0.08 - 0.15$ keV, and $Z_{eff} \sim 2 - 3$. The operational diagnostic systems includes Rogowskii coils for plasma current measurements, Single turn loops for Loop voltage measurements, Mirnov coils for poloidal magnetic field and its fluctuation measurements, Microwave interferometry for density and density profile measurements, Soft X-ray detectors for temperature measurements, Bolometers for plasma radiation measurements, Diamagnetic loops for plasma stored energy measurements, visible spectroscopy for different emission measurements.

In chapter 3, the complete description of the developmental and experimental efforts towards carrying out electrode biasing experiments in Aditya tokamak has been presented. The major emphasis has gone in the development of the electrode assembly and biasing power supply. Also included are the developments of Langmuir probe array for measurements of radial profiles of density and floating potential, magnetic probe array for current profile measurements and MHD sensing trigger circuit for real time control experiment of disruptions. A brief description of electrode assembly, biasing power supply, trigger circuit and diagnostic system is given below. A special electrode-holding assembly by which the electrode dimension can be varied in-situ along with its position movement inside the Aditya tokamak. The electrode used in the experiments is made of a high purity (99.9%) molybdenum (Mo) rod of 5 mm diameter. To apply biasing voltage pulse to the electrode a

pulsed power supply based on a capacitor bank consisting of electrolyte capacitors has been designed. The total capacitance of the bank is $\sim 37.5mF$ which can deliver a maximum current $\sim 150A$ at $900V$ for $\sim 30ms$ with a drop of only $\sim 50 V$. A SCR switch with force commutation is used to switch on/ off the biasing power. A trigger circuit based on PIC18F45J10-I/P micro-controller IC is designed for triggering the SCRs in the biasing pulsed power supply at desired times. A MHD oscillations sensing feed- back circuit is designed for active control of disruption avoidance by biased electrode induced by H_2 gas puffing. In this experiment only delay in current quench obtained. An array of 6 single Langmuir probes designed and fabricated to measure radial profile of floating potential and electron density. The probe tips are made of Molybdenum and each cylindrical probe has a length and diameter of $2mm$ and $3mm$ respectively. The centre to centre distance between two adjacent probes is $\sim 7mm$. No noticeable change in discharges regarding its reproducibility in terms of achieving same plasma current, density and temperature compared to typical ADITYA discharges without the electrode is observed by placing the electrode up to 3.5 cm inside the LCFS with an exposed length of ~ 20 mm. It has been observed that the improvement in confinement and disruption mitigation are obtained with keeping the electrode tip at $r_{elec} = 22$ cm with an exposed length of 20 mm in typical ADITYA discharges. The application of positive bias voltage in typical discharges of Aditya tokamak led to observation of improvement confinement as observed in many previous experiments with all the signatures such as profile modification of plasma potential and increase in radial electric field in the edge plasma region, reduction in reduction of H_α emission (656.2 nm) intensity, increase in line average density, steepening of radial density profile in edge region, substantial reduction in electrostatic fluctuations along with the observation of suppression of magnetic (MHD) fluctuations.

A novel technique of disruption mitigation using biased electrode placed at the edge of Aditya tokamak plasma is presented in Chapter 4. For this experiment the Aditya tokamak has been operated for normal discharges having maximum $I_p \sim 65 - 70kA$, electron density $\sim 1.0 - 1.5 \times 10^{19} m^{-3}$ and electron temperature $T_e \sim 350 - 450eV$. These values of I_p and B_ϕ have been chosen so as to keep the $q = 3$ rational surface near the radial position of the electrode. Electrode was introduced from the top port of the machine. The deliberately induced disruptions using H_2 gas-puff in the flat-top duration of the plasma current [I_p] are successfully mitigated by applying a positive bias voltage on the Molybdenum electrode

placed inside the LCFS. The injection of H₂ gas-puff leads to a considerable rise in MHD perturbation amplitudes due to the growth of magnetic islands, which then stop rotating by being locked through overlapping of grown islands and causing disruption of the plasma. By applying positive bias voltage larger than some threshold value to the electrode placed inside the LCFS prior to the gas injection leads to significant reduction in the growth of magnetic islands corresponding to m/n = 3/1, 2/1 MHD modes, which in turn prevents them from locking and delays or avoids the current quench. The stabilization of MHD-modes or suppression of magnetic islands by plasma rotation has been established both experimentally [26, 27] and theoretically [28-30] with flows arising from variety of causes such as unbalanced neutral beam injection, radio frequency heating or as a by-product of micro-turbulence. It has also been shown analytically as well as numerically that sheared plasma toroidal or poloidal flow can change the linear stability of resistive tearing modes, hence suppressing the magnetic islands. In this work, the sheared (shear refers to the radial gradient of E_r) poloidal plasma rotation through $E_r \times B_\phi$ force generated by biased electrode has been exploited to linearly stabilize the conventional tearing modes leading to suppression of magnetic island growth and delaying or avoidance of disruptions. This approach towards avoidance of disruption opens up a completely new area where disruptions can be controlled through maintaining a proper shear of plasma poloidal rotations in the edge region of tokamaks.

Chapter 5 is focused on understanding the effect of biasing on electrostatic and magnetic fluctuations and chronology of events. With the application of bias voltage above some threshold voltage in typical discharges of Aditya tokamak, significant reduction in both magnetic and electrostatic fluctuations is observed leading to two distinct regimes of improved confinement with different characteristics. The important observation is that the magnetic fluctuations are reduced prior to that of electrostatic fluctuations. With the onset of bias first the magnetic fluctuations are suppressed due to substantial reduction in m/n=3/1 mode and the H_α decreased with an increase in plasma confinement. After ~ 4 – 8 ms of the application of bias voltage, the electrode current falls sharply with the electrode voltage remaining constant, indicating higher cross - field resistivity. Simultaneously, the electrostatic fluctuations are suppressed and confinement improves further. This state does not last long and magnetic fluctuations associated with m / n = 2 / 1 mode increases leading to increase in H_α emission and confinement degrades. However, the electrostatic fluctuations

remains suppressed compared to their values before biasing till the end of the biasing pulse. Further investigation revealed that the possible cause of transition to the improved state might be the suppression of drift-Alfven waves due to bias, which exists before biasing.

In summary, we have successfully mitigated plasma disruptions in ADITYA tokamak using a biased electrode. Signatures of confinement improvement observed in other tokamaks also obtained using electrode biasing in Aditya tokamak. Both the electrostatic and magnetic fluctuation suppressions have been observed. The major conclusions of the thesis are as following.

- The Electrode assembly and biasing pulsed power supply single are designed and installed in ADITYA tokamak to study physics of L-H transition and for mitigation of disruptions. A single Langmuir probe array designed and installed to measure edge parameters like floating potential and electron density. For real time disruption avoidance experiments MHD oscillation sensing circuit designed and developed.
- The improvement in confinement as well as disruption mitigation has been observed mainly with electrode-exposed length of 20 mm placed at $r_{elec} = 22$ cm in typical discharges of ADITYA tokamak.
- First experimental demonstration of successful mitigation H_2 gas puff induced plasma disruption in ADITYA tokamak using a biased electrode at the plasma edge by stabilizing MHD tearing modes ($m/n=2/1$ and $3/1$) through generation of large poloidal flow shear near $q=3$ surface is present. Observations indicate that MHD tearing modes ($m/n=2/1$ and $3/1$) islands do not grow in increased poloidal sheared flow and disruptions are avoided through prevention of mode locking.
- Both the magnetic and electrostatic fluctuations are suppressed with biasing with magnetic fluctuation suppression occurred prior to that of electrostatic fluctuations.
- Suppression of Drift-Alfven modes may be the cause of improvement confinement observed in typical Aditya plasma discharges.

Future works include mitigation of disruptions with a reciprocating electrode controlled by some precursor of disruption, as fixed electrodes cannot be put inside the LCFS of big tokamaks. More systematic electrode position, electrode exposed length and biasing voltage scans along with reciprocating electrode system are envisaged for best optimisation of above three parameters in real time disruption avoidance. The effect of negative bias on disruption

mitigation and other global parameters of Aditya have to be carried out. The biasing experiments can be expanded in future towards better understanding of underlying physics with different toroidal magnetic field and with field reversed.

Summary and future scope is presented in Chapter 6.

References

- [1] F. Wagner *et al.*, *Phys. Rev. Lett.* **49**, 1408 (1982)
- [2] J.W. Connor and H.R. Wilson, *Plasma Phys. Control.Fusion* **42**, R1–74 (2000)
- [3] K.C. Shaing and E.C. Jr Crume *Phys. Rev. Lett.* **63**, 2369 (1989)
- [4] P.H. Diamond and Y.B. Kim, *Phys. Fluids B* **3**, 1626 (1991)
- [5] H. Biglari, P.H. Diamond and P.W. Terry, *Phys. Fluids B* **2**, 1 (1990)
- [6] K. Toi, J. Gernhardt, O. Kluber and M. Kornherr, *Phys.Rev. Lett.* **62**, 430 (1989)
- [7] J.P. Christiansen and J.G. Cordey, *Nucl. Fusion* **30**, 599 (1990)
- [8] K. Toi *et al.*, *Phys. Rev. Lett.* **64**, 1895 (1990)
- [9] N. Ohyabu, G.L. Jahns, R.D. Stambaugh and E.J. Strait, *Phys. Rev. Lett.* **58**, 120 (1987)
- [10] B.E. Chapman *et al.*, *Phys. Plasmas* **7**, 3491 (2000)
- [11] J.Y. Hsu and M.S. Chu, *Phys. Fluids* **30**, 1221 (1987)
- [12] E. Minardi, *Plasma Phys. Control. Fusion* **30**, 1701 (1988)
- [13] T.S. Hahm and P.H. Diamond *Phys. Fluids* **30**, 133 (1987)
- [14] R.J. Taylor, M.L. Brown, B.D. Fried, H. Grote, J.R. Liberati, G.J. Morales, P. Pribyl, D. Darow and M. Ono, *Phys. Rev. Lett.* **63**, 2365 (1989)
- [15] G. Van Oost *et al.*, *Plasma Phys. Control. Fusion* **45**, 621 (2003)
- [16] R.R. Weynants *et al.*, *Nucl. Fusion* **32**, 837 (1992)
- [17] L.G. Askinazi *et al.*, *Nucl. Fusion* **32**, 271 (1992)
- [18] E.Y. Wang *et al.*, *Nucl. Fusion* **35**, 467 (1995)
- [19] C. Silva *et al.*, *Nucl. Fusion* **44**, 799 (2004)
- [20] K.K. Jain *et al.*, *Research Report, Plasma Physics Laboratory, University of Saskatchewan*, PPL-145 (1994)
- [21] Joydeep Ghosh *et al.*, *Nucl. Fusion* **47**, 331 (2007)
- [22] Debjyoti Basu *et al.*, *Phys. Plasma* **19**, 072510 (2012)
- [23] I.C. Nascimento *et al.*, *Nucl. Fusion* **47**, 1570 (2007)
- [24] Debjyoti Basu *et al.*, *Phys. Plasma* **20**, 052502 (2013)
- [25] S.B. Bhatt *et al.*, *Indian J. Pure Appl. Phys.* **27**, 710 (1989)

- [26] P.C. De Vries, *et al.*, *Plasma Phys. Control. Fusion* **38**, 467 (1996)
- [27] R.J. La Haye, *et al.*, *Phys. Plasmas* **10**, 3644 (2003)
- [28] M. Persson, *Nucl. Fusion* **31**, 382 (1991)
- [29] D. Chandra, *et al.*, *J. Plasma Fusion Res. SERIES* **9**, 457 (2010)
- [30] D. Chandra, *et al.*, *Nucl. Fusion* **47**, 1238 (2007)

List of Figures

Figure 2.1. Opposite \hat{z} - direction drift in ions and electrons caused by grad- B drift and curvature drift results a charge polarization, which induces an electric field. Both ions and electrons drift outward ($\mathbf{E} \times \mathbf{B}$). Consequently, plasma is not confined in a simple toroidal magnetic field. 23

Figure 2.2. Helical structure of magnetic field: Plasma current (I_p) generates a poloidal magnetic field (\mathbf{B}_θ), which together with toroidal magnetic field (\mathbf{B}_ϕ) produce helical magnetic field lines $\mathbf{B} = \mathbf{B}_\phi + \mathbf{B}_\theta$. In helical field lines polarization is short circuited, as charged particles can move freely along the line of force. 23

Figure 2.3. Circular flux surface is displaced by a distance (Δ_s) with respect to boundary flux surface whose centre is at a distance R_0 from the major axis. The outwards displacement (Δ_s) is known as the ‘Shafranov shift’ 26

Figure 2.4. (a) Magnetic island with magnetic shear with no flow shear and q increasing with major radius R . (b) Magnetic island with flow shear added. 40

Figure 2.5. Hugill diagram shows limitation of stable operational regime of the tokamak in a region of (q_a, \bar{n}) space, where q_a denotes the safety factor at the edge of the plasma and \bar{n} denotes the mean electron density. In this diagram operating regime is shown as a function of $1/q_a$, which is proportional to plasma current (I_p), and of the Murakami parameter $\bar{n}R/B_\phi$. ‘low- q disruptions’ and ‘density limit disruptions’ limit this region. Operating regime is reduced for contaminated OH-plasmas and extended beyond the $Z_{\text{eff}} = 1$ boundary when auxiliary heating is employed. 41

Figure 2.6. Restoring force produced by concave field lines against vertical (\hat{z} -direction) displacement 45

Figure 2.7. Vertical cross-section of TF coil, OT (or TR) coil, B_V coils in ADITYA 46

Figure 2.8. Anti transformer arrangement to nullify mutual inductance between Ohmic Transformer (OT) coil and Vertical Field (B_V) coil 48

Figure 2.9. Temporal profile of current signal in (a) toroidal field magnetic coil (I_{TF}), (b) Ohmic transformer coil (I_{OT}), (c) Vertical magnetic field coils (I_{BV}) for a typical ADITYA tokamak discharge (#26571). Time of hydrogen gas pre-fill is shown by red dotted line. 50

Figure 2.10. Temporal profile of typical ADITYA tokamak discharge (#22761). (a) Loop voltage (V_L), (b) plasma current (I_p), (c) Vertical magnetic field (B_V), (d) H_α line radiation, (e) SXR signal, (f) HXR signal 51

Figure 3.1. (a) Cross-sectional view of electrode assembly and (b) electrode holder. 59

Figure 3.2. (a) Electrode assembly mounted on top of ADITYA tokamak and (b) inner view of ADITYA showing electrode mounted on top of the machine.....	60
Figure 3.3. Schematic diagram of pulsed power supply depicts positive biasing arrangement	62
Figure 3.4. Pulsed Power Supply used for biasing experiments	63
Figure 3.5(a). Block diagram of electronic circuit of SCR trigger circuit (T1)	64
Figure 3.5(b). Output trigger pulse.....	64
Figure 3.5(c). Block diagram of MHD generated trigger circuit (T2).....	66
Figure 3.5(d). Functional flow chart of operation of multi-channel Micro-Controller based timing circuit with comparator.....	67
Figure 3.6. Demonstration of pulsed power supply working with the plasma load in shot #26427. Electrode exposed length in plasma and radial position of its tip from plasma center are $L_{exp} \sim 20$ mm and $r_{elec} \sim 22$ cm, respectively. Temporal profile of (a) plasma current (I_P), (b) drawn electrode current (I_B) and (c) biasing voltage (V_B) across electrode and ground. At $t \sim 41$ ms electrode is biased at $V_B \sim 190$ V and electrode draws $I_B \sim 80$ A current. At $t \sim 57$ ms electrode biasing is switched off using commutation circuit in the pulsed power supply. Before the biasing is switched on electrode is at floating potential of plasma and no current is drawn by the electrode.	68
Figure 3.7. Top view of ADITYA tokamak shows location of electrode assembly, Langmuir probe array, B-dot probe array, Gas puffing system, Mirnov garland and limiter	70
Figure 3.8. (a) Inner view of ADITYA showing Langmuir probe array mounted on top of machine and (b) Langmuir probe array. Each probe's neck is covered with ceramic sleeve.....	71
Figure 3.9. Circuit descriptions of plasma floating potential and density measurements by Langmuir probe array. A floating power supply was used to measure plasma density. Red coloured lines show grounding scheme for the measurements.....	71
Figure 3.10. (a) Plasma current, (b - g) floating potential (Φ_f) measured by 6 Langmuir probes, (h) electrode voltage, and (i) electrode current for shot no #26260.	72
Figure 3.11. Radial profile of floating potential (Φ_f) for discharge #26260 measured by Langmuir probe prior to biasing (~ 40 ms) and after biasing (~ 42 ms).	73
Figure 3.12. Schematic drawing of a section of B-dot probe array. There are five such sections in the array, which measure radial profiles of radial and poloidal magnetic field. Figure (a) shows cross-section of the two B-dot probes measuring radial and poloidal magnetic field. Figure (b) is another cross-sectional view of same section of the B-dot probe at 90° angle of the figure (a).	75
Figure 3.13. Construction of magnetic probe array: (a) array of magnetic probes to measure radial and poloidal magnetic fields, (b) electric connections of the probes, (c) probes covered with ceramic and (d) magnetic probe assembly.	76
Figure 3.14. Helmholtz coil arrangement	77

Figure 3.15. Poloidal magnetic field measurement by magnetic probe array at different radial locations for discharge #26332	78
Figure 3.16. Detectors integrate the local emission, $g(r, \theta)$ along lines-of-sight, L , defined by (p, ϕ) . The emitting region must be completely contained within the circular region.....	80
Figure 4.1. Schematic diagram of electrode biasing set-up for positive biasing.	84
Figure 4.2. (a) Comparison of plasma current from two discharges (#26501 without bias in red dashed line and #26512 with bias in black solid line) with electrode placed at $r_{elec} \sim 21.5$ cm with an exposed length $L_{exp} \sim 25$ mm in the biased discharge. (b) Electrode voltage, V_B and (c) electrode current, I_B in biased discharge # 26512.....	85
Figure 4.3. Variation of electrode current (I_B) as a function of biasing voltage (V_B) for different electrode tip positions (r_{elec}) of 2 cm – 3.5 cm inside the LCFS with various electrode exposed lengths (L_{exp}) of 10 mm – 25 mm.	86
Figure 4.4. Comparison of temporal evolution of electrode current for three electrode exposed lengths of 10 mm (#25343, black dot-dash line), 15 mm (#26292, red dash line), and 20 mm (#26477, blue solid line).....	87
Figure 4.5. Time evolution of (a) \dot{B}_θ fluctuation at high field side, (b) density fluctuation (\tilde{n}_e), (c) Bias voltage (V_B) and (d) electrode current (I_B)	88
Figure 4.6. Comparison of \dot{B}_θ without bias (#26570 black) and with bias (#26571 red) discharges with H_2 gas injection: (a) plasma current (I_P), loop voltage (LV), (b) plasma density (n_e), (c) electron temperature (T_e), (d) SXR emission, (e) stored energy, (f) H_2 gas-puff pulse (g) biasing voltage (V_B), (h) bias current (I_B) and (i) H_α emission. Disruption is avoided in #26571 with application of bias. The dotted line in (b) represents the density measurements and temperature measurements with uncertainties during the disruption phase respectively. $L_{exp} \sim 20$ mm and $r_{elec} \sim 22$ cm.	90
Figure 4.7. Comparison of without bias (#26714 black) and with bias (#26719 red) with H_2 gas injection: (a) I_P , (b, c) \dot{B}_θ at midplane, low field side (d, e) Time-frequency spectrum of \dot{B}_θ , (f, g) Island width of $m = 2, 3$ modes, (h, i) spatial structures of $m = 2, 3$ modes. Disruption (by gas puffing at $t \sim 42$ ms) is avoided in #26719 with application of bias at $t \sim 41$ ms.....	91
Figure 4.8. Reconstructed radial profiles of toroidal current density and safety factor	92
Figure 4.9. (a) Position of three magnetic probes of Mirnov garland in a poloidal plane used to detect mode rotation direction. (b) and (c) show time evolution of magnetic fluctuations of the three probes shown in (a) indicate that modes rotate in the ion diamagnetic direction in discharge #26714 and #25719, respectively.	93
Figure 4.10. Tomographic results using SVD analysis of the reconstructed SXR emissivity in ADITYA Tokamak of (a) shot # 26714 and (b) #26719 in different time interval. Spatial eigen modes (topos) show time evolution of $m/n=1/1$ island for both the discharges.	94

Figure 4.11. Radial profiles of (a) plasma potential (b) radial electric field (c) poloidal flow velocity and (d) radial shear in normalised poloidal flow, with and without bias.	96
Figure 4.12. Short Time FFT analysis of $m=2$ and $m=3$ fluctuations computed by SVD analysis shows that modes $m/n = 3/1$ and $2/1$ rotate with same frequency in #26714 ((a) and (b)) and #26719 ((c) and (d)).	97
Figure 4.13. Time evolution of island rotation speed in without bias discharge (#26714) and with bias discharge (#26719) measured by phase difference of two \dot{B}_θ coils separated $\Delta\theta = 24^\circ$ from each other.	98
Figure 4.14. (a) Time evolution of island width of $m = 2$ mode, W (black) with an exponential fit (red) in the disruptive discharge #26714 after the gas-puff and (b) dW/dt of (a). (c) dW/dt versus $(1 - W/W_s)$ close to saturation and linear fit (red solid line).	99
Figure 4.15. Variation of saturation island width (W_s) and $(\Delta'a)$ as a function of poloidal flow shear for $m = 2$ and $m = 3$ modes.	100
Figure 4.16. Synchronization of bias application with Mirnov signal: (a) Comparison of two repeatable plasma discharges (#25362 without bias in red and #25367 with bias in black. H_2 Gas is puffed at 51ms (also shown in (b), (c) and (d) by vertical blue dotted line). (d) On puffing gas MHD oscillation amplitude crosses a set threshold value (0.5V in #25367, shown by horizontal red line) in trigger circuit, triggers SCR and thereby switch on the bias voltage on the electrode (shown in (b), (c) and (d) by vertical red dotted line). $L_{exp} \sim 15$ mm and $r_{elec} \sim 22.5$ cm.	102
Figure 5.1. Temporal evolution of (a) electrode current (I_B), (b) bias voltage (V_B) and (c) cross – field plasma resistance calculated as V_B/I_B . Figure depicts that after ~ 46.5 ms electrode current decreases indicating increase in cross – field plasma resistance.	108
Figure 5.2. Leaky capacitor model of the rotating plasma along with biasing circuit. V_E is biasing power supply voltage and R_X is current limiting resistor. Voltage at electrode is V_B . Rotating plasma under influence of toroidal magnetic field and radial electric field is modelled as parallel combination of plasma capacitance and cross-field plasma resistance in series with plasma inductance.	109
Figure 5.3. Comparison of electrode voltage (V_B) and electrode current (I_B) calculated from leaky capacitor model with those of experimentally measured for plasma shot #26477.	110
Figure 5.4. Temporal profile of (a) plasma current (I_P), (b) density fluctuations (\tilde{n}_e), (c) \dot{B}_θ signal (in A.U.) measured by one of Mirnov coil at the high field side, (d) $ \tilde{B}_\theta /B_\theta$, (e) H_α line intensity, (f) CIII signal, (g) SXR signal (A.U.), (h) cross field plasma resistance (R_\perp) calculated using (i) electrode current and (j) electrode voltage signal. Discharge has been divided into time zones A-E based on behaviour of electrostatic and magnetic fluctuations. (k) Reduced H_α intensity time zones B	

and C together have been defined as first regime of improved confinement. Time zone D of higher H_α intensity has also been termed as second regime of improved confinement. 113

Figure 5.5. Time behaviour of MHD modes, $m/n=3/1$ and $2/1$, in discharge #26477. During first regime of improved confinement (time zone B and C) island size of $m/n=3/1$ tearing mode reduce. No effect on island size of $m/n=2/1$ tearing mode observed during this regime. In second regime of improved confinement island width of $m/n=2/1$ mode increase significantly, triggering larger recycling at the edge. 114

Figure 5.6. Effect of biased electrode on floating potential at the plasma edge measured by radial array of six Langmuir probes..... 115

Figure 5.7. Modification in radial profile of (a) radial electric field and (b) its shear during first and second improved confinement regimes. As soon as the biasing is switched on electric field and its shear increase at the beginning of first regime ($t \sim 41.9\text{ms}$). Afterwards both the parameters reduce to previous value during first regime ($t \sim 42.5\text{ms}$ and $\sim 45.5\text{ms}$). During second regime ($t \sim 47.9\text{ms}$) a stronger electric field and shear again develops, which persists during throughout the biasing pulse. After biasing is switched off ($t \sim 52.5\text{ms}$), E_r and its shear (dE_r/dr) achieve their respective values before bias..... 116

Figure 5.8. (a) \dot{B}_θ signal measured by one of Mirnov coil, (b) electrode current, (c) bias voltage for shot #26282 and (d) radial profile of toroidal current density modifies at the plasma edge before biasing ($t \sim 41\text{ms}$), during first regime ($t \sim 43\text{ms}$) and second regime ($t \sim 49\text{ms}$) of improved confinement for #26282. In first confinement regime current density profile flattens, stabilising $m=3$ tearing mode. Steepening of current density profile causes growth in both $m=3$ and $m=2$ modes during second improved confinement regime. 118

Figure 5.9. Temporal profile of (a) plasma current (I_P), (b) loop voltage (V_L), (c) central electron temperature (T_e), (d) H_α line intensity and (e) electrode current (I_B). In second regime at $t \sim 46\text{ms}$ loop voltage decreases due to electron temperature rise..... 119

Figure 5.10. Comparison of power spectral properties of (a) magnetic fluctuations measured by Mirnov coil and (b) electrostatic fluctuations measured by Langmuir probes for time zones A - E. Shown power spectrum is average over eight similar discharges..... 121

List of Tables

<i>Table 1.1. Electrode biasing experiments worldwide.....</i>	<i>21</i>
<i>Table 2.1. Scaling laws for Ohmic plasmas.....</i>	<i>29</i>
<i>Table 2.2. Scaling laws for auxiliary heated L-mode and H-mode plasmas.....</i>	<i>29</i>
<i>Table 2.3. Plasma parameters of ADITYA tokamak.....</i>	<i>43</i>
<i>Table 3.1. Frequency response measurement of radial and poloidal probes.....</i>	<i>77</i>

Chapter 1

Introduction

1.1 A quest towards Controlled Thermonuclear Fusion

To meet energy requirement of the world in future an economical and abundant source of energy will be needed. Nuclear fusion reactions, which are source of enormous power can achieve this requirement. In these reactions light elements fuse together and form heavier elements. The resulting heavier elements have slightly less mass than the fusing elements and this mass difference results in the release of large amount of energy. The D-T (D = H², T = H³) reaction (Deuterium – tritium fusion: ${}^2_1D + {}^3_1T \rightarrow {}^4_2He + {}^1_0n + E$) is the most probable reaction (having largest reaction cross-section) at attainable temperatures in fusion reactors.

To fuse deuterium and tritium nuclei against electrostatic repulsive force, a mixture of D-T nuclei is heated to a temperature of the order of ~10 keV (i.e. ~100 million °C), the resulting process is known as thermonuclear fusion.

1.1.1 Lawson criterion

To achieve break-even condition ($Q = P_{fusion} / P_{in} = 1$), i.e., self – sustained burning plasma critical minimum condition for a fusion plasma must be satisfied, which is usually known as the Lawson criterion [1.1, 1.2]: $n_e T_e \tau_E > 5 \times 10^{21} m^{-3}.keV.s$, which states that for a plasma the product of plasma density (n_e), energy confinement time (τ_E), and electron temperature (T_e) should have a minimum required value to maintain the plasma against all losses without external power input. In other words, when this condition is satisfied released fusion energy equals the energy required to produce and confine the plasma. This condition can be obtained through the power balance equation at steady state.

1.1.2. Development of fusion research based on tokamaks

To achieve fusion on the Earth in a controlled manner in confined plasma magnetic and inertial confined fusion devices have been developed. The major research effort in the area of controlled nuclear fusion is focused on the confinement of hot plasmas by means of strong magnetic fields. Among all the toroidal magnetic confinement devices tokamaks are most studied and most advanced fusion machine and have been making steady progress through international collaboration and competition.

Tokamaks are toroidal axially symmetric magnetic confinement systems, have no open end and plasma is confined in a simple toroidal field. As will be discussed in chapter 2, for a toroidal plasma to be effectively confined, toroidal magnetic field lines must be twisted, i.e., a poloidal component of the magnetic field is essential for the equilibrium. In tokamaks plasma current is used to generate the poloidal magnetic field.

TFTR [1.3] has demonstrated $Q = 0.27$ in D-T experiments and JET [1.4] demonstrated $Q = 0.62$ in D-T experiments. JET and JT60U [1.5] achieved break-even condition ($Q = 1$) by D-D plasma [1.6].

1.2 Confinement regimes in Ohmic discharges

For Ohmic discharges, there are different confinement regimes in a tokamak in principle [1.7]. The linear Ohmic confinement (LOC) regime stands for the relatively low density, where the confinement time in Ohmic plasmas is found to increase linearly with density up to some critical value. In this regime confinement time is scaled as $\tau_E \sim n_e a^2 q^{1/2}$ [1.8]. This favourable linear dependence ($\tau_E \sim n_e$) was first found in Pulsator [1.9] and Alcator-A [1.10]. This is also called “neo-Alcator or (Alcator-INTOR)” scaling. The confinement time τ_E in this linear (with density) Ohmic confinement (LOC) regime depends neither on the plasma current nor the toroidal field.

In larger machines [1.11, 1.12] above a critical density, the confinement time saturates, which is called the saturated Ohmic confinement (SOC) regime. In this situation radiation losses from the plasma edge dominate the power balance. This regime shows a linear increase in energy confinement time with plasma current.

The saturation of τ_E with n_e could be overcome by controlling the density. With the reduced gas-puffing rate, superior confinement is obtained, with the original Alcator-INTOR scaling, i.e., $\tau_E \sim n_e$ up to the extended density limit. This improved state is characterized by peaked

density profiles. This improved Ohmic confinement (IOC) regime [1.7, 1.13] was observed in ASDEX [1.7].

Ohmic H-mode was achieved in TUMAN-3 [1.14] and DIII-D [1.15] tokamak. In DIII-D spontaneous H –mode observed in Ohmically heated discharges at low toroidal field ($\leq 1.5T$) and low density, which was always initiated by a sawtooth collapse and terminated because of increased impurity radiation. Ohmic H –mode shows all qualitative features as that in the case H-mode with auxiliary heating like rapid increase in density, a sudden drop of H_α (or D_α), edge localized modes (ELMs). Decrease in plasma internal inductance during the Ohmic H-mode indicates a broadening of the toroidal current density profile. In this confinement regime the energy confinement time have values near those predicted by Neo-Alcator scaling and a factor of two above those of non-H-mode Ohmic discharges at similar densities. In contrast to the improved Ohmic confinement (IOC) regime, the electron density profile is broadened in the Ohmic H-mode.

High density mode (HDM) was achieved on the TUMAN-3 [1.14] tokamak with additional gas puffing during magnetic compression accompanied by a fast second current ramp- up. At the moment of transition D_α reduced. After the transition to the HDM, steep density gradient formed near the limiter, fluctuation induced particle flux dropped by a factor of 10 and relative density fluctuation (\tilde{n}_e / n_e) reduced.

Pellet-enhanced-performance mode (PEP mode) were observed in TFTR [1.16] and JET [1.17] discharges that were fuelled by pellets, particles of frozen hydrogen or deuterium. This PEP regime was characterized by high central q , $q_0 (> 1)$ and reversed magnetic shear, $s = (r/q)\partial q/\partial r < 0$ near the magnetic axis following the pellet injection. First internal transport barriers (ITBs) were seen in JET plasmas that were pellet fuelled [1.17]. PEP mode in TFTR also exhibited $q_0 > 1$, but with weak positive, not negative magnetic shear.

1.3 Confinement regimes with auxiliary heating

One of the main goals in fusion-oriented tokamak research is the production and investigation of high – temperature, high- β plasmas. The stimulation for these efforts is the requirement of high β values for a fusion reactor device in order to achieve high fusion power output at low investments of magnetic field energy.

The temperature corresponding to the optimum reaction rate for D–T fusion lies in the region 10–20 keV. The tokamak current heats the plasma through Ohmic heating (typically to

temperatures of a few keV) but as the temperature rises, Ohmic heating becomes less and less effective and on its own is unable to heat the plasma to the stage where alpha particle heating can sustain fusion. Additional power is needed and auxiliary heating in tokamaks is provided by neutral beam injection (NBI) and radio frequency (RF) heating (ECRH, ICRH, LHCD).

In 1982 Wagner et al [1.18] exposed ASDEX plasma to intense heating by the neutral beam (NB) and they confronted by a totally unexpected "transition". Plasma confinement suddenly improved by a factor of two and the turbulences at the plasma edge greatly reduced. This new confinement regime known as the "H-mode" (High confinement mode) appeared first as "a strong and sudden change in plasma characteristics"

In ASDEX two different types of discharges developed with neutral beam injection. In one case with injection power $P_{NI} \sim 1.6MW$ low value of poloidal β (β_p) achieved indicating reduction in confinement throughout the NB pulse. These discharges are called L- type discharges. In these discharges electron and ion temperatures increase. However, global energy confinement time (τ_E) and particle confinement time (τ_p) reduced.

At marginally increased injection power $P_{NB} \sim 1.9MW$ a higher value of β_p was obtained and particle and energy confinement suddenly improved. This discharge type is called H-type. Sudden improvement in particle confinement and energy confinement were seen in H-type discharges, which resulted in increase in density and central temperature.

In the following years, H-mode was observed in PDX and DIII-D, the Joint European Torus (JET) and JT-60, then on several other tokamaks. In 1993, H-mode was also achieved in the German W7-AS stellarator, thus demonstrating it was a "generic feature" of all toroidal configurations.

1.3.1 L- mode discharge

One of the key observations of L-mode discharge, which was observed in all devices, was that for injected powers greater than approximately twice the Ohmic power, the energy confinement time decreased at the onset of neutral beam injection (NBI) by a factor of 1.4 to 4 from that observed during the Ohmic phase (see Ref. [1.19] and references therein). On increasing neutral beam power confinement time decreased, although the degradation of τ_E was less than linear. τ_E was observed to vary as $P_{heat}^{-1/3}$ to $P_{heat}^{-2/3}$, where P_{heat} is the total heating power.

The main features of these modes are as follows:

1. Average plasma density decreases in L-modes with the onset of the additional heating as compared to their values in Ohmic regime.
2. The out flux of the plasma ions with energies $\geq 100\text{eV}$ in ASDEX clearly reflected the degradation of the particle confinement time (τ_p) during L-mode operation.
3. The recycling at the edge increases as the H_α , D_α line radiation increases during the L-mode phase.
4. Another indication of the degraded confinement is an increase in hard X-ray radiation caused by an enhanced out flux of runaway electrons produced during the initial phase of the discharge.

1.3.2 The H- mode

H-mode enables improvement of confinement times by a factor of nearly 2 in comparison with L mode. Since the improved-confinement regime, "H- mode" was discovered in the poloidal divertor tokamak ASDEX, it has been achieved in divertor and limiter configurations. The discovery of this mode of enhanced confinement was crucial to thermonuclear fusion, and the H- mode is still today the reference scenario for the next step machine ITER. The profiles of density and temperature are much steeper at the edge in the H-mode than in the L-mode. The amplitude of turbulent fluctuations is dramatically reduced during L-H transition. The velocity of poloidal rotation and the radial electric field grow very significantly during the transition [1.20- 1.23]. The typical length scale of the electric field profile is of the order of 1cm [1.24].

The transition from the L to the H regime can be triggered artificially either by injecting a neutral beam into the periphery, by a minor radius compression of a tokamak, or by driving a current from a biased electrode immersed into a plasma inside a separatrix [1.25 – 1.28]. The L-H transition can also be shown to occur when triggered by short and powerful gas puff impulses [1.29, 1.30] or pellet injection of small pellets into the vicinity of the separatrix [1.31]. Data obtained on many tokamaks suggests that a growth in poloidal rotation is a fundamental feature of the L-H transition.

Poloidal rotational equilibrium arises from the balance between the viscous damping force F_{visc} and the forces resulting from the radial ambipolar loss or charging currents, capable of torquing up the plasma. The latter can be set up in the plasma edge in different ways: fast ion

losses resulting from NBI [1.32, 1.33] or ICRH enhanced thermal ion losses induced by fluctuations [1.34, 1.35], or simply by means of a electrode. In the latter case the driving force is simply given by $j_r B_\phi$, where the current density $j_r = I_E / A$ and A is the area of the magnetic surface at the electrode radial position.

1.4 Biasing experiments in tokamaks

Biased electrode experiments have been carried out in various machines to impose radial electric fields externally to understand possible importance of radial electric fields in L- H transition phenomenon. In these experiments radial electric fields are created by applying a voltage difference between electrode protruding beyond the Last Closed Flux Surface (LCFS) and limiter or divertor plate. Present section aims to give brief review about the main experimental findings of the electrode biasing experiments of some of the tokamaks.

A detailed comparison of tokamak configuration, electrode material, electrode geometry, electrode area, electrode orientation, electrode tip position, biasing polarity, transition voltage and current for observing higher confinement modes in different tokamaks is presented in Table 1.1.

CCT [1.25, 1.36]

First electrode biasing experiment (polarised electrode experiment) inducing L-mode to H-mode transition was reported in Constant Current Tokamak (CCT) by Taylor et al [1.25]. Negatively and positively biased electrodes were used to drive radial current externally across the edge magnetic surface. The experiment confirmed significance of radial electric field and associated poloidal rotation of plasma for H-mode confinement, for the first time. Radial electric field was excited by cross-field currents from electrodes well ($\sim 0.125 \times a$, ' a ' is plasma minor radius) in the interior of the Last Closed Flux Surface (LCFS) by biasing plasma to a potential $> \pm 10T_e / e$ (T_e is electron temperature at electrode location in eV). Similar results were obtained on drawing sufficient current ($\sim 20A$) by electron emissive injectors (W, LaB₆) used in negative biasing and cold -ion collectors (Graphite) in positive biasing to induce L-mode to H-mode (L-H) transition.

$E_r \times B_\phi$ rotation flow in plasma took place in a region of rapid potential rise between electrode and first wall. During biasing applied radial current decreased rapidly in ion-ion collision time scale ($\sim 100\mu s$) in association with electric field and plasma rotation increase. This phenomenon was termed as bifurcation in plasma rotation. Bifurcation exhibited L-H

transition, which was followed by increase in particle confinement ($> 10\times$), identified by reduction in Hydrogenic (H_α and H_β) line radiation emission and increase in plasma density.

During transition radial conductivity $\sigma_r = I_r / (2\pi R)(2\pi r)E_r$ averaged over the magnetic surface at electrode location (r_{elec}) dropped sharply. Sharp gradients in temperature and density near edge were also observed, which represented ‘transport barrier’. Moderate improvement in energy confinement ($\sim 1.5\times$) was also reported.

It was argued by Taylor et al. that applied radial current overcome neoclassical viscous damping through $J_r \times B_\phi$ force. Mathematically, $J_r B_\phi = nm_i v_\theta / \tau_p = nm_i E_r v_{ii} / B_\phi$, where m_i is ion mass and τ_p is viscosity damping time scale, which is reciprocal of the ion-ion collision time (ν_{ii}).

Poloidal asymmetry was observed in density fluctuations monitored with a poloidal array of reflectometers at L-H mode transition in CCT tokamak [1.36]. It was observed that on the outboard midplane the fluctuations decrease significantly at the H- mode transition while those on the inboard midplane generally exhibit little or no reduction. It was interpreted by the argument that poloidal variation in $E_r \times B_\phi$ rotation velocity observed due to difference in the magnetic field on the high and low field sides. Different values of electric field shear at different poloidal locations, was considered as possible mechanism. The fluctuations located at the top and bottom of the tokamak show an intermediate behaviour. It was suggested that local neutral density or impurity content strongly affect the turbulence.

Tuman 3 [1.29]

High confinement modes were achieved with positive and negative voltages in Tuman-3 electrode biasing experiments. Although they reproduced all the results of CCT biasing experiments, external radial current was quite high in TUMAN -3 than that in CCT, because of the higher plasma density in TUMAN -3. More improvement in confinement in case of negative bias than in positive bias was depicted by larger improvement in particle confinement and higher reduction rate of recycling. Particle confinement time was more by a factor of two in negative bias. Authors also reported that spontaneous Ohmic H – mode caused by natural enhancement of the negative radial electric field at the plasma periphery could be terminated by applying the external positive field. They invoked anomalous viscosity and inertia driven by turbulence within the framework of standard neoclassical

theory to explain high current densities during biasing and presented a theoretical expression for the perpendicular conductivity

$$\sigma_{\perp} = \sqrt{\pi/2n\varepsilon^2} \sqrt{m_i T_i} / \theta B_{\phi}^2 r,$$

and maximum electrode current

$$I_{\max} = 7\sqrt{2\pi^{5/2} R n T_i \varepsilon^2} / B_{\phi}, \text{ where } \theta = \varepsilon / q, \text{ } q \text{ is local safety factor, } B_{\phi} \text{ is toroidal magnetic field, } \varepsilon = a / R \text{ is inverse aspect ratio.}$$

These theoretical results matched well with the measured values in Tuman-3 and CCT for weak biasing voltages (of ~100V) and current of ~100A. They further pointed out that decrease in electrode current with growing potential in both TUMAN-3 and CCT was due to the diminishing viscosity as a function of the poloidal rotation velocity.

SINP tokamak [1.37 – 1.40]

In SINP tokamak biasing experiments were carried out at different q_a regimes to study the influence of radial electric field and current profile modification induced by applying fast (\sim ion – ion collision time, i.e., $\sim 20\mu s$) positive and negative bias electrode placed at top and bottom ports of tokamak using various materials in electrode. Increase in confinement was observed with bias voltage $< -50V$ and $> 40V$ with modified current density profile (j_{ϕ}) at the edge at $1 < q_a < 2$ discharge regime [1.37]. It was found that with the application of negative voltage from $-50V$ to $-200V$ plasma current duration increased, i.e., more the biasing voltage, plasma current lasted longer. Drop in loop voltage was observed with application of bias. It was argued that drop in the loop voltage is due to the increase in electron temperature and/or decrease in inductance.

It was inferred that loop voltage drop ($\sim 0.5V$) was mainly due to an increase in the core plasma temperature. After the bias onset j_{ϕ} -profile modification started within $100\mu s$, the E_r -profile modification came after more than $200\mu s$. In another regime of discharge with edge safety factor $q_a = 6 - 7$ [1.38], It was again reported that edge current density profile modifies due to fast edge biased electrode which leads to better confinement and longer ($\sim 40\%$) duration of plasma current.

It was reported that electrostatic fluctuations caused by drift wave modes and magnetic fluctuations caused by excitation of slow compressional Alfvén (magneto-acoustic) waves

were suppressed due to current profile modification by biased electrode in discharges having edge safety factor $q_a > 5$ [1.39].

Spontaneous plasma disruption controlled by biased electrode [1.40] was reported first time in SINP tokamak by the stabilization of $m/n = 3/1$ and $m/n = 2/1$ tearing modes. It was proposed that stabilization of tearing modes is due to current redistribution due to biasing. Biasing made current profile steeper near electrode position and affected current – driven tearing modes.

Phaedrus - T tokamak [1.41]

In Phaedrus –T tokamak H –mode plasma of hydrogen, deuterium and helium gases was produced by inserting a positively biased graphite electrode from either top or bottom of the machine [1.41].

H-mode was triggered very quickly after the application of the positive bias and particle confinement time (τ_p) increased by a factor of ~ 2 during biasing. Data showed that in the plasma edge the particle flux due to turbulence and the RMS amplitudes of both the ion saturation current (i_s) and poloidal electric field (E_θ) in the SOL are reduced during electrode biasing as compared with before biasing.

It was observed that during H- mode current (I_B) drawn by the electrode increased. H- mode degraded when I_B starts to decreased. It was found that recycling coefficient was much closer to 1 in helium plasma in Phaedrus–T as compared with hydrogen and deuterium plasmas. Therefore, τ_p was already quite large in Ohmic helium discharges and therefore, maximum line averaged density was smaller for the helium discharge.

Two –dimensional camera measurement of D_α emission (normalized to density) the four poloidal quadrant depicted that D_α emission with the onset of H-mode was poloidally asymmetric. Greatest relative decrease occurred on the low-field side. It was argued that D_α emission depended not only on n_e fluctuations but also on E_θ fluctuations, as well as on the phase and coherency between n_e and E_θ fluctuations. The change of edge fluctuations was much faster than the change in the H_α or D_α level. Edge fluctuation level decays with a time scale of 0.1ms, H_α or D_α level decayed with a time scale of 1 to 5ms and n_e and τ_E increased on a 10 to 20ms time scale. This suggested that the transition from small to large E_r , resulted in a reduction in edge fluctuations, the reduction in edge fluctuations resulted in a reduction

of the radial transport of edge particles, and the reduction in the radial transport of edge particles caused decrease in the H_α or D_α emission and the increased in density and energy.

ISTTOK Tokamak [1.42]

Improved confinement mode was achieved in ISTTOK tokamak with positive and negative bias, provided bias current was larger than 20A. In case of negative bias to draw large current two approaches were followed - (1) use of smaller limiter, inserted deep inside the main limiter radius and (ii) use of emissive electrode made of LaB_6 . It was found that as the polarization voltage is increased, the bias current started to increase linearly with the radial electric field and reached a saturation value, after which it decreases. This is in qualitative agreement with the expression for the electric current density derived by Stringer [1.43].

Threshold voltage for negative bias found to be $<-140V$. In emissive (negative) electrode bias E_r -profile is modified in less than $50\mu s$. During negative bias in the region just inside the limiter as the bias is applied a double – peaked structure of radial profile of the large radial electric field was observed. As the density increased towards its maximum and collected current amplitude decreased, E_r profile relaxed to a single – peaked structure without a significant increase in the maximum magnitude of E_r during improved confinement mode. It was considered that these structures were related to the non-linear solutions of the equation for the radial electric field, discussed by Kasuya *et al* [1.44].

In large positive electrode voltage (+140V) radial electric field modification led to plasma density increase. Modest increase in particle confinement was also observed. In positive bias no double-peaked structures are observed in the radial electric field, suggesting that these (double – peak E_r profile) structures were related with transitory localized negative space charge formation in a radial position close to the electrode, caused by the emitted electrons during emissive electrode bias.

TCABR [1.45- 1.47]

In TCABR [1.45, 1.46] regimes of strong and weak MHD activity were obtained using a biased electrode near magnetic island. In bias excited MHD activity regime mode $m/n = 2/1$ was found to be dominant. In totally or partially suppressed MHD burst regime dominant mode was $m/n = 3/1$. A strong decrease in radial electric field was detected with destruction of the transport barrier during both regimes.

In bias excited MHD regime first plasma turbulence was suppressed, but again increased with the growth of MHD oscillations. It was found that at onset of biasing edge transport barrier formed which was inferred from increase in radial electric field to $\sim 100\text{V/cm}$ value and plasma density at the edge. Also, average density measured by microwave interferometer was increased and H_α emission decreased. Decrease in turbulent – driven particle transport $\Gamma = \langle \tilde{n}_e \tilde{v}_r \rangle$ was resulted by decreased poloidal electric field and plasma density oscillations. At latter time during onset of strong MHD activity transport barrier is deteriorated indicated by decrease in radial electric field and edge plasma density and increase in H-alpha emission and turbulent transport. Excitation of MHD activity was due to change of radial plasma profiles, produced by accumulation of impurities in the central region of the plasma column. In bias suppressed MHD activity regime at the onset of bias edge transport barrier was formed like in excited MHD regime, which on latter time followed by further sudden drop in plasma turbulence and related transport similar to L-H transition with slightly reduced radial electric field. But contrastingly, no drop in electrode current observed and H-alpha line spectral density increased slightly. Possible explanation of excitation of the $m/n = 3/1$ mode in this regime were impurity contribution and due to modification of current density gradient at the plasma edge due to the skin effect.

STOR–M [1.48, 1.49]

STOR–M tokamak registered confinement enhancement in both positive and negative electrode biasing. Electrode current was nearly equal in both cases, but decayed much more rapidly for negative biasing. All the characteristics of H-mode were obtained for both the cases. Effect of biasing was more prominent in case of negative bias. Toroidal and poloidal plasma rotation profile at the edge were investigated during biasing.

It was observed that without bias plasma poloidal rotation was in ion diamagnetic drift direction, which during negative biasing changed to electron diamagnetic drift direction due to significant decrease in E_r (increased negative E_r) and large density steepening. During positive bias smaller negative E_r slowed down the poloidal rotation in the electron diamagnetic drift direction.

With no bias applied, the plasma toroidally flows in the direction of the plasma current. It was observed that increased negative E_r during negative bias reduced the toroidal flow throughout the edge, while the smaller negative E_r during positive bias significantly increased toroidal flow and its shear at the plasma edge.

TEXTOR [1.28, 1.50, 1.51]

In TEXTOR H-mode could be achieved by either bias polarity and named as H_+ and H_- modes for radially outward and radially inward electric field, respectively. Experiments were performed in Ohmic and NBI heated plasmas. A canoe shaped carbon electrode was used for the experiments. But confinement properties of these modes were different. Energy confinement in H_+ mode was found to be similar or somewhat higher than in H_- mode. In contrast to this, the particle confinement in the H_- mode was substantially higher than that in the H_+ mode although radial electric field shear was comparable in both cases. Confinement modification accompanied with establishment of transport barrier in the high electric field zone inside the limiter radius. For positive biasing threshold electrode current was about $130 \pm 20 A$. It was reported that threshold value for transition depended on the TEXTOR wall conditions. For boronized walls it laid 400-500V and with carbonized walls the threshold is typically 100V higher. In Ohmic discharge transition current was of the order of 30-40A for negative bias, which was appreciably lower than the observed current in the case of positive bias. Ohmic H_- mode was readily obtained using emissive electrodes, capable of drawing higher current similar to positive bias case. It was observed that with positive bias strong localized radial electric field built up in the immediate vicinity of the limiter on a time-scale of 1.2ms upon the L-H transition.

Recently experiments [1.51] were performed at TEXTOR to demonstrate role of zonal flows in triggering the H – mode transition by controlling the $E_r \times B_\phi$ shear rate by biasing the electrode above the critical voltage needed for H-mode transition. They presented first experimental observations of stretching and splitting of eddy structures in sheared flow during the transition to an improved confinement regime.

1.5 Different models to explain L- H transition

The development of the $E_r \times B_\phi$ shear stabilization model is considered the explanation of the formation of transport barrier in magnetic confinement devices since the last two decades [1.52]. The effect of sheared flow has been widely demonstrated. Sheared poloidal flow can influence turbulence by shear decorrelation [1.53]. The development of methods to control the sheared $E_r \times B_\phi$ flows is considered to be a key issue in the control of plasma turbulence and the optimization of plasma confinement. Numerous mechanisms on the generation of poloidal sheared flow have been proposed, including Reynold stress [1.54 – 1.56], external

biasing [1.25, 1.57- 1.59], injected radio-frequency waves [1.60, 1.61], orbit loss [1.32] and non –symmetric transport [1.62, 1.63] etc. Among them, biasing experiments, an effective means of controlling the radial electric field E_r , have been conducted in a variety of devices, including tokamak and non - tokamak [1.57, 1.64, 1.65].

Role of current density profile modification is also considered as a candidate for the observed precursor magnetic oscillations to the H- mode transition [1.66]. It has been observed in the H-mode discharge [1.66], the electron temperature and density at the plasma edge ($T_{e,a}, n_{e,a}$) rise significantly just after the L- to H- transition, but there is also a continuous rise in $T_{e,a}$ prior to the transition in many cases when there is a delayed transition. It was interpreted that $T_{e,a}$ reaches a certain threshold due to sawtooth crash to initiate the transition. The initiation by a sawtooth mostly occurs at low heating power and high plasma current. However, the transition is often initiated without a sawtooth in discharges with high heating power in ASDEX [1.66]. H-mode discharges initiated without a sawtooth in the Poloidal Divertor Experiment (PDX) tokamak [1.67] showed that there was no simple threshold for the transition in $T_{e,a}$. It was found that as an alternative to the requirement of sufficiently high $T_{e,a}$, the H mode could be triggered by the formation of finite current density at the edge ($j_{\phi,a}$).

In ASDEX change in the current density (j_{ϕ}) profile were analysed with the help of MHD modes detected by Mirnov probes in H- mode discharges which do not show rise in $T_{e,a}$ prior to transition. It was found that coherent magnetic oscillations prior to the H-mode transition suggested evolution of the j_{ϕ} profile from the peaked L- type to the H- type with finite $j_{\phi,a}$. The behaviour of the oscillations suggested that the current-density profile plays an important role in the transitions. Some Theories [1.68–1.70] suggest that current-density profile with finite $j_{\phi,a}$ is relevant to the H-mode from energy principle. These theories predict that the increased edge magnetic shear may suppress edge turbulence in the divertor configuration and trigger the H-mode transition. Another theory [1.71] predicted that the stabilization of the ideal ballooning mode due to finite $j_{\phi,a}$ in a divertor plasma.

Hahm et al [1.72] discussed theoretically that increased global shear near separatrix causes reduction in the effective step size of turbulent diffusion process at the edge and improves heat and particle confinement in diverted tokamak geometry. This fact was elucidated in JIPP T-IIU limiter tokamak by Toi et al [1.73]. They demonstrated that H-mode transition was readily triggered by the enhancement of global magnetic shear near the edge.

1.6 Recent results and renewed interest in electrode-biasing experiments

Observations of modifications in poloidal rotations generated due to the setting up of radial electric field during L – H transition is thought to be one of causes of L - H transition. Although, there is substantial support for the paradigm of sheared radial electric field (E_r) causing enhanced local $E_r \times B_\phi$ shear flows, which suppresses the electrostatic turbulence leading tokamak plasma to attain higher confinement regimes, however, no single theory explains all the observations [1.74]. Different mechanisms of shear generation, e.g., ion-orbit loss, neutral particle effect, Reynolds stress and pressure gradients lead to bifurcation in different situations in tokamaks [1.32, 1.53, 1.74, 1.75]. On the other hand, experiments [1.66, 1.73, 1.76 – 1.78] and theories [1.70, 1.72, 1.79] have also been put forward establishing the significant role of toroidal current density (j_ϕ) profile modification in the L–H transition. The importance of an increased $E_r \times B_\phi$ shear in confinement improvement during the H-mode was also strengthened by the edge plasma biasing experiments [1.25, 1.80], where E_r -profile modification is created by a biased electrode. Electrode biasing experiments have been carried out in many tokamaks [1.25, 1.28, 1.29, 1.41, 1.42, 1.49, 1.80] with different magnetic configurations for decades after it was first demonstrated in CCT tokamak [1.25] to understand improved energy confinement in tokamaks. Majority of the high confinement mode features observed in L - H transition with auxiliary heating such as sharp transport barrier formation, reduction of H_α emission (656.2 nm) intensity, substantial reduction in electrostatic fluctuations reproduced with placing a biased electrode inside the last closed flux surface of many tokamaks. But, the effect of sheared rotation generated due to induced radial electric field by biased electrode on magnetohydrodynamic (MHD) fluctuations have been overlooked till very recently and have generated renewed interest in electrode biasing experiments through observations of substantial modifications in magnetic fluctuations as well as in toroidal current density (j_ϕ) profiles due to biasing. Physical mechanisms of interplay between induced electric fields generated rotations and MHD activities are not well understood. In very low q_a (VLQ) and normal q_a discharges of SINP-tokamak improved confinement with extension of plasma current duration are observed with inserting biased electrode and the results are attributed to the observed edge toroidal current profile modification due to the biased electrode [1.37, 1.39]. They have shown that radial electric field profile modification comes much later in time than the toroidal current profile modification. In TCABR tokamak, both suppression and excitation of MHD activity has been

observed using voltage polarised electrode placed in the edge region [1.46]. Very recent experiments in SINP tokamak, spontaneous disruptions are successfully mitigated with biased electrodes placed in the edge region of this tokamak [1.40].

1.7 Interplay between radial electric fields and MHD activity

The interplay of rotating magnetic island and background plasma in toroidal devices has been a subject of theoretical and experimental study since the very beginning of tokamak research. However, until now no clear picture exists that is capable of describing all the observed phenomena. One of the most important problems is a possible mutual influence of island evolution, radial electric field and plasma confinement.

According to the linear theory, an MHD island in the tokamak rotates due to the joint impact of electron diamagnetic drift and $E_r \times B_\phi$ drift [1.81] and the island velocity in the lab frame is a sum of the electron diamagnetic drift and the $E_r \times B_\phi$ drift velocities, i.e., $v_m = v_{dia} + v_{E \times B}$, where v_m , v_{dia} and $v_{E \times B}$ are mode velocity, electron diamagnetic velocity and $E_r \times B_\phi$ drift velocity, respectively. In the non-linear stage, no such simple relation for the island rotation velocity exists. Nevertheless, this velocity is expected to remain greater than the plasma rotation velocity outside the island [1.82].

In experiments done in TUMAN-3M [1.82- 1.84], it was found that H-mode initiated by strong negative peripheral E_r generation was hampered by a potential positive radial electric field generated by poloidally rotating large MHD island in a nearby region. It was also speculated that a positive (directed outwards) $E_r(\Delta)$ may generate near the rotating island. $E_r(\Delta)$ depends on the island size Δ , and plays a role only if the island is large enough. It was argued that large MHD burst with coexistence of $m = 2, 3$ and 4 produced the field line's stochastization. Electrons are lost due to stochastical perturbation of the magnetic field lines in the vicinity of the island [1.85] and positive E_r generated.

In a neoclassical approach Kaveena and Rozhansky [1.86] calculated E_r inside and outside the island combining anomalous ion viscosity effect. It was found that poloidal rotation of an island with angular velocity ω generates a potential radial electric field $E_r^{island} = \langle B_\phi \rangle \omega r / m$ in a nearby region with the radial scale δ depending on the ratio of anomalous ion viscosity to neoclassical one, η^{an} / η^{neo} . The value and direction of this field are such as to provide

rotation of the nearby plasma together with the island. Outside this region E_r decreases to the neoclassical level.

Theoretical treatments [1.86, 1.87] reveal that if island rotation velocity differs from the neoclassical rotation velocity of background plasma, plasma rotates with a velocity close to the magnetic island rotation's one in vicinity of the island. Thereby, plasma rotation is sheared near the rational flux surface. Thus, a tearing mode excitation may assist in the transport barrier formation near the rational flux surface.

1.8 Motivation of the thesis work

The primary objective of the work described in this thesis is to investigate the effect of the radial electric field and its shear generated by biased electrode on MHD oscillations. Further, the study envisaged the detail investigation of effect of biasing on resistive tearing modes ($m/n = 3/1$ and $2/1$). Further, controlling these MHD modes using biased electrode, we aim to control plasma disruptions initiated by growth in MHD instabilities, as the success of ITER and big tokamaks as fusion systems depend heavily on avoidance of disruptions. As suppression of both the electrostatic and magnetic fluctuations is observed in different tokamaks, we further seek to answer the temporal chronology of events, i.e., which event is the cause and which one is the effect. Furthermore, there exists no definite criterion for achieving L – H transitions using biased electrode in different tokamaks, which have used different electrode dimensions, have drawn different electrode currents using different biasing voltages to achieve transition. In this thesis we intend to find most effective parameter responsible for the transition by designing a special electrode-holding assembly by which we can change the electrode dimension by changing its exposed length (L_{exp}) in-situ along with its position (r_{elec}) movement inside the ADITYA tokamak.

1.9 Thesis Outline

This thesis consists of six chapters. First chapter is an introduction to biased electrode experiments carried out in different tokamaks and also includes the motivation and objective of the thesis. Second chapter describes tokamaks, especially ADITYA tokamak, its parameters, operational regimes and diagnostics. Third chapter includes experimental set up, design and fabrication of electrode holding assembly, design and fabrication of biasing power supply and its sub-systems along with various diagnostics especially developed for biasing experiments. Fourth chapter describes the novel approach of mitigating tokamak plasma

disruption using biased electrode and its physical mechanism. Fifth chapter discusses the effect of biased electrode on electrostatic and magnetic fluctuations leading to better confined state. Conclusions and future outlook are presented in the sixth chapter.

1.10 References

- [1.1] John Wesson, Tokamaks, 3rd Edition, Oxford University Press
- [1.2] Lawson, J.D., “Some Criteria for a Useful Thermonuclear Reactor”, *Atomic Energy Research Establishment*, Culham Report No: A.E.R.E. GP/R – 1807 (1955)
- [1.3] J. D. Strachan, et al., *Plasma Phys. Control. Fusion* **39**, B103 (1997)
- [1.4] D. Stork, IEA workshop W60 “Burning Plasma Physics and Simulation”, Tarragona, 4-5 July, 2005
- [1.5] Shirai Hiroshi, Division of Plasma Physics Meeting, American Physical Society, November 17-21, 1997
- [1.6] K. Miyamoto, Plasma Physics for Nuclear Fusion, The MIT Press, 1989
- [1.7] F. X. Soldner, E. R. Muller, F. Wagner, et al., *Phys. Rev. Lett.* **61**, 1105 (1988)
- [1.8] Fusion Physics, edited by M. Kikuchi et al., IAEA, Vienna, 2012
- [1.9] O. Kluber et al., *Nucl. Fusion* **15**, 1194 (1975)
- [1.10] M. Gaudreau et al., *Phys. Rev. Lett.* **39**, 1266 (1977)
- [1.11] S. Fairfax et al., in *Proceedings of the Eighth International Conference on Plasma Physics and Controlled Nuclear Fusion Research*, Brussels, 1980 (IAEA, Vienna, 1981), **Vol. 1**, p. 439
- [1.12] S. Ejima et al., *Nucl. Fusion* **22**, 1627 (1982)
- [1.13] M. Greenwald, D. Gwinn, S. Milora, et al., *Phys. Rev. Lett.* **53**, 352 (1984)
- [1.14] T. Yu Akatova, et al., in *Plasma Physics and Nuclear Fusion Research 1990* (Proc. 13th Int. Conf. Washington, 1990) **Vol 1**, IAEA, Vienna 509 (1991)
- [1.15] T. H. Osborne, et al., *Nuclear Fusion* **30**, 2023 (1990)
- [1.16] S. L. Milora, et al., *Plasma Phys. Control. Fusion* **28**, 1435 (1986)
- [1.17] G. L. Schmidt, et al., *Plasma Phys. and Control. Fusion* (Proc. 12th Int. Conf. on Fusion Energy, Nice, 1988) **1**, 215 (1989)
- [1.18] F. Wagner, et al., *Phys. Rev. Lett.* **49**, 1408 (1982)
- [1.19] S. M. Kaye, *Phys. Fluids* **28**, 2327 (1985)
- [1.20] R. J. Groebner, et al., *Phys. Rev. Lett.* **64**, 3015 (1990)
- [1.21] K. Ida, S. Hidekuma, Y. Miura, et al., *Phys. Rev. Lett.* **65**, 1364 (1990)

Chapter 1: Introduction

- [1.22] K. Ida, S. Hidekuma, M. Kojima, et al., *Phys. Fluids B* **4**, 2552 (1992)
- [1.23] A. R. Field, G. Fussman, J. V. Hofmann, and the ASDEX Team, *Nucl. Fusion* **32**, 1191 (1992)
- [1.24] K. T. Tsang and E. A. Frieman, *Phys. Fluids* **19**, 747 (1976)
- [1.25] R. J. Taylor, et al., *Phys. Rev. Lett.* **63**, 2365 (1989)
- [1.26] R. Van Neinwenhove, G. Van Oost, R. Weynants et al., in *Proc. 18th European Conference on Controlled Fusion and Plasma Physics*, **Vol. 15C, Part 1**, Berlin (1991), p. 405
- [1.27] L. G. Askinazi, V. E. Golant, E. R. Its, et al., in *Proc. 18th European Conference on Controlled Fusion and Plasma Physics*, **Vol. 15C, Part 1**, Berlin (1991), p. 401
- [1.28] R. R. Weynants, et al., *Nucl. Fusion* **32**, 837 (1992)
- [1.29] L. G. Askinazi et al., *Nucl. Fusion* **32**, 271 (1992)
- [1.30] Z. A. Pietrzyk, et al., *Nucl. Fusion* **32**, 1735 (1992)
- [1.31] L. G. Askinazi, et al., *Phys. Fluids B* **5**, 2420 (1993)
- [1.32] K. C. Shaing, et al., *Phys. Rev. Lett.* **63**, 2369 (1989)
- [1.33] T. Ohkawa, R. L. Miller, *Nucl. Fusion* **30**, 1616 (1990)
- [1.34] H. Biglari, et al., in *Plasma Physics and Controlled Nuclear Fusion Research 1990* (Proc. 13th Int. Conf. Washington, 1990) **Vol -2**, IAEA, Vienna, IAEA-CN-53/D-III-5 (1991)
- [1.35] A. Hassam, et al., in *Plasma Physics and Controlled Nuclear Fusion Research 1990* (Proc. 13th Int. Conf. Washington, 1990) **Vol -2**, IAEA, Vienna, IAEA-CN-53/D-IV-11 (1991)
- [1.36] T. L. Rhodes, *Nuclear Fusion* **33**, 1787 (1993)
- [1.37] Joydeep Ghosh et al., *Nucl. Fusion* **47**, 331 (2007)
- [1.38] Debjyoti Basu and R. Pal, *J. Plasma Fusion Res. SERIES* **8**, 446 (2009)
- [1.39] Debjyoti Basu et al., *Phys. Plasma* **19**, 072510 (2012)
- [1.40] Debjyoti Basu et al., *Phys. Plasma* **20**, 052502 (2013)
- [1.41] E. Y. Wang, et al., *Nucl. Fusion* **35**, 467 (1995)
- [1.42] C. Silva, *Nucl. Fusion* **44**, 799 (2004)
- [1.43] T. E. Stringer, *Nucl. Fusion* **33**, 1249 (1993)
- [1.44] N. Kasuya, K. Itoh and Y. Takase, *Nucl. Fusion* **43**, 244 (2003)
- [1.45] I. C. Nascimento et al., *Nucl. Fusion* **45**, 796 (2005)
- [1.46] I. C. Nascimento et al., *Nucl. Fusion* **47**, 1570 (2007)
- [1.47] Z. O. Guimaraes-Filho, et al., *Phys. Plasma* **15**, 062501 (2008)
- [1.48] Xiao, C., et al., *Phys. Plasma* **1**, 2291 (1994)

Chapter 1: Introduction

- [1.49] K. K. Jain et al., *Research Report, Plasma Physics Laboratory, University of Saskatchewan*, PPL-145 (1994)
- [1.50] R. R. Weynants, et al., in *Plasma Physics and Controlled Nuclear Fusion Research*, 1990 (Proc. 13th Int. Conf. Washington, 1990) **Vol -1**, IAEA, Vienna 473 (1991)
- [1.51] I. Shesterikov, et al., *Phys. Rev. Lett.* **111**, 055006 (2013)
- [1.52] K. H. Burrell, *Phys. Plasma* **4**, 1499 (1997)
- [1.53] H. Biglari, et al., *Phys. Fluids B* **2**, 1 (1990)
- [1.54] G. G. Craddock and P. H. Diamond, *Phys. Rev. Lett.* **67**, 1535 (1991)
- [1.55] P. H. Diamond et al., *Phys. Rev. Lett.* **72**, 2565 (1994)
- [1.56] C. Hidalgo, et al., *Phys. Rev. Lett.* **83**, 2203 (1999)
- [1.57] O. Sakai, et al., *Phys. Rev. Lett.* **70**, 4071 (1993)
- [1.58] G. R. Tynan, et al., *Phys. Rev. Lett.* **68**, 3032 (1992)
- [1.59] C. Wang, et al., *Chin. Phys. Lett.* **18**, 257 (2001)
- [1.60] B. Leblanc, et al., *Phys. Plasma* **2**, 741 (1995)
- [1.61] B. Leblanc, et al., *Phys. Rev. Lett.* **82**, 331 (1999)
- [1.62] T. E. String, *Phys. Rev. Lett.* **22**, 770 (1969)
- [1.63] A. B. Hassam, et al., *Phys. Rev. Lett.* **66**, 309 (1991)
- [1.64] R. C. Isler, et al., *Phys. Fluids B* **4**, 2104 (1992)
- [1.65] D. Craig, et al., *Phys. Rev. Lett.* **79**, 1865 (1997)
- [1.66] K. Toi et al., *Phys. Rev. Lett.* **62**, 430 (1989)
- [1.67] R. Fonck, et al. , in *Proceedings of the Fourth International Symposium on Heating of Toroidal Plasmas*, Rome, 1984, edited by H. Knoepfel and E. Sindoni (International School of Plasma Physics, Varenna, 1984), p. 37
- [1.68] D. Biskamp, Natural current profiles in tokamaks, *Comments Plasma Phys. Controlled Fusion* **10**, 165 (1986)
- [1.69] B. B. Kadomtsev, *Comments Plasma Phys. Controlled Fusion* **11**, 153 (1987)
- [1.70] J. Y. Hsu and M. S. Chu, *Phys. Fluids* **30**, 1221 (1987)
- [1.71] C. M. Bishop, *Nucl. Fusion* **26**, 1063 (1986)
- [1.72] T. S. Hahm and P. H. Diamond, *Phys. Fluids* **30**, 133 (1987)
- [1.73] K. Toi et al., *Phys. Rev. Lett.* **64**, 1895 (1990)
- [1.74] J. W. Connor and H. R. Wilson, *Plasma Phys. Control. Fusion* **42**, R1–74 (2000)
- [1.75] P. H. Diamond and Y. B. Kim, *Phys. Fluids B* **3**, 1626 (1991)
- [1.76] J. P. Christiansen and J. G. Cordey, *Nucl. Fusion* **30**, 599 (1990)

Chapter 1: Introduction

- [1.77] N. Ohya, G. L. Jahns, R. D. Stambaugh and E. J. Strait, *Phys. Rev. Lett.* **58**, 120 (1987)
- [1.78] B. E. Chapman, et al., *Phys. Plasmas* **7**, 3491 (2000)
- [1.79] E. Minardi, *Plasma Phys. Control. Fusion*, **30**, 1701 (1988)
- [1.80] G. Van Oost et al., *Plasma Phys. Control. Fusion* **45**, 621 (2003)
- [1.81] J. C. Hosea, F. C. Jobes, R. L. Hickok and A. N. Dellis, *Phys. Rev. Lett.* **30**, 839 (1973)
- [1.82] V. V. Bulanin, et al., *Plasma Phys. Control. Fusion* **48**, A101 (2006)
- [1.83] L. G. Askinazi et al., *Plasma Phys. Control. Fusion* **48**, A85 (2006)
- [1.84] V. V. Bulanin, et al., *33rd EPS Conference on Plasma Phys.*, Rome, 19 - 23 June 2006 ECA **Vol. 30I**, P-4.106 (2006)
- [1.85] V. V. Bulanin, V. V. Dyachenko, L. A. Esipov et al., *Proc. Int. Workshop on Strong Microwaves in Plasmas (Nizhniy Novgorod)* **Vol 1**, p. 398 (2003)
- [1.86] E. Kaveeva and V. Rozhansky, *30th EPS Conf. on Controlled Fusion and Plasma Physics (St Petersburg, Russia, 7–11 July 2003)* **Vol. 27A**, (ECA) P-3.150 (2003)
- [1.87] C. Shaing, *Phys. Plasmas* **9**, 3470 (2002)
- [1.88] G. Van Oost, et al., *Plasma Phys. Control. Fusion*, **45**, 621–643 (2003)
- [1.89] J. Stockel et al., *Problems of Atomic Science and Technology, No 6 Series: Plasma Physics* **12**, 19 (2006)

Chapter 1: Introduction

Table 1.1. Electrode biasing experiments worldwide

Tokamak	$\epsilon = a / R$	Limiter	Electrode Material	Electrode Geometry	Electrode area (cm ²)	Electrode orientation	Electrode tip position inside limiter (cm)	r_{elec} / a	Biasing Polarity	Transition Voltage	Transition Current
CCT [1.25, 1.36]	40/150=0.267	Poloidal limiter	W, LaB ₆ , Graphite	Cylindrical	50.3	Top	15	0.63	Positive and Negative bias	<-150V	20A
TEXTOR [1.28, 1.50, 1.51]	40/175=0.263	Toroidal belt	Carbon	Canoe shaped	39.0	Bottom	6.0 & 4.5	0.85	Positive and Negative bias	<-900V & >(400-500)V	(30-40) A (-) & (130±20)A(+)
TUMAN-3 [1.29]	22/53= 0.415	Poloidal limiter	Molybdenum		3.0		3.0-4.0	0.82	Positive and Negative bias	$\leq -250V$ & $\geq 500V$	(150-250)A(+), 40A(-)
PHAEDRUS-T [1.41]	26/93= 0.279	Poloidal limiter	POCO graphite	Cylindrical	23.6	Top & Bottom	3.0	0.88	Positive bias only	300V	150A
STOR-M [1.48, 1.49]	12/46= 0.261	Poloidal limiter, Horizontal rail	Stainless Steel	Cylindrical	14.5	Radial	3.8 & 1.5	0.68	Positive and Negative bias	-350V and 150V	15A(-) & 15A(+)
SINP [1.37- 1.40]	7.5/30= 0.250	Poloidal limiter	Tungsten	Cylindrical	0.57-1.89	Top	1.8	0.76	Positive and Negative bias	(-50 to -200)V & >40V	No dependency
ISTTOK [1.42]	7.8/46= 0.170	Poloidal graphite limiter	LaB ₆	Disk	2.0	Radial	1.2	0.85	Positive and Negative bias	-175V & 70V	15A(-) & 20A(+)
CASTOR [1.88, 1.89]	8.5/40= 0.213	Poloidal limiter	Carbon	Mushroom	8.0	Top	0.5	0.5	Positive bias only	100V	10A
TCABR [1.45-1.47]	18/615= 0.293	Poloidal limiter	Graphite	Disk	5.65	Radial	2.0	0.89	Positive bias only	300-400V	150A
ADITYA [1.90]	25/75= 0.33	Two semicircular poloidal ring	Molybdenum	Cylindrical	1.57	Top	1.0- 3.5	0.88	Positive bias only	150V	40 - 50A

Chapter 2

Tokamaks and ADITYA Tokamak

This chapter introduces the basic physics of tokamaks and ADITYA tokamak with its subsystems and operational diagnostics.

2.1 Tokamaks

In thermonuclear fusion research using magnetic confinement, tokamak is the most promising candidate to demonstrate fusion as achievable energy source. A tokamak (**T**oroidal**n**aya **K**amera **M**agnitnaya **K**atushka or "Toroidal Vessel with Magnetic Coils") is a toroidal device which uses a strong toroidal magnetic field, B_ϕ to confine high temperature plasma within the torus for a sufficiently long time. Final goal of the tokamak research is to reach fusion of deuterium and tritium nuclei for production of electricity.

In a tokamak toroidal magnetic field magnitude has gradient and curvature in $-\hat{\mathbf{R}}$ direction. Charged particles (electrons and ions) gyrate under the influence of these fields and feel drift (Fig. 2.1).

Because of grad- B drift and curvature drift ions drift in $\hat{\mathbf{z}}$ direction and electrons drift in opposite direction. This charge separation produces an electric field perpendicular to toroidal magnetic field (in $-\hat{\mathbf{z}}$ direction). The force qE of electric field along with B_ϕ results in outward (in $\hat{\mathbf{R}}$ direction) collective drift $\mathbf{v}_{E \times B} = -\mathbf{E}_z \times \mathbf{B}_\phi / B^2$ on charge particles and makes plasma unstable.

The outward drift tendency of charged particles in a toroidal magnetic field is compensated by adding a poloidal magnetic field (\mathbf{B}_θ) generated by toroidal plasma current (I_P) (Fig. 2.2). The resultant magnetic field lines ($\mathbf{B} = \mathbf{B}_\phi + \mathbf{B}_\theta$) are twisted into helical shapes. Electrons flowing along field lines neutralize the charge-separation and instability originated from grad- B and curvature drifts are removed.

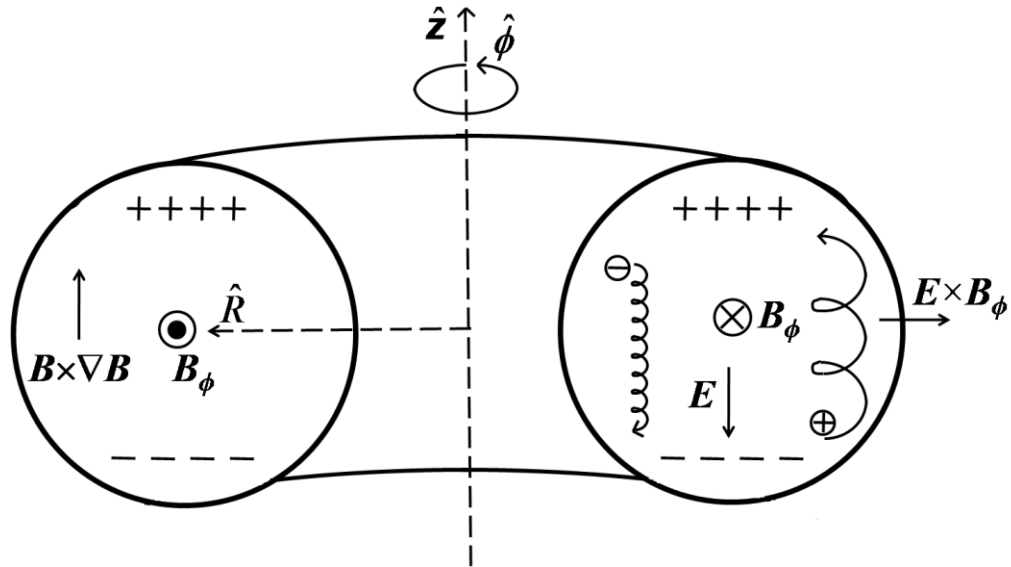


Figure 2.1. Opposite \hat{z} - direction drift in ions and electrons caused by grad- B drift and curvature drift results a charge polarization, which induces an electric field. Both ions and electrons drift outward ($E \times B$). Consequently, plasma is not confined in a simple toroidal magnetic field.

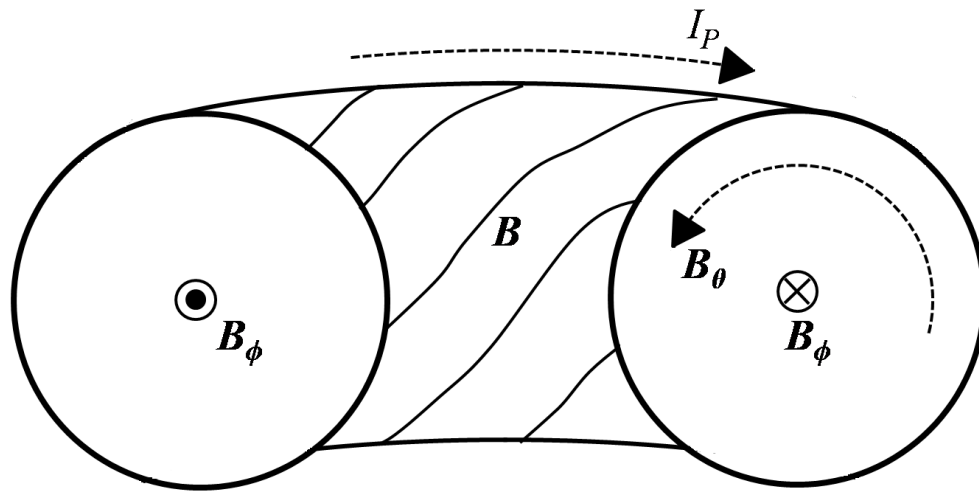


Figure 2.2. Helical structure of magnetic field: Plasma current (I_P) generates a poloidal magnetic field (B_θ), which together with toroidal magnetic field (B_ϕ) produce helical magnetic field lines $B = B_\phi + B_\theta$. In helical field lines polarization is short circuited, as charged particles can move freely along the line of force.

In a tokamak a fast time varying current in Ohmic transformer (OT or TR) coils produce a time varying magnetic flux, which in turn produce a toroidal electric field (generally expressed in terms of loop voltage). Under the influence of electric field plasma is produced

inside the vacuum vessel. Plasma current (I_P) induced via this transformer action is understood as secondary circuit of transformer. Plasma is confined by toroidal magnetic field, which is produced by external electric currents flowing in poloidal coils (toroidal field (TF) coils) wound around the torus. Poloidal magnetic field caused by plasma current (I_P) and vertical magnetic field produced by a set of vertical magnetic field coil (B_V coils) is used to keep plasma in equilibrium. A detailed description of coil arrangement and plasma discharge is discussed in section 2.4.1.1 and 2.4.2.

2.1.1 Equilibrium of tokamak plasma

On short timescales tokamak plasmas show a variety of oscillations and turbulent phenomena. On sufficiently long timescales the plasma behaviour is governed by diffusive losses, gradual changes in the magnetic configuration and changes caused by plasma heating. The timescale in which the plasma pressure and the magnetic forces balance, tokamak plasma is understood to be in “equilibrium”. In ideal MHD, which treats the plasma as an ideally conducting fluid, Maxwell equations are subject to the low frequency and Ampere’s law shows no displacement current ($\mathbf{j} = \nabla \times \mathbf{B}$). Ideal MHD equilibrium satisfies the force balance:

$$\nabla p = \mathbf{j} \times \mathbf{B} \quad (2.1)$$

From which we have, $\mathbf{B} \cdot \nabla p = 0$, i.e., there is no pressure gradient along a field line; magnetic flux surfaces are surfaces of constant pressure. Also from eqn. 2.1, we have $\mathbf{j} \cdot \nabla p = 0$, so that current lines lie in a magnetic surface. Therefore, in equilibrium configurations, \mathbf{B} and \mathbf{j} lie on constant pressure surfaces, which if closed, appear as continuous windings of intersecting magnetic field and current lines; these are said to lie on ‘magnetic surfaces’.

Safety factor

As discussed in a tokamak, plasma is confined by a toroidal magnetic field lines. Plasma current generates poloidal magnetic field, which in combination with toroidal field lines forms helical field lines (Fig. 2.2) and keeps plasma in equilibrium. Field lines lay on nested surfaces centred on magnetic axis. These nested surfaces are termed as magnetic flux surface. In an axi-symmetric equilibrium each magnetic field line has different twisting, which is expressed by its ‘ q ’ value and termed as ‘*rotationl transform*’ or ‘*safety factor*’.

General definition of safety factor can be expressed as the pitch of the field: $q = d\phi / d\theta$, where ϕ and θ are toroidal and poloidal angle, respectively. If after change of $\Delta\phi$ toroidal

angle a field line returns to its poloidal position (i.e., after $\Delta\theta = 2\pi$) at some poloidal plane, its q -value is defined as $q = \Delta\phi / 2\pi$. In other words, safety factor is defined as number of toroidal turns in one poloidal turn.

Field lines associated with rational flux surfaces with $q = m/n$, where m and n are integers, the field line joins up on itself after m toroidal and n poloidal rotations around the torus. Rational values of q play an important role in stability. Effect of magnetic shear on mode stability and its localization at mode rational surface ($r = r_s$) is of great interest. Generally, higher value of q leads to greater stability. In tokamaks, the radial profile of q usually has its minimum value at, or close to, the magnetic axis and increases outwards. Its behaviour is determined by the toroidal current density profile $j_\phi(r)$.

2.1.2 Grad- Shafranov equation and the Shafranov shift

In studying tokamak equilibria it is convenient to introduce the stream function ψ to reduce equilibrium equations to a single partial differential equation in one unknown. The stream function is proportional to the poloidal flux function $\psi = \psi_{pol} / 2\pi$ within each surface.

In cylindrical coordinates (R, φ, z) , an axi-symmetric toroid, ($\partial/\partial\varphi = 0$), poloidal magnetic flux can be expressed in terms of the toroidal component of the vector potential A_φ alone, i.e., $\psi(R, z) = RA_\varphi$. Assuming that there is no pressure gradient along a field line, the equation for pressure balance in equilibrium is given by $\nabla p = \mathbf{j} \times \mathbf{B}$. With these assumptions ideal magnetohydrodynamic equations reduce to an elliptical partial differential equation for the poloidal magnetic flux, also known as Grad- Shafranov equation [2.1, 2.2]

$$-\mu_0 R j_\varphi = R \frac{\partial}{\partial R} \left(\frac{1}{R} \frac{\partial \psi}{\partial R} \right) + \frac{\partial^2 \psi}{\partial z^2} \quad (2.2)$$

Above equation is solved in order to reconstruct the magnetic flux surface inside an isotropic plasma.

The Shafranov shift

For low- β , large aspect ratio tokamak plasmas of nearly circular cross section when toroidal effects are included, it is seen that magnetic flux surfaces form non-concentric circles, i.e., the centers of the magnetic flux surfaces are displaced with respect to the center of the bounding surface (Fig. 2.3). This displacement is called the Shafranov shift (Δ_s). The origin

of Shafranov shift can be easily understood. Current is bent in axi-symmetric tokamak plasma. So, average value of the major radius is smaller on the inside surface than the outside surface. A given amount of poloidal flux ψ on the outside of the torus must be squeezed into a smaller cross sectional area on the inside (small r). Therefore, poloidal magnetic field at large r is smaller. Magnitude of the magnetic field is greater on the in-board side than on the out-board side and the lines are packed more closely together on the inside [2.3].

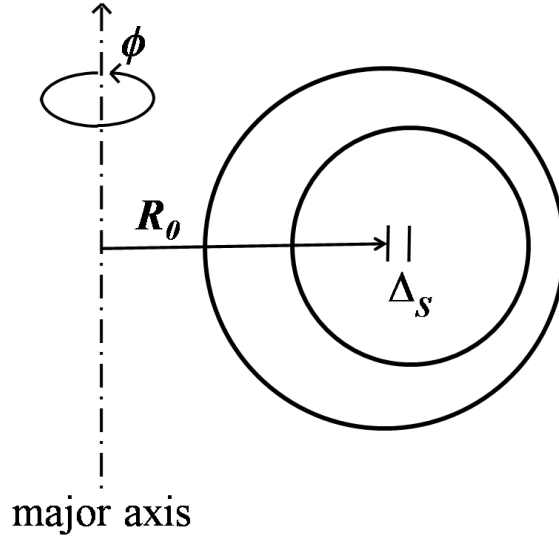


Figure 2.3. Circular flux surface is displaced by a distance (Δ_s) with respect to boundary flux surface whose centre is at a distance R_0 from the major axis. The outwards displacement (Δ_s) is known as the ‘Shafranov shift’.

Since an excessive shift will inefficiently lose the plasma either to the limiter or to the wall of the vacuum vessel, it is customary in tokamak devices to control the shift with an externally provided vertical magnetic field. The necessary vertical field to maintain the tokamak plasma in equilibrium, is given by [2.4]

$$B_V = -\frac{\mu_0 I_p}{4\pi R_0} \left(\ln \frac{8R_0}{a} + \Lambda - \frac{1}{2} \right), \quad (2.3)$$

where $I_p (= 2\pi a B_{\theta 0}(a) / \mu_0)$ is the plasma current and $\Lambda = \beta_p + \frac{l_i}{2} - 1$.

β_p , the poloidal beta, is given by $\beta_p = \frac{8\pi \langle p \rangle}{B_{\theta 0}^2}$.

The interaction of the toroidal plasma current with vertical magnetic field, B_V , pushes the plasma inwards in major radius to balance the outward forces. Necessary condition for vertical magnetic field to keep plasma in equilibrium is discussed in section 2.4.1.1.

2.1.3 Tokamak confinement

As described in the section 2.1.1, in a tokamak plasma is confined in the nested magnetic surfaces. In the zeroth order approximation, while moving along the nested surfaces, trajectories of particles on the inner surfaces do not mixed up with those on the outer surfaces. In the central region high temperature plasma is confined and separated from the cold plasma at the edge. Plasma parameters (temperature and density) gradually decrease from centre to the edge. But this inhomogeneity in the plasma brings main problem of plasma confinement. In the first approximation, plasma energy and density is lost due to temperature gradient, density gradient, electric fields and gradients in magnetic field. Particles migrate across \mathbf{B} to the walls along the gradients.

In straight cylindrical plasma diffusion understood in terms of Coulomb collisions is termed as '*classical transport*'. In classical transport particles suffer collisions with a collision frequency ν and collision allows the particle to step length equal to the Larmour radius, ρ . This gives a diffusion coefficient $D_{\perp} \sim \nu \rho^2$ and hence diffusion coefficient across the magnetic field scaled as $1/B^2$. To keep the distinction clear, the collisional transport in a toroidal geometry is termed as '*neoclassical transport*'. In toroidal plasma, transport fluxes enhance above the straight cylinder geometry because of internal convective flows and loss of poloidal symmetry because the toroidal field is stronger on the inside than on the outside of the torus.

Based upon the collisionality tokamak plasma can be differentiate in three regimes: (1) banana regime, (2) Pfirsch-Schluter regime and (3) plateau regime.

In collisionless regime trapped particles exist in the weaker region of the tokamak magnetic field due to inhomogeneity of magnetic field and average time between collisions is long compared to the time required for a particle to complete a banana orbit and plasma is said to be in a *banana regime*. Thus in banana regime effective collision frequency is smaller than the bounce frequency: $\nu < \epsilon^{3/2} \nu_{th} / Rq$.

If the time between collisions is less than the time required for a particle to complete an untrapped orbit, then the form of the trapped orbit cannot be relevant to the diffusion process and the plasma is in *collisional regime*: $\nu > \epsilon^{3/2} \nu_{th} / Rq$. In the collisional regime, particles

move along the field lines between collisions. The transport in highly collisional fluid regime is called *Pfirsch-Schluter* transport.

The regime of intermediate collisionality, connecting low collisional banana regime to the highly collisional Pfirsch-Schluter regime is called *plateau regime* ($\varepsilon^{3/2} v_{th} / Rq < \nu < v_{th} / Rq$). In this regime diffusion coefficient has no dependence on the collision frequency.

The measured values of transport across the magnetic field in tokamaks often exceeds the predicted values calculated using the classical or the neo-classical theories. These enhanced losses are termed as *anomalous transport*. The anomalous transport in plasma is believed to arise from turbulent diffusion caused by electrostatic or electromagnetic fluctuations caused by micro-instabilities.

Confinement of plasmas is among the most important subjects in fusion research. To achieve thermonuclear conditions the plasma in a tokamak has to be confined for sufficient time. The energy confinement time is defined as the ratio of plasma energy content to the plasma energy loss rate. The energy confinement time is usually defined via the energy balance equation as

$$\frac{dW_p}{dt} = P_{in} - \frac{W_p}{\tau_E}, \quad (2.4)$$

where W_p is the total plasma energy and P_{in} is the power supplied to the plasma.

Experiments have revealed that the energy confinement time turns out to be strongly dependent on the plasma temperature. High temperature plasmas are generated by use of the intense heating. The confinement behaviour can be conveniently put into three categories. The first covers Ohmically heated plasmas and the other two relate to plasmas with additional heating. These two basic modes of auxiliary heated plasma confinement are the so-called L (for low) and H (for high) confinement regimes. The scaling laws for Ohmically heated plasmas and those for externally heated plasmas are summarized in Table 2.1 and 2.2.

2.1.4 Heating

Plasma heating is essential problem in controlled fusion. In tokamak plasma the energy losses are balanced by the plasma heating. Fusion reaction rate is strong function of temperature and is negligible at low temperatures. Thus, to reach the temperature required for ignition it is necessary to provide some form of heating. Neutral beam injection (NBI) and radio-frequency heating (RFH) are commonly used for additional heating task.

Scaling law	$\tau_E [s]$
Intor scaling	$5 \times 10^{-21} \bar{n}_e a^2$
Neo-Alcator	$7 \times 10^{-22} \bar{n}_e a R^2 q_a^{1/2}$
Merezhkin-Mukhovatov	$3.5 \times 10^{-21} \bar{n}_e a^{0.25} R^{2.75} T(eV)^{-0.5} q_a$
Goldston [2.5]	$7.1 \times 10^{-22} n_e [cm^{-3}] a^{1.04} [cm] R^{2.04} [cm] q^{0.5}$

Table 2.1. Scaling laws for Ohmic plasmas

Scaling law	$\tau_E [s]$
Goldston (L-mode) [2.5]	$6.4 \times 10^{-8} \kappa^{0.50} I_P [A] P_{heat}^{-0.50} [W] a^{-0.37} [cm] R^{1.75} [cm]$
Kaye-Goldston (L-mode) [2.6]	$2.77 \times 10^{-8} \kappa^{0.28} I_P^{1.24} [kA] B_\phi^{-0.09} [T] n_e^{0.26} [10^{23} cm^{-3}]$ $P_{heat}^{-0.58} [MW] a^{-0.49} [cm] R^{1.65} [cm]$
ITER89P (L-mode) [2.7]	$0.048 M^{0.5} \kappa^{0.5} I_P^{0.85} [MA] B_\phi^{0.2} [T] n_e^{0.1} [10^{20} m^{-3}]$ $P_{heat}^{-0.5} [MW] a^{0.3} [m] R^{1.2} [m]$
ITER98y, 2 [2.8] (H-mode)	$0.0562 M^{0.19} \kappa_a^{0.78} I_P^{0.93} [MA] B_\phi^{0.15} [T] n_e^{0.41} [10^{19} m^{-3}]$ $P_L^{-0.69} [MW] a^{0.58} [m] R^{1.39} [m]$
McDonald-Cordey-Thomsen (H-mode) [2.9]	$0.0593 M^{0.08} \kappa_a^{0.84} I_P^{0.86} [MA] B_\phi^{0.21} [T] n_e^{0.39} [10^{19} m^{-3}]$ $P_L^{-0.69} [MW] a^{0.68} [m] R^{1.31} [m]$

Table 2.2. Scaling laws for auxiliary heated L-mode and H-mode plasmas**Neutral injection heating**

The concept of neutral injection as a heating technique is the most successful to date. In this technique high energy neutrals are injected into magnetically confined plasma as they are unaffected by the confining fields. These neutrals are converted into ions inside the plasma. The fast ions that result are then slowed down by Coulomb collisions, transferring most of their energy to the plasma particles if they are confined long enough, causing heating of both electrons and ions. Since heating the center of the plasma is desirable, injection of neutrals normal to the field lines is generally preferred, distance of penetration of a neutral beam into plasma before “ionization” increases with the energy of the beam particles.

Radio frequency heating

Since the collisional process scales as $T_e^{-3/2}$, plasma heating by the direct collisional mechanism saturates with temperature and becomes weak in high temperature plasmas. Electromagnetic waves in plasmas are subject to resonant absorption which is collisionless process and produces strong heating. Radio frequency heating transfers energy from an external source to the plasma by means of electromagnetic waves. When an electromagnetic wave propagates through plasma the electric field of the wave accelerates the plasma ions and electrons which then heat the plasma through collisions. Because of the nonuniform magnetic field and density in most plasmas, the non-collisional absorption of energy of electromagnetic waves in a magnetized plasma is allowed at variety of resonance frequencies by many different radio frequency heating schemes. However, all these schemes consist of the same general layout, namely, an efficient high power generator remote from the plasma, a low-loss transmission line and an efficient antenna which couples the electromagnetic energy to the plasma.

Radio frequency heating has been used to heat magnetically confined plasmas since the early days of fusion research. Three schemes have emerged as the most successful, namely, ion cyclotron, lower hybrid and electron cyclotron heating.

Ion Cyclotron Resonance Heating ($\nu \sim 50\text{MHz}$)

In a tokamak, the toroidal field falls off with major radius as R^{-1} and the ion cyclotron resonance is localized at a value of R for which the wave frequency, ω , satisfies $\omega = \omega_{ci}(R)$. Ion cyclotron heating in tokamaks is accomplished by launching a fast magnetosonic (compressional Alfvén) wave to transport energy from the antenna to the absorption region of plasma, where $\omega_{pe}^2 / \Omega_e^2 \leq 1$ and $\omega_{pi}^2 / \Omega_i^2 \geq 1$.

Lower Hybrid Resonance Heating (LHRH) ($\nu \sim 1-8\text{GHz}$)

In dense plasmas of interest, $\omega_{pi} \gg \omega_{ci}$, and the lower hybrid resonance frequency is then given to a good approximation by $\omega_{LH} = \omega_{pi} / \sqrt{(1 + \omega_{pe}^2 / \omega_{ce}^2)}$, which lies typically in the range about 1-8GHz. The use of lower hybrid waves was originally proposed with the object of heating the ions. For this purpose it is essential to choose conditions such that the lower hybrid resonance occurs in the plasma. The condition for this is

$$n_{res} = \frac{2.3 \times 10^{19} A_i f^2}{(1 - 2.3 A_i f^2 / B_0^2)} m^{-3} \quad (f \text{ is in GHz}), \quad (2.5)$$

where n_{res} is the electron density at the lower hybrid resonance, A_i is the atomic mass number of the ions, f is the frequency, and B_0 is the magnetic field.

Electron Cyclotron Resonance Heating (ECRH) ($\nu \sim 50 - 200 \text{GHz}$)

Since $\Omega_e \geq \omega_{pe} \gg \omega_{pi}$, only the electrons can respond to waves in the 50 GHz to 200 GHz ECRH frequency range, but ion heating can result from collisional energy transfer from the heated electrons. Electron cyclotron heating has been made possible by the invention of the gyrotron millimetre wave source. When the source frequency is comparable to the electron gyro-frequency or its harmonics, then cyclotron damping by electrons can take place when the resonance condition is satisfied. Because of the variation in the tokamak magnetic field with major radius, R , this limits the spatial extent of the resonance region. Because extremely high frequencies employed, electromagnetic waves propagate freely into the plasma until quite high densities are reached and power can be fed simply and efficiently to the plasma from wave-guides.

2.1.5 Instabilities

MHD instabilities and low-frequency micro-instabilities of magnetically confined plasmas are two important areas of modern plasma physics research. Tokamaks are subject to a variety of macroscopic instabilities. These strong instabilities are mainly MHD modes and arise from (1) *current gradients* and (2) *pressure gradients* in combination with *adverse magnetic field curvature*. The resulting instabilities are divided into two categories: (i) *Ideal modes*- Instabilities which would occur even if the plasma were perfectly conducting, and (ii) *Resistive modes*- which are dependent on the finite resistivity of the plasma.

Instabilities in which wavelength of the fluctuations is comparable to the ion Larmor radius are termed as micro-instabilities. Fine scale plasma turbulence can be explained by micro-instabilities. Therefore, these are important for understanding plasma turbulence.

In confined plasma there are processes by means of which the plasma evolves towards a state of lower free energy. In this process free energy is converted into kinetic energy to drive instabilities. The generalized energy conservation relation from the linearized MHD equations is given by

$$\begin{aligned} \frac{\partial}{\partial t} \int \left(\frac{1}{2} \rho_0 \mathbf{V} \cdot \mathbf{V} + \frac{\mathbf{B} \cdot \mathbf{B}}{8\pi} + \frac{1}{2} \frac{\mathbf{J}_0}{c} \cdot (\boldsymbol{\xi} \times \mathbf{B}) + \frac{1}{2} \mathcal{P}_0 (\nabla \cdot \boldsymbol{\xi})^2 + \frac{1}{2} (\boldsymbol{\xi} \cdot \nabla p_0) (\nabla \cdot \boldsymbol{\xi}) \right) d^3r \\ + \oint \left(\frac{c}{4n} \mathbf{E} \times \mathbf{B} + p\mathbf{V} \right) \cdot d\mathbf{S} = 0 \end{aligned} \quad (2.6)$$

for a plasma in which the pressure is isotropic and bounded by a rigid, perfectly conducting wall, where the boundary conditions are:

$$\hat{\mathbf{n}} \cdot \mathbf{V} = 0 \quad \hat{\mathbf{n}} \times \mathbf{E} = 0 \quad \hat{\mathbf{n}} \cdot \frac{\partial \mathbf{B}}{\partial t} = 0, \quad (2.7)$$

where $\hat{\mathbf{n}}$ is the unit normal to the boundary, \mathbf{V} is fluid velocity, $\boldsymbol{\xi}$ is linear displacement vector defined by $\frac{d\boldsymbol{\xi}}{dt} = \mathbf{V}$, $d\mathbf{S} \equiv \hat{\mathbf{n}}dS$ and S is the surface bounding the volume of integration.

Under boundary conditions (2.7) surface integral vanishes and eqn 2.6 reduces to

$$\frac{\partial}{\partial t} (K + \delta W) = 0, \quad (2.8)$$

where $K \equiv \int \frac{1}{2} \rho_0 \mathbf{V} \cdot \mathbf{V} dV$ is the total kinetic energy of the plasma. δW is identified as the potential energy of the perturbation and given by

$$\delta W = \int \left(\frac{\mathbf{B} \cdot \mathbf{B}}{8\pi} + \frac{1}{2} \frac{\mathbf{J}_0}{c} \cdot (\boldsymbol{\xi} \times \mathbf{B}) + \frac{1}{2} \mathcal{P}_0 (\nabla \cdot \boldsymbol{\xi})^2 + \frac{1}{2} (\boldsymbol{\xi} \cdot \nabla) p_0 (\nabla \cdot \boldsymbol{\xi}) \right) d^3r \quad (2.9)$$

A number of conclusions can be drawn from equation for the conservation of energy (eqn. 2.8). Since we have assumed that there is no flow without perturbation in equilibrium, it follows that K is always positive definite. From the definition of instability K increases unboundedly in time. If $\delta W > 0$, system must be absolutely stable. In order to have instability, $\delta W < 0$ such that $|\delta W|$ grows in time so as to balance exactly the increase in K .

Equation 2.9 shows that the energy required to perturb the equilibrium magnetic field (either field line bending or compression) is positive definite and therefore stabilizing. The third term is also positive definite so that incompressible perturbations may be expected to be the most unstable. The second and fourth terms are potentially destabilizing ones. The driving mechanism in the second term is due to the equilibrium current and in the fourth term is due to the equilibrium pressure gradient.

With some algebraic manipulations equation 2.9 can be derived into following form

$$\delta W = \frac{1}{2} \int d^3r \left(\frac{1}{4\pi} |\mathbf{B}_\perp|^2 + 4\pi \left| \frac{\mathbf{B}_\parallel}{4\pi} - \frac{\mathbf{B}_0 \boldsymbol{\xi} \cdot \nabla p_0}{B_0^2} \right|^2 + \mathcal{P}_0 |\nabla \cdot \boldsymbol{\xi}|^2 + \frac{\mathbf{J}_0 \cdot \mathbf{B}_0}{|\mathbf{B}_0|^2} \mathbf{B}_0 \times \boldsymbol{\xi} \cdot \mathbf{B} - 2\boldsymbol{\xi} \cdot \nabla p_0 \boldsymbol{\xi} \cdot \boldsymbol{\kappa} \right)$$

(2.10)

where \perp and \parallel denote components of \mathbf{B} perpendicular and parallel to \mathbf{B}_0 , κ is the normal field line curvature, $\kappa = \hat{\mathbf{B}} \cdot \nabla \hat{\mathbf{B}}$, where $\hat{\mathbf{B}}$ is a normal vector parallel to \mathbf{B}_0 . In equation (2.10), first three terms are always positive and are the energies associated with the shear Alfvén, magneto-sonic and sound waves. The fourth term is the energy – driving kink modes and is created by the presence of the plasma current. This term can be negative. The fifth term is the energy – driving interchange modes. It can be negative if the curvature is in the same direction as the pressure gradient. If the pressure gradient is anti-parallel to κ , the last term is always positive.

From the above discussion it is quite clear that the instabilities in tokamak plasma are mainly attributes of equilibrium toroidal current and equilibrium pressure gradient. At high β they start to interact but at low β they can be studied separately.

Instabilities due to magnetic energy of plasma current

Gradient in toroidal current drives instabilities in tokamak plasmas. These instabilities grow at rational surfaces where helicity of the perturbation matches with that of the magnetic field. These MHD instabilities may be ideal or resistive. Kink instability is a strong ideal MHD instability. Kink instability with low mode number is driven by radial gradient of the toroidal current density. It is so named because it leads to the kinking of the magnetic surfaces and the plasma boundary. Tearing modes are also driven by radial gradient of the equilibrium toroidal current density. These modes grow at rational surfaces due to tearing and rejoining of magnetic field lines as consequence of finite resistivity.

Instabilities due to pressure gradient

High- n modes tend to be strongly stabilized by the energy required to perturb the magnetic field. A necessary condition for the stability for a large aspect ratio tokamak of circular cross-section was given by Mercier criterion

$$\frac{rB_\phi^2}{8\mu_0} \left(\frac{q'}{q} \right)^2 > (-p')(1 - q^2) \quad (2.11)$$

The term $p'q^2$ represents the stabilizing contribution of the average curvature of the toroidal magnetic field. For $q > 1$ this is sufficiently large that the resultant curvature is good and a negative pressure gradient is stabilizing.

In the usual case with $(dp/dr) < 0$, both the pressure gradient and shear term are stabilizing if $q(r) > 1$. For toroidal current density distributions that peak at the centre of the plasma and decrease with minor radius, r , the safety factor, $q(r)$, increases with r . Thus, $q(0) > 1$ is sufficient to ensure the stability of localized, high- m interchange modes, as long as $(dp/dr) < 0$.

At sufficiently large values of the plasma pressure, the pressure gradient may become large enough in regions of bad curvature in a tokamak to produce “ballooning” instability. The deformation is flutelike and is larger on the outside of the torus. This deformation bends the field lines, which provides a restoring force. If the driving force, which is proportional to the product of the pressure gradient and the curvature (inverse major radius), is greater than the restoring force due to the resistance of the field lines to bending, then these ballooning modes will limit the achievable plasma pressure.

Non-linear instabilities

These instabilities are not fully understood but they can be attributed to identifiable MHD modes. The three major types of non-linear activities related to the MHD perturbations are Mirnov oscillations, Sawtooth oscillations and Disruptions.

Mirnov Oscillations

There are small magnetic fluctuations, which can be detected by placing magnetic pick-up loops just outside the plasma. These magnetic oscillations are observed as the island passes under the pick-up loop at the drift frequency (typically 1-20kHz). These small oscillating helical perturbations in the poloidal magnetic field can be separated into their Fourier components around the plasma in poloidal direction.

Sawtooth oscillations

Observations of x-rays emitted from the centre of the plasma often reveal oscillations, having a period of the order of the millisecond. The emission increases slowly through most of this period and falls back rapidly. X-rays observed from the outer part of the plasma have the inverse profile, a slow decay being followed by a rapid rise. The interpretation of these oscillations is that there is a tendency of tokamak plasma to a unstable concentration of current in the central, hotter region. As a result of this the axial current density j_0 rises. Thus for sufficiently large j_0 , q_0 falls below unity and a $q = 1$ surface appears. The presence of

$q = 1$ surface now allows $m = 1$ instability to occur, producing a magnetic island. The value of q on this island is larger than unity.

Disruption

The most serious problem caused by magnetic islands is the major disruption. Disruption is sudden and complete loss of plasma confinement and a collapse of the plasma current, which result in large electromagnetic and pressure forces in the surrounding structure. These generally occur at the sufficiently high plasma density or high plasma current.

One mechanism for the disruption is nonlinear coupling of two islands which generate a large stochastic magnetic region within the plasma volume destroying the plasma confinement. Magnetic islands, when uncoupled or only loosely coupled to each other, grow on a time scale of milliseconds. This growth rate is too slow to explain the sudden nature of the hard disruption which happens on a microsecond time scale. If, however, two magnetic islands of different helicity were to grow and overlap, the resulting region engulfed by the islands may explosively grow into a stochastic magnetic region of poor confinement, and if the initial islands were large enough, a large percentage of the plasma confinement would be destroyed thus terminating the discharge.

2.2 Resistive tearing instability

Plasma instabilities may be divided into two general categories: magneto-hydrodynamic (MHD) and kinetic instabilities. The former may pose the most stringent limitations to plasma performance and detrimental effects on plasma confinement, and are described by a magneto-hydrodynamic model of the plasma. Instability drive may arise predominantly from plasma current or pressure gradients.

The poloidal field magnetic energy excites the helical instabilities owing to the helical perturbations. Perturbations may be decomposed into different modes. A growing perturbation increases the internal energy of the plasma. If all of them are stable in the plasma, they will attenuate and the perturbation will vanish. On the contrary, if some modes are unstable, they will grow in time. Perturbation having a form $\exp(im\theta - in\phi)$, is periodic in θ and ϕ angles and represents a sum of harmonics, where m and n are integers. This perturbation is called the m/n mode. m and n specify the poloidal and toroidal mode numbers, respectively. As discussed in Section 2.1.1, in a tokamak device, along different flux surfaces, the ratio between the poloidal and toroidal magnetic fields changes. Each field

line is defined as function $q = m/n$. In general modes of greatest interest and importance are those whose perturbation structure lies along the direction of the magnetic field lines somewhere inside the plasma. Around these magnetic surfaces the pitch of the perturbation matches to that of the magnetic field. They are then said to be resonant at that point, and if they possess a field component perpendicular to the equilibrium magnetic surfaces, they will cause the field topology to change and thereby the formation of magnetic islands.

2.2.1 Ideal and resistive instabilities

Plasma instabilities that occur when resistivity (η) is null are called ideal instabilities. In ideal MHD theory unstable modes are expected to be evolve in a very fast Alfvén time scale ($\tau_A = \sqrt{\mu_0 \rho a} / B$), where ρ is the plasma density, B is the magnitude of the magnetic field, and μ_0 the magnetic permeability of vacuum.

In an ideal plasma with zero electrical resistivity, taking into account Ohm's law $\mathbf{E} + \mathbf{v} \times \mathbf{B} = 0$,

$$(2.12)$$

the evolution of the magnetic field is governed by the following equation:

$$\frac{\partial \mathbf{B}}{\partial t} = \nabla \times (\mathbf{v} \times \mathbf{B}), \quad (2.13)$$

where \mathbf{v} is the plasma flow, \mathbf{B} is the magnetic field, \mathbf{E} is the electric field. Eqn. 2.13 equation describes the convection of the magnetic field with the plasma flow. The significance of above equation is that in the absence of resistivity, magnetic flux is *frozen* to the plasma fluid. This frozen flux relation implies that magnetic flux through an arbitrary surface that moves with the plasma fluid is constant, that is, the topology of the magnetic surfaces does not change and island formation is inhibited.

In a resistive-MHD plasma, taking into account Ohm's law

$$\mathbf{E} + \mathbf{v} \times \mathbf{B} = \eta \mathbf{j}, \quad (2.14)$$

the time variation of the magnetic field is given by

$$\frac{\partial \mathbf{B}}{\partial t} = \nabla \times (\mathbf{v} \times \mathbf{B}) + \frac{\eta}{\mu_0} \nabla^2 \mathbf{B} \quad (2.15)$$

The first term in the RHS describes the convection of the magnetic field with the plasma flow, i.e., *frozen in* condition of magnetic field lines with the fluid. The second term (known as diffusive or inertial term) in the RHS is the resistive diffusion of the field across the plasma, i.e., resistivity allows the plasma to diffuse relative to the magnetic field lines. The

rate at which the magnetic field lines diffuse through the plasma is proportional to the plasma resistivity, gives rise to another time scale defined by $\tau_r = \mu_0 a^2 / \eta$ (resistive diffusion time). Validity of the ideal MHD approximation is expressed in terms of the magnetic Reynolds number or *Lundquist number* (S), which is the ratio of Alfvén transit time and resistive diffusion time. Ideal instabilities grow in Alfvén transit time (τ_A) typically measured in micro-seconds for tokamaks, whereas, resistive diffusion time (τ_r) in seconds. Resistive tearing instabilities grow on time-scales that are intermediate between the very short MHD time-scale, τ_A , and the very long resistive time-scale, τ_r . These modes grow faster than the resistive diffusion time scale ($\tau_r = \mu_0 a^2 / \eta$) but slower than the Alfvén time scale.

2.2.2 Tearing modes

If Reynolds number (S) is small then the diffusive (inertial) term becomes important and the magnetic field lines can move through the plasma and even tear and reconnect to form a completely new topology. Because the magnetic Reynolds number is very high for normal tokamak operation, one could say that the motion conforms to ideal MHD. There are certain thin layers (*tearing layer*) within a tokamak plasma that have very short system length scales and a small S value, which means that resistivity is important to consider and that magnetic reconnection can become favourable. Because of this, these regions can become susceptible to the growth of a type of resistive plasma instability called a neoclassical tearing mode (NTM).

The non-zero η in the resistive layer allows magnetic field lines to "tear" or break and reconnect across a closed magnetic field line at rational surface which supports a resonant perturbation, via a finite value of B_r to form a new and different magnetic configuration, called magnetic islands. A magnetic island is characterized by its helicity number and its width. The helicity numbers, which are the m and n numbers indicate the island location and with what magnetic surface it interacts with. The relationship between the m and n numbers is $nq - m = 0$.

Radial magnetic field perturbation is needed to produce magnetic islands or to change it in time. The width of the island is defined as the maximum radial width across the island region in the poloidal plane. It is approximately

$$w = \sqrt{\frac{r_s L_s \tilde{B}_{rs}}{m B_z}}, \quad (2.16)$$

where r_s is the radius of the resonant surface, \tilde{B}_{rs} is the perturbed radial magnetic field, and $L_s = q^2 R_0 / q' r_s$, both evaluated at the rational surface of the mode.

The major effect of magnetic islands is enhanced transport. Since the islands have a width, they provide a transport short circuit by the destruction of closed magnetic surfaces. Magnetic islands cause the flattening of the temperature and the density profiles in the plasma interior. When islands of different helicity overlap a stochastic magnetic field region is produced. This results in a region with no confinement since the particles will traverse this region on a time scale of the thermal velocities, rather than the diffusion time scale. During the tokamak discharge, there occur sawtooth oscillations and Mirnov oscillations and disruptions, which are understood to be due to tearing modes.

2.2.3 Growth of tearing modes

The linear stability analysis of the tearing mode was originally given by Furth et al [2.10], which is based on the boundary layer theory around the rational surface. The growth rate of the linear tearing mode is obtained by matching the ideal MHD solution for the outer layer and the resistive MHD solution for the inner layer.

In resistive MHD, tearing mode stability is determined by parameter ‘stability index, Δ' ’, which is defined as the discontinuity in the radial magnetic field perturbation across the rational surface (r_s):

$$\Delta' \equiv (\tilde{\psi}'_{r_s + \varepsilon} - \tilde{\psi}'_{r_s - \varepsilon}) / (a \tilde{\psi}(r_s)), \text{ where } \varepsilon \rightarrow 0 \quad (2.17)$$

A positive Δ' implies instability. Its value is related to the growth rate of the mode by:

$$\gamma \approx 0.55 \tau_R^{-3/5} \tau_A^{-2/5} (\Delta' a)^{4/5} \left(\frac{a}{R} n \frac{aq'}{q} \right)^{2/5} \quad (2.18)$$

where γ is the growth rate of the mode, q' is the radial derivative of q , and n refers to the mode number (m, n). The expression above shows that the development of the instability takes place in a hybrid time scale, faster than the resistive diffusion time scale but slower than the Alfvén time scale.

2.2.4 Linear and non-linear tearing mode growth

As long as the island width is much smaller than the resistive boundary layer thickness, island grows exponentially. The mechanism for saturation of mode growth can be explained as follows [2.11]:

As the perturbation on \mathbf{B} diffuses around the resonant surface, a similar diffusion occurs for the perturbation on \mathbf{j} . The cross product of the former with the equilibrium current density promotes the occurrence of a perturbation in the fluid velocity field. The convection caused by the perturbation of velocity causes an increase in the magnetic field and its perturbation. In turn, the increase in the magnetic perturbation will generate an increase in the velocity perturbation. This process will account for an exponential growth in the early development of the perturbation.

Rutherford [2.12] showed that when the magnetic island width grows to be as large as the boundary layer width, a new force becomes important and the growth rate of the instability is greatly reduced and finally the island width saturates. Instead of growing like an exponential function in time, the island width starts to grow like a linear function in time. At this time, the growth of the island is related to Δ' by

$$\frac{dW}{dt} = 1.66\Delta' \frac{\eta}{\mu_0} \left[1 - \frac{W}{W_s} \right] \quad (2.19)$$

where W is the island width, and W_s is the saturation island width.

2.2.5 Effect of sheared flows on growth of tearing modes

Shear flow has significant influence on tearing modes by changing the value of stability index Δ' . In the case when flow shear is very small inertial term dominate the convection term. When flow shear is larger than the magnetic field shear the convection term overtakes the inertial term, kinetic energy overpowers the magnetic energy and growth rate of mode is changed. In this case the flow freezes the magnetic field and suppresses the tearing instability. An explanation for stabilizing effect of magnetic shear and flow shear on tearing mode instability was presented by La Haye [2.13], which says that-

Magnetic shear (with no flow shear) varies the field line pitch with q increasing with major radius. Thus the singularity at the rational surface is limited in radial extent. The resonant condition $(1 - nq/m)$ becomes $-(r - r_s)/L_q$ (L_q is the magnetic shear length $q/(dq/dr)$ and r_s is radial location of rational surface), which makes tearing "harder", i.e., it takes more energy to bend field lines, and this makes the linear classical Δ' more negative, i.e., more stable. When flow shear is added, the island is distorted as shown in Fig. 2.4 due to the viscous drag of a sheared flow and the flow shear provides an additional means to limit the radial extent of the resonance.

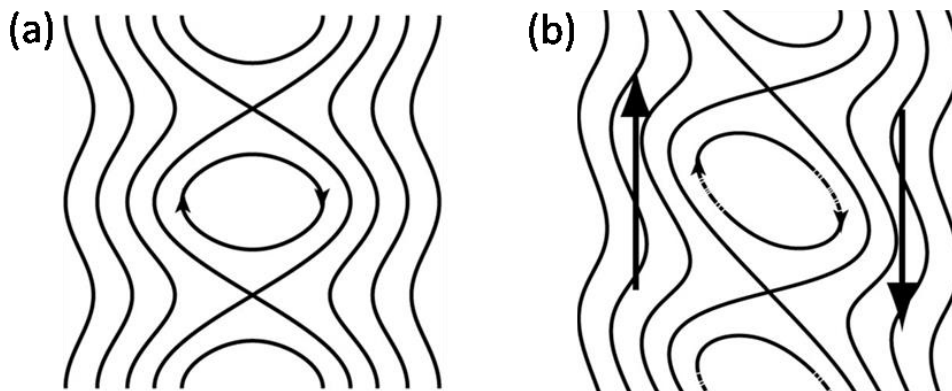


Figure 2.4. (a) Magnetic island with magnetic shear with no flow shear and q increasing with major radius R . (b) Magnetic island with flow shear added.

2.3 Disruptions in tokamak

Tokamak plasma can last up to hours within some operational limits. Beyond these limits major plasma instabilities result termination of discharge on the millisecond timescale, known as disruption. Plasma density, current and pressure are limited by MHD instabilities and any attempt to raise these parameters above the stable value ends in a disruption. Disruption is preceded by growth of MHD modes, which destroy magnetic flux surfaces creating magnetic field lines, which fill the whole plasma in a stochastic manner. As a consequence of the ergodicity of the magnetic field the plasma energy confinement is lost. This phase is called thermal quench and is followed by the increase of the plasma resistivity and by the Ohmic dissipation of the plasma current. A disruption causes the loss of significant thermal loads and mechanical forces on the plasma facing components and therefore must be avoided.

2.3.1 Causes of disruptions

There are several identified causes of disruptions. Operating limits for steady operation are imposed by both low- q disruptions and density limit disruptions. These are thought to be due to unstable current profiles which lead to large amplitude tearing modes. These two operational limits can be combined in a diagram which was found by Hugill [2.14]. In this diagram (Fig. 2.5) the boundary of operation as limited by disruptions is plotted against $1/q_a$ and Murakami parameter $(\bar{n}R/B_\phi)$ [2.15].

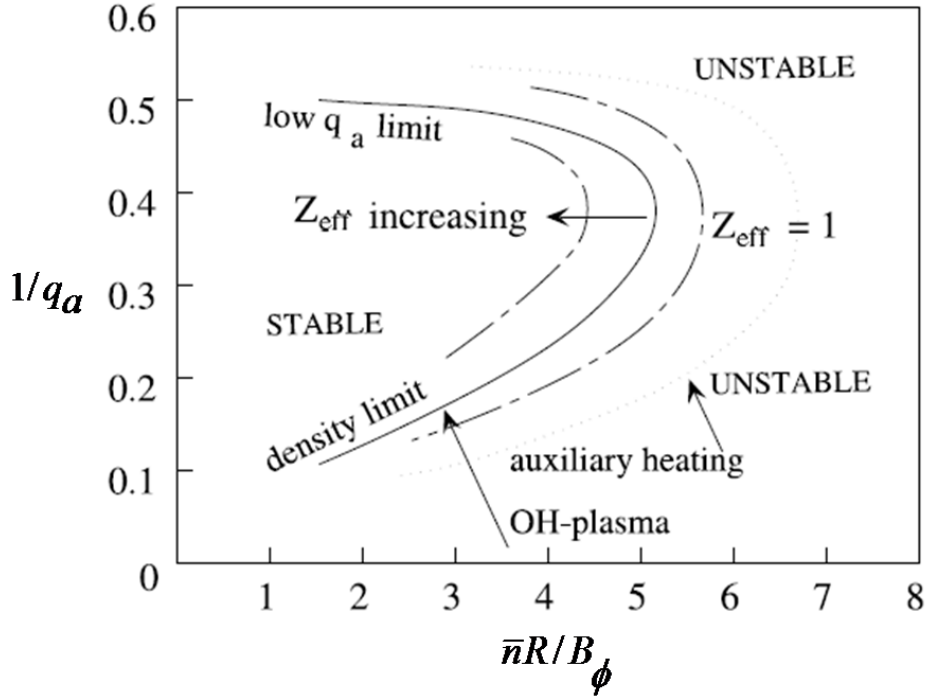


Figure 2.5. Hugill diagram shows limitation of stable operational regime of the tokamak in a region of (q_a, \bar{n}) space, where q_a denotes the safety factor at the edge of the plasma and \bar{n} denotes the mean electron density. In this diagram operating regime is shown as a function of $1/q_a$, which is proportional to plasma current (I_P), and of the Murakami parameter $\bar{n}R/B_\phi$. ‘low- q disruptions’ and ‘density limit disruptions’ limit this region. Operating regime is reduced for contaminated OH-plasmas and extended beyond the $Z_{\text{eff}} = 1$ boundary when auxiliary heating is employed.

Density limit disruptions

The plasma density achievable in a tokamak is roughly proportional to the toroidal current density. Highest achievable density for a stable tokamak operation is known as ‘density or Murakami limit’ [2.15]. Above this critical plasma density disruptions occur. An empirical formula for this critical density in tokamaks is

$$\bar{n}_{\text{crit}} \approx 10^{20} B_\phi A_i^{1/2} / q_a Z_{\text{eff}} R_0 (m^{-3}), \quad (2.20)$$

where $A_i = (\text{ion mass})/(\text{proton mass})$ [2.16]. Attempt of increasing the density with gas puffing leads to further cooling of cold high density plasma edge due to rise of radiation. Cooling is more localized on the high field side, which is called MARFE (multifaceted asymmetric radiation from the edge). In this process resistivity increases at the edge, the toroidal current contracts and leads to steepening the profile. In this scenario peaked current

profile may develop tearing modes on rational flux surfaces, which form magnetic islands. These islands grow and trigger major disruption. The cooling of the edge plasma, i.e., the shrinkage of the temperature profile can be postponed by additional heating hence shifting the density limit to higher values.

Low- q disruptions

High β plasmas can be achieved either by increasing the plasma current or by decreasing the external magnetic fields. In both the cases when $q_a = 2$ approaches at the plasma boundary and $q_0 \leq 1$, the $m/n=2/1$ tearing mode, driven to large amplitude at the $q(r) = 2$ surface, alters $J_r(r)$ so that neighbouring modes (3/2) or (5/3) also become destabilized and island overlap and field line becomes stochastic, magnetic flux surfaces are destroyed, particles flowing along magnetic field lines cross through the entire region and confinement is spoiled, leading to plasma disruption.

When the plasma current is concentrated along the plasma centre, then $q(0)$ at the centre becomes less than 1 even if q_a is much larger than 1. It has been observed that the tearing mode grows at the rational surface $q_a = 1$ and triggers disruptive instability.

Beta limit or ballooning modes limit disruptions

Ballooning modes are pressure- driven instabilities. These are local bulges in the plasma surfaces. These are high-mode-number interchange modes. Plasma flux surfaces bulges out due to the ballooning instabilities created by the high plasma pressure at the place where the curvature of magnetic fields are worst, such as at the tips of a vertically elongated plasma. These instabilities lead to disruptions and hence set upper limit to the plasma pressure or plasma beta for stable tokamak operation.

Stability against ballooning depends upon the magnitude of the curvature and on the connection length, which are related to q and R_0/a . For circular plasma in an axisymmetric torus, a simplified theoretical estimate is $\beta \leq a/R_0 q^2$ for stability.

2.4 ADITYA Tokamak

ADITYA is a medium size tokamak [2.17, 2.18]. This is a poloidal limiter tokamak with circular cross-section plasma and with air core transformer. It has minor radius $a = 25\text{cm}$ and major radius $R = 75\text{cm}$. ADITYA design parameters are listed in Table 2.3.

Design Parameters	Design value
Major radius; R	75cm
Minor radius; a	25cm
Toroidal magnetic field; B_ϕ	1.5T
Plasma current; I_p	250kA
Edge safety factor; q_a	2.5
Central electron temperature; T_{eo}	400eV
Length of the pulse duration	300 ms

Table 2.3. Design parameters of ADITYA tokamak

2.4.1 ADITYA tokamak subsystems

Major subsystems of ADITYA tokamak are: magnetic coils, vacuum vessel, pumping systems, gas puff systems, wall conditioning systems, limiters, pulsed power system and data acquisition and control system.

2.4.1.1 Magnetic coils in ADITYA

In a tokamak electromagnetic coils are used to produce magnetic field for various purposes. Ohmic heating (OH) power generates the transformer flux that produces and heat the plasma. Toroidal magnetic field (B_ϕ) confines the plasma and vertical or equilibrium field keeps the plasma in an equilibrium position.

Ohmic Transformer (OT or TR) coils

In a tokamak plasma current is generated by the transformer action. Ohmic transformer initiates plasma discharge and drive plasma current. Plasma currents forms poloidal magnetic field (B_θ) and heats plasma Ohmically. In ADITYA in this set of coils central solenoid TR1, which acts as primary of transformer produces total flux swing $V_{Loop} \times \Delta t \sim 1.2V\text{-sec}$ required to produce and maintain plasma current $I_p \sim 250kA$ for a duration $\sim 300ms$. Stray fields produced by TR1 in the plasma region are minimised by compensating coils TR2, TR3, TR4 and TR5. Vertical cross-section of OT (or TR) coils is shown in Fig. 2.7.

Toroidal Field (TF) coils

Toroidal magnetic field causes charged particles to spiral around field lines. Plasma particles are lost to the vessel walls only by relatively slow diffusion across the field lines. Toroidal magnetic field is produced by 20 numbers of equidistant rectangular coils. These coils are designed to generate a magnetic field of 1.5T at the plasma centre. Discreteness of coils causes <2.5% ripple in toroidal magnetic field. Vertical cross-section of TF coils is shown in Fig. 2.7.

Vertical Field (B_V) Coils

Under the uniform plasma kinetic pressure and non-uniform magnetic field pressure on a flux surface plasma current ring expands as net pressure is stronger at the in-board side than on the out-board side. It is necessary to eliminate this net force by adding a vertical field. This radially outward directed force on the plasma is balanced by vertical magnetic field generated by quadrupole of poloidal magnetic field. Necessity of vertical magnetic field (B_V) coils can be explained by following argument.

Stability relative to displacement along the axis of symmetry (\hat{z})

With a purely vertical dipole magnetic field, $B_V = B_z$, the plasma is neutrally stable relative to its displacement along vertical direction (\hat{z}). However, if the line of force of the confining field are slightly concave towards the major axis (Fig. 2.6) and $\mathbf{B}_V = B_z + B_R$, then the accidental displacement in vertical direction is opposed by restoring force $F \sim I_p \times B_R$ produced by interaction of the R -component of the field with the current and plasma position is stable with regard to up and down motion.

The concavity of vertical field line is written as decay index. $n = -\frac{R}{B_z} \frac{\partial B_z}{\partial R}$ is radial decay

index of the externally applied magnetic field. It is linked to the curvature of B_z and the vertical variation of its radial component.

The condition of stability of the equilibrium position of the plasma column relative to vertical displacements can be written as $n > 0$ [2.19, 2.20].

Stability relative to horizontal displacement (\hat{R})

To maintain plasma column in equilibrium against horizontal axisymmetric displacement, the interaction of the z -component of the external field and the plasma current produces a radially

inward directed force that just offsets the imbalance in the plasma pressure and poloidal magnetic field pressure,

$$F_R = -I_p R B_v \quad (2.21)$$

The variation of this force with radial position is given by

$$\partial F_R / \partial R = -I B_z \left(\frac{R}{I_p} \frac{\partial I_p}{\partial R} + 1 - n \right), \quad (2.22)$$

where B_z is vertical magnetic field in absence of plasma. For horizontal stability the condition on the field index is given by $n < 3/2$ to ensure $\partial F_R / \partial R < 0$. Hence the condition for stability of the equilibrium against displacements is expressed in terms of the field index as: $0 < n < 3/2$.

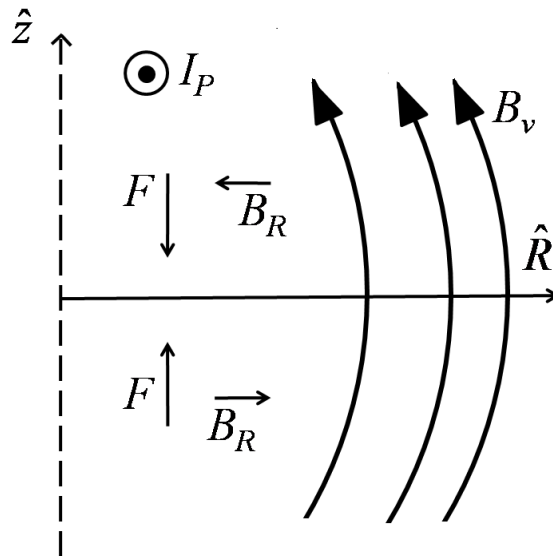


Figure 2.6. Restoring force produced by concave field lines against vertical (\hat{z} -direction) displacement

In ADITYA to maintain plasma column in equilibrium position a set of two vertical magnetic field (B_v) coils, B_{v1} and B_{v2} are placed symmetrically around the mid - plane. These coil position and Ampere-turns are chosen such that $n > 0.4$ and < 1.2 . Vertical cross-section of B_v coils is shown in Fig. 2.7.

2.4.1.2 Vacuum vessel and associated systems

ADITYA vacuum vessel is a ultra-high vacuum compatible and made out of SS-304L material with major radius 75cm and square cross- section of side 60cm. Vessel is assembled

in four quadrants. At one toroidal location electrical discontinuity is provided to allow fast poloidal magnetic field penetration into the vessel. Base pressure of $\sim 1 \times 10^{-7}$ Torr is achieved by three turbo-molecular pumps and one cryogenic pump. Each turbo-molecular pump has pumping capacity of 2,000 l/s for N_2 . Cryogenic pump has pumping capacity of about 9,500 l/s for water vapour and condensed hydro-carbons.

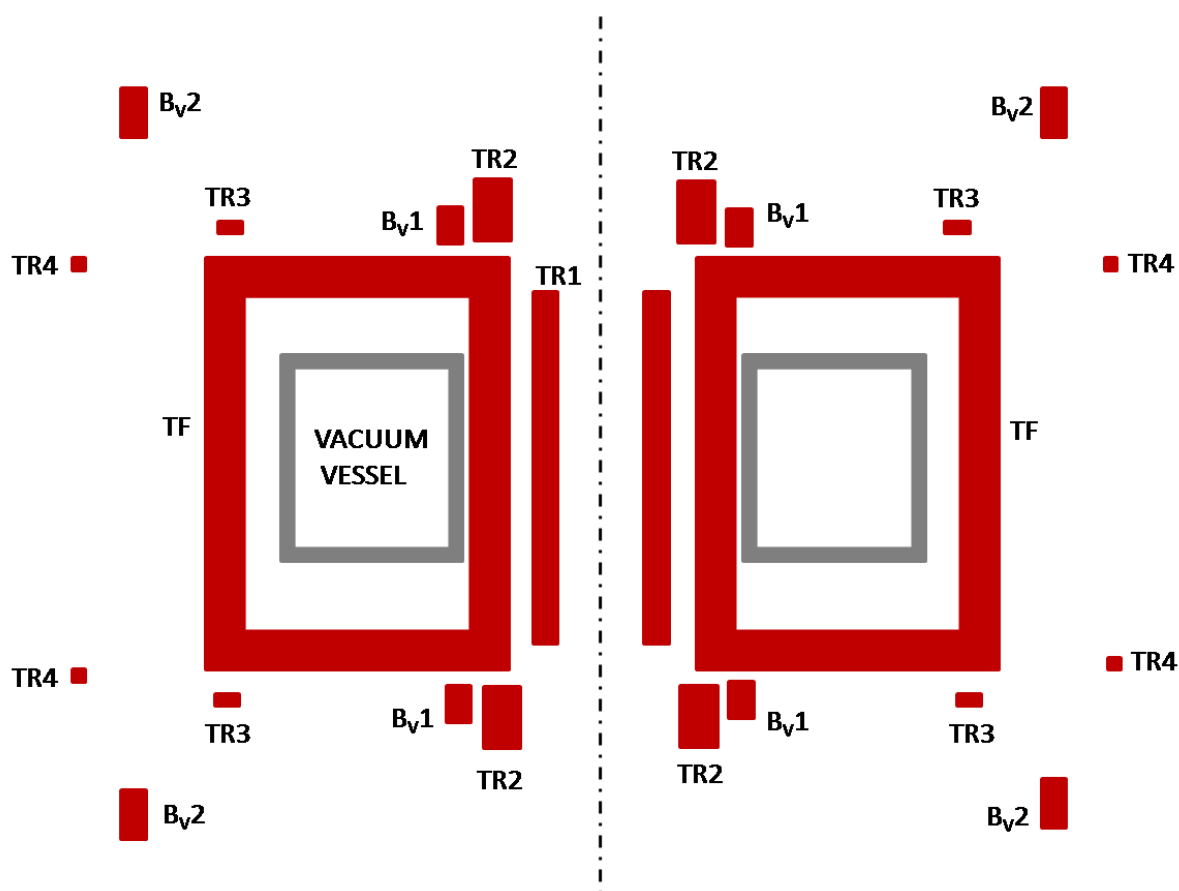


Figure 2.7. Vertical cross-section of TF coil, OT (or TR) coil, B_v coils in ADITYA

2.4.1.3 Wall conditioning

Normally, vacuum vessel surface is covered with a layer of adsorbed gas atoms with weak binding energy. These impurities can be desorbed by incident ions, neutrals, electrons and photons back into the plasma. This process is called *particle recycling*. Desorbed atoms radiate away the energy and result cold boundary plasma. In order to minimize recycling due to plasma –wall interaction during plasma discharge various wall treatment procedures have been adopted before plasma discharge. In order to condition ADITYA vacuum vessel wall (1) glow discharge cleaning, (2) pulse discharge cleaning in combination with glow discharge cleaning and (3) electron cyclotron resonance cleaning are carried out.

2.4.1.4 Gas puff system

Hydrogen gas is injected from a constant pressure reservoir through fast response piezo electric valve. There are two stages of gas filling: (1) Pre-filling of torus to a specific pressure prior to the initiation of a tokamak discharge, (2) Pre-programmed gas feed for building up plasma density and to control HXR. At working pressure of $\sim 1 \times 10^{-5} \text{ Torr}$ plasma is produced.

2.4.1.5 Limiter

Limiter is the first material surface to come into contact with the hot plasma. Limiter receives particle and heat load. ADITYA has two poloidal limiters of graphite material- working limiter and safety limiter. Working limiter receives all heat loads and has graphite tiles mounted on two semi-circular rings. This limiter has radius of 25cm and defines plasma size. Safety limiter generally does not receive significant particle and heat load. It is designed to take the full load in the event of failure of working limiter.

2.4.1.6 ADITYA Pulsed Power System (APPS)

ADITYA Pulsed Power System (APPS) mainly consists of three pulsed power supplies. Its main function is to deliver current pulses of specified shape, amplitude and duration to Ohmic transformer (OT or TR) coils, TF magnet coils and vertical field (B_v) coils.

APPS consists of two major sub-systems namely the 132kV/ 11kV sub-station including the reactive power compensation system and the DC system comprising of the line commutated converters, pulse shaping units and the control instrumentation.

The power system consists of 12-pulse thyristor-based wave-shaping dc converter system for Ohmic power supply ($\pm 25 \text{ kA}$, 2000 V), TF power supply (25 kA, 425 V), the ripple frequency is 600 Hz and voltage ripple is 6%. With total load inductance is 6mH, the current ripple is estimated 0.0045%.

Ohmic power supply

Ohmic power supply initiates the gas breakdown and drives the plasma current. To ionize the gas and start current build-up a relatively large voltage is required, which is followed by a lower loop voltage for slower plasma current changes and less runaway electron generation. To produce a desired plasma loop voltage and current an active wave shaping circuit is connected between the dc power converter and the OT coils.

OT power supply, which is also called converter consists of four thyristor bridges. Two bridges are in series, which are in parallel of other two bridges in series. Each thyristor produces 3 pulse output and each series combination gives 12.5kA. In this way the converter is 12 pulse 25kA output.

Vertical field power supply

Vertical field power supply is a thyristor based power supply, which delivers power to B_V coil. This power supply can be operated by two methods- (a) by pre-programming and (b) by I_p -control or feed- back control. In second method current in B_V coil is supplied in such a way that it produces $B_V \propto I_p$.

Toroidal field power supply

Toroidal field power supply (50 kA, 425 V) is a simple thyristor based converter. A 132/11 kV transformer of 50 MVA rating supplies the input power to the converter system.

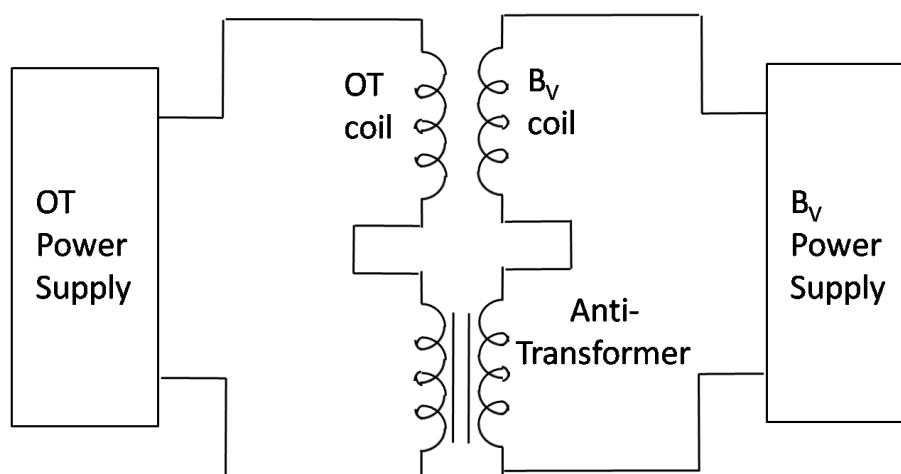


Figure 2.8. Anti transformer arrangement to nullify mutual inductance between Ohmic Transformer (OT) coil and Vertical Field (B_V) coil

Anti-transformer and its significance

In ADITYA tokamak OT (or TR) coil and B_V coil are very close to each other. So there is mutual inductance between the two coils $M = k\sqrt{L_{OT}L_{BV}}$, where k is the coupling coefficient between the two coils, L_{OT} is the inductance of the OT coil, and L_{BV} is the inductance of the B_V coil. To nullify effect of mutual inductance an anti-transformer is used. Primary coil of anti-transformer is connected in series with OT coil and secondary coil is

connected in series with B_V coil. Flux linkage between primary and secondary coil is such that it nullifies the flux linkage due mutual inductance between OT and B_V coil.

2.4.1.7 ADITYA Data acquisition system and control system

The data acquisition and control of the entire tokamak system is carried out using control system based on Computer Automated Measurements And Control (CAMAC) concept. It is designed to provide various channels with selectable sampling rates and different selectable time slots synchronized for pulsed experiments.

The analog signals coming from various diagnostics are passed through opto-isolators and sent to digitizers. The digitizers are software/ hardware settable for appropriate sampling rate and memory length depending upon the frequency of interest and viewing time interval during plasma discharge. The time synchronisation between the plasma discharge and acquisition is achieved with the help of appropriate trigger signal derived from control process and timer modules. During the interval between successive discharge the local memory of digitizer is read by computer and the data is stored on hard disk for immediate and future processing.

2.4.2 Typical ADITYA tokamak discharge

As discussed in previous section, in ADITYA tokamak vacuum vessel is evacuated to a base pressure $\sim 10^{-7}$ torr. At ~ -2 s TF power supply is turned on (Fig. 2.9). At ~ -0.5 s current in TF coil reaches to flat – top, which remains flat till ~ 0.2 s. Toroidal magnetic field during TF current flat – top is maintained at ~ 0.70 - 0.8 T. Ohmic power supply is used for plasma breakdown and current drive. At ~ -1.1 s Ohmic transformer (OT) power supply is switched on which reaches to maximum value at ~ -0.3 s. At $t \sim -0.2$ s H_2 gas is filled up to produce $\sim 1 \times 10^{-5}$ torr pressure. At 0ms fast change in current (dI_{OT} / dt) induces toroidal electric field (loop voltage) inside vacuum vessel. In this electric field H_2 gas plasma is produced. Simultaneously, vertical field power supply is switched on. Vertical field is applied for the control of radial motion of plasma. It is maintained as proportion to plasma current all the time so that the plasma can be kept at center.

Toroidal electric field $E_\phi = V_{Loop} / 2\pi R$ accelerates free electrons, which are always present due to the cosmic radiation. But their amount is not sufficient to produce fast discharge. Additional free electrons are produced by pre-ionization filament to produce fast and reproducible discharge. At breakdown H_α intensity is at its maximum value. After

breakdown, H_α intensity reduces and electron density n_e increases. Temporal profile of typical ADITYA tokamak discharge (#22761) is shown in Fig. 2.10.

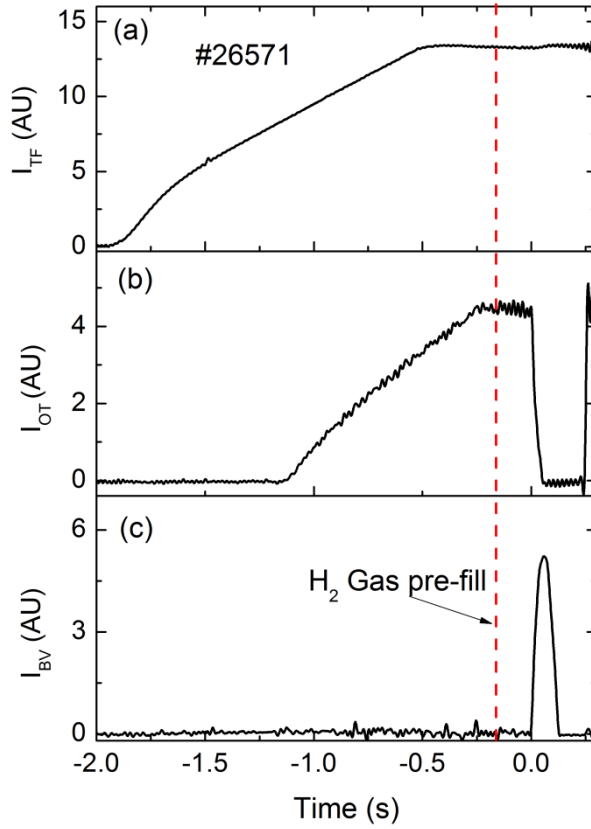


Figure 2.9. Temporal profile of current signal in (a) toroidal field magnetic coil (I_{TF}), (b) Ohmic transformer coil (I_{OT}), (c) Vertical magnetic field coils (I_{BV}) for a typical ADITYA tokamak discharge (#26571). Time of hydrogen gas pre-fill is shown by red dotted line.

In ADITYA rate of plasma current increase (dI_p/dt) just after breakdown is kept $\sim 7\text{--}9\text{MA/s}$. During current rise phase run-away electrons are generated which are detected by HXR detectors. These initial run-away electrons are removed by puffing H_2 gas. After the removal of these run-away electrons part, plasma current takes a dip and then rises again. After the plasma current reaches to plateau ($\sim 60\text{--}90\text{kA}$), $\sim 2\text{--}3\text{V}$ loop voltage is sufficient to drive plasma Ohmically.

It is observed that during plasma disruption negative spikes occur. These negative spikes are due to plasma inductance decrease. The sudden decrease of the inductance is due to expansion of the plasma radius across the strong magnetic field [2.21 – 2.23].

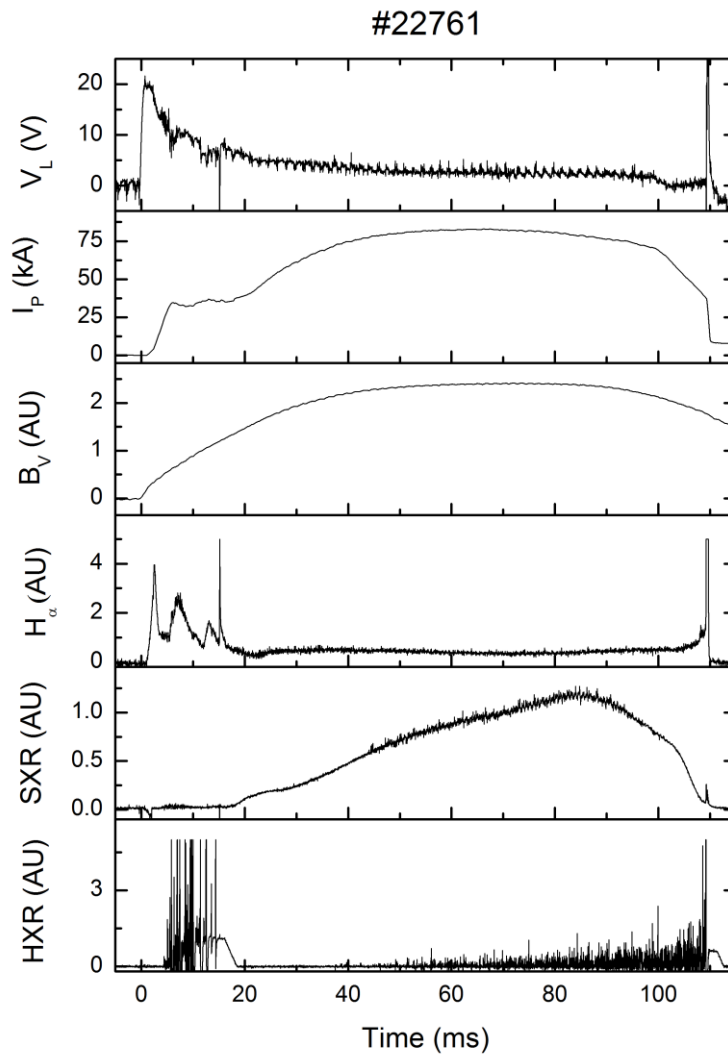


Figure 2.10. Temporal profile of typical ADITYA tokamak discharge (#22761). (a) Loop voltage (V_L), (b) plasma current (I_P), (c) Vertical magnetic field (B_V), (d) H_α line radiation, (e) SXR signal, (f) HXR signal

2.4.3 Operational diagnostics in ADITYA tokamak

Diagnostics for tokamaks have generally been developed to run tokamaks by measuring plasma parameters and to study particular topics in tokamak research.

2.4.3.1 Magnetic measurements

Magnetic measurements in tokamaks are carried out to setting up stable plasmas, investigate MHD instabilities, determine energy confinement time etc.

2.4.3.1.1 Loop voltage measurement

The Loop voltage also called the Volts per Turn or Surface Voltage, is used in calculating the Ohmic power input to the plasma. It also allows a calculation of the plasma parallel resistivity. Loop voltage is simply measured by a single turn pickup coil toroidally wound close to the plasma. In ADITYA tokamak during plasma current flat-top loop voltage remains ~2-3V.

2.4.3.1.2 Rogowski coil

Plasma current is measured by a ‘Rogowski coil’, which is multi- turn solenoid completely enclosing the current to be measured. The transient plasma current generates a voltage

$$\varepsilon = \frac{\mu_0 N \pi r^2}{2\pi R} \frac{dI_p}{dt}, \quad (2.23)$$

where N is number of turns, r and R are minor and major radius of the Rogowski coil. I_p is deduced from the time integration of equation (2.23). In ADITYA plasma current is measured by a Rogowski coil with square cross-section of $4 \times 10^{-4} \text{ m}^2$ and side length 0.64m [2.18]. It has 4600 turns and made of Teflon insulated copper wire.

2.4.3.1.3 Mirnov coil

In tokamaks it is expected that magnetic islands play a role in determining transport. Their structure is expressed in the form of helical Fourier modes $e^{i(m\theta+n\phi)}$ (m and n being poloidal and toroidal mode numbers), and they are located at rational surfaces. Mirnov [2.24] first studied their presence using array of B_θ coils in a single poloidal plane, measuring dB_θ/dt outside the plasma. Poloidal mode structure of such perturbation is determined by Mirnov coils. Toroidal mode structure is determined from a toroidal array of B_θ coils. In ADITYA a poloidal array of 30 magnetic probes (15 B_θ coils and 15 saddle coils) [2.25] mounted inside the vacuum vessel at $r = 27\text{cm}$ allows measurements of fast dB_θ/dt and dB_r/dt oscillations. Frequency response of these probes linear up to ~30kHz.

2.4.3.1.4 Diamagnetic loop

Energy confinement time measurement is a subject of particular interest. This is carried out by determining the energy content, W , using a diamagnetic loop and calculating the confinement time from $\tau_E = W/P$, where P is the input power to the plasma. The quantities

which require to be measured to determine the thermal energy and internal inductance (or poloidal beta) are the magnitude and direction of the magnetic field at the measuring surface, and the diamagnetic flux. The diamagnetic flux is the difference between the total toroidal flux with plasma and that in the absence of plasma. This flux is measured with loop enclosing the plasma, encircling it poloidally, called diamagnetic loop.

Relation between the diamagnetic flux and the poloidal beta derived from simplified equilibrium relation

$$\beta_p = 1 + \frac{8\pi B_{\phi 0} \delta\phi}{\mu_0^2 I_p^2} \quad (2.24)$$

where $B_{\phi 0}$ is the toroidal magnetic field in the absence of the plasma which can be obtained by the magnetic probe,

$$\beta_p = \frac{8\pi^2 a^2 \langle p \rangle}{\mu_0 I_p^2} \quad (2.25)$$

for a circular cross-section, I_p is the plasma current which can be obtained by the rogowski coil. ,

$$\delta\phi \equiv \pi a^2 (\bar{B}_\phi - B_\phi(a)) \quad (2.26)$$

is the change in the toroidal flux due to plasma pressure and \bar{B}_ϕ is the average toroidal magnetic field. The energy confinement time τ_E can be calculated from β_p and plasma resistance $R_p (= P/I_\phi^2)$ using the relation

$$\tau_E = (3/8)\mu_0\beta_p(R/R_p) \quad (2.27)$$

In ADITYA diamagnetic flux is measured by a single-turn loop (diamagnetic loop) [2.26] and a compensating loop of six turns made of polyimide-insulated shielded wire. Its shield ensures complete immunity to electrostatic pick-up. Flux measurement channels use low pass filters at 157Hz. Signal is converted from analog to digital by CAMAC module at sampling rate of 5 kHz.

2.4.3.2 Microwave interferometry

Microwave interferometer technique is a well known method of measuring plasma density. This method gives line averaged electron density along the line of sight through the measurement of the phase shift in the microwave beam due to the plasma. Microwave beam during its passage through plasma suffers a phase shift (ϕ) due to the change in the refractive

index of the medium. For propagation path length, L , average density is given as $\bar{n} = 2\varepsilon_0 m_e c \omega \phi / e^2 L$, where ω is frequency of microwave.

In ADITYA a seven chord millimetre wave interferometer at 100GHz homodyne interferometer system is used to measure the radial electron density profile [2.27]. Each chord is separated by a distance of 7cm at the median plane of plasma. The phase changes are detected by Schotky diode.

2.4.3.3 Soft X-ray measurements

Two identical detectors with different thickness of thin metallic foils, usually Beryllium, provide the possibility of measurement of electron temperature (T_e) by means of the absorber foil technique [2.28]. The time evolution of the X- ray flux provides information about MHD activity also.

The two foil method or absorption method

The two foil method of determining T_e relies on the fact that the continuous X-ray power spectrum depends upon $\exp(-E/T_e)$, and the transmission properties of X-ray through thin foils. The transmission coefficient through a thin metal foil is strongly energy dependent and a foil of particular thickness will effectively have a cut-off energy, E_1 , below which it is opaque to incident X-rays. A thicker foil will have a higher cut-off energy, E_2 , and so if the X-rays from a region of hot plasma are viewed by two detectors shielded by the two different foils, then the ratio of the observed power in each detector may be written very approximately as

$$R = \frac{P1}{P2} = \frac{\int_{E_1}^{\infty} \exp(-E/T_e) dE}{\int_{E_2}^{\infty} \exp(-E/T_e) dE} = \exp(-(E_2 - E_1)/T_e) \quad (2.28)$$

The measurement of R and knowledge of E_1 and E_2 will then determine T_e . The expression for R has been evaluated in an exact manner by Jahoda et al [2.28] for a variety of different foil thickness and temperatures.

In ADITYA Soft X-rays are detected by silicon surface barrier diodes, which measure the integrated X-ray power above a threshold energy determined by Beryllium, placed in front of

the detectors. Central line averaged electron temperature was measured with the transmission ratios of soft X-ray flux through two Beryllium foils of 25 and 70 micron thickness [2.29].

2.4.3.4 Hard X-ray measurements

Hard X rays are photons with energy greater than hundreds of keV. These radiations arise when fast relativistic electrons (runaway electrons) strike the limiter or the first wall. In present day tokamaks, runaway electrons constitute a serious concern. The first and the most common goal of HXR measurement is simple evidence of the presence of runaway electrons in tokamak plasmas. In ADITYA NaI(Tl) scintillators coupled with photomultipliers are used to detect HXRs. The calibration of detector is done by the standard source of the Caesium-137 or Cobalt. Normally in ADITYA, it is kept at the 1V output signal corresponding to the 1MeV of radiations.

2.4.3.5 Spectroscopy

Because electron temperature edge value range from few eV to few tens of eV, atoms are neutral or in state of low ionization and visible radiation are emitted over a wide spectral range in tokamaks. Line emissions (H_α , CIII, OI etc) are observed with visible light spectrometers or monochromators to monitor plasma discharge performance. Ruled grating are used as dispersing elements and photomultiplier tubes as detectors. The aim of much of this work is to determine impurity influxes. Impurity content is often determined from the intensity of the visible continuum radiation. Measurement of continuum radiation intensity in the visible spectral region is carried out to estimate the effective charge of plasma ions Z_{eff} . UV spectral region is used for particle transport studies. Grazing incidence and normal incidence monochromators are used to measure the intensity of resonance line radiation from impurity. A multi-track spectrometer is used to monitor time and space resolved visible spectral lines [2.30].

2.5 References

- [2.1] John Wesson, Tokamaks, 3rd Edition, Oxford University, 2004
- [2.2] V. D. Shafranov, *Review of Plasma Physics (ed. Leontovich, M.A.)* Vol 2, 103, Consultants Bureau, New York (1966)
- [2.3] J. P. Freidberg, Plasma Physics and Fusion Energy, Cambridge University Press (2008)
- [2.4] V. S. Mukhovatov and V. D. Shafranov, *Nucl. Fusion* **11**, 605 (1971)

- [2.5] R. Goldston, *Plasma Phys. Control. Fusion* **26**, 87 (1984)
- [2.6] S. M. Kaye, R. J. Goldston, *Nucl. Fusion* **25**, 65 (1985)
- [2.7] P. N. Yushmanov, T. Takizuka, K. S. Riedel, et al., *Nucl. Fusion* **30**, 1999 (1990)
- [2.8] ITER Physics Basis, *Nucl. Fusion* **39**, 2175 (1999)
- [2.9] D. C. McDonald, J. G. Cordey, K. Thomsen, et al., *Nucl. Fusion* **47**, 147 (2007)
- [2.10] H. P. Furth et al., *Phys. Fluids* **6**, 459 (1963)
- [2.11] G. Bateman, MHD Instabilities, The MIT Press, 1980
- [2.12] P. H. Rutherford, et al., *Phys. Fluids* **16**, 1903 (1973)
- [2.13] R. J. La Haye, et al., *Phys. Plasma* **17**, 056110 (2010)
- [2.14] S. J. Hugill, et al., *Nucl. Fusion* **17**, 1382 (1977)
- [2.15] M. Murakami, J. D. Callen, and L.A. Berry, Some Observations on Maximum densities in Tokamak Experiments, *Nuclear Fusion* **16**, 347 (1976)
- [2.16] Equipe TFR, 'Tokamak Scaling Laws, With Special Emphasis On TFR Experimental Results', *Nuclear Fusion* **20**, 1227 (1980)
- [2.17] Conceptual Design of ADITYA, Plasma Physics Programme, February (1983)
- [2.18] S. B. Bhatt, et al., *Indian Journal of Pure and Applied Physics*, **Vol. 27 September-October**, 710 (1989)
- [2.19] S. M. Osovets, *Plasma Physics and the problems of controlled Thermonuclear Reactions*, **2**, 238 (1958)
- [2.20] S. Yoshikawa, *Physics Fluids* **7**, 278(1964)
- [2.21] Kenro Miyamoto, Plasma Physics for Nuclear Fusion, The MIT Press, 1980
- [2.22] H. P. Furth, The 3rd International Symposium on Toroidal Plasma Confinement, Garching, March 1973, paper B9-I.
- [2.23] R. A. Jacobsen, *Plasma Phys.* **17**, 547 (1975)
- [2.24] S. V. Mirnov and I. B. Semenov, *Atomnaya Energiya* **30**, 20 (1971) [*Soviet atomic energy* **30**, 22 (1971)]
- [2.25] D. Raju, et al., *Pramana – journal of physics*, **Vol. 55**, Nos 5 & 6, Nov. & Dec. 2000, pp. 727-732
- [2.26] Sameer Kumar, et al., *Rev. Sci. Instrum.* **81**, 123505 (2010)
- [2.27] P. K. Atrey, et al., *Indian J. Phys.* **66B (5 & 6)**, 489 (1992)
- [2.28] F. C. Jahoda, et al., *Phys. Rev.* **119**, 843(1960)
- [2.29] C.V.S. Rao and S.K. Mattoo, Technical Report, Physical Research Laboratory, Ahmedabad, May, PPP/TR-21/86 (1986)
- [2.30] S. Bannerjee et al., *Meas. Sci. Technol.* **19**, 045603 (2008)

Chapter 3

Experimental Set-up

Ohmic discharges cannot produce confinement required for the fusion reactors. For H-mode plasmas transport barrier is necessary to be formed. Different techniques such as NBI, ECRH, ECCD, LHCD, edge biasing are implemented to induce transport barriers at the edge. Electrode biasing techniques change edge current density profile and produce higher radial electric field at the plasma edge by drawing cross-field current and thereby generate high sheared poloidal flow to make plasma more confined. Not being complicated these experiments have been carried out in ADITYA to understand physics of L-H transition and other tokamak related physics issues. For biasing experiments in ADITYA an electrode holding assembly and pulsed power supply were designed and fabricated. Arrays of Langmuir probe and B-dot probe developed to measure edge plasma parameters such as plasma density, floating potential and toroidal current density. Design, fabrication and working of these systems have been discussed in this chapter.

3.1 Electrode and its holding assembly

3.1.1 Design criteria

Different tokamaks have used electrodes of different dimensions for achieving L–H transitions in respective experiments and there exists no definite criterion for choosing the electrode dimensions in this kind of experiments. Electrodes of different sizes, inserted from different locations of tokamak, such as from radial, top and bottom ports, and different radial currents were reported in different tokamaks depending upon the size and the plasma parameters, for achieving improved confinement. For example, in the CCT tokamak [3.1] a bias voltage of 1.5 kV was necessary to draw a radial current only of 20 A through an electrode surface area of approximately 50 cm^2 to enable the *L–H* transition, whereas in the TUMAN-3 tokamak [3.2] only 150 V was sufficient to draw over 100 A of radial current through an electrode exposed area of only 3 cm^2 for achieving the transition. Further, the

electrode had to be placed at different radial locations inside the limiter and also had to be biased with different polarities (positive or negative) to achieve the transition in different tokamaks. Although a broad criterion is followed in all biasing experiments that the electrode should be big enough to be able to charge the flux surface and should be small enough not to act as a limiter, no systematic studies had been carried out along these lines. To undertake a parametric study on the effect of a biased electrode of variable dimensions of the electrode on plasma confinement and especially on MHD modes, we have designed a special electrode-holding assembly by which we can change the electrode dimension by changing its exposed length (L_{exp}) in-situ along with its position (r_{elec}) movement inside the ADITYA tokamak. Instead of using a fixed electrode, the electrode-exposed length has been varied inside the plasma by means of an especially designed electrode holding assembly.

3.1.2 Electrode Material

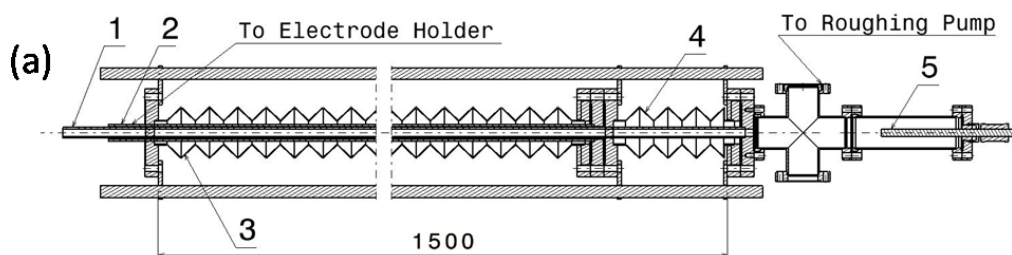
Since the first electrode biasing experiments done in CCT tokamak, different materials have been chosen for the electrode in different tokamaks keeping in mind the melting point and current drawing capability of the material. Generally, electron emissive injectors (W, LaB₆) were used in negative biasing to draw sufficient current and Graphite, Molybdenum, Stainless Steel were used in positive biasing to induce L-mode to H-mode (L-H) transition. The electrode used in the experiments done in ADITYA tokamak is made of a high purity (99.9%) molybdenum (Mo) rod of 5 mm diameter procured from Teknis Elecsys Llc.

3.1.3 Electrode holding assembly

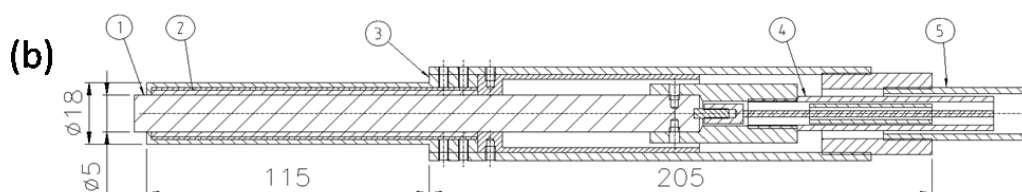
For the experiments we have employed an electrode assembly at the top of ADITYA tokamak which can be used to put electrodes of variable length and different diameter at various radial position (up to 10cm max.) inside the limiter. Although for the experiments only 5mm diameter electrode was used, system can accommodate electrodes of different diameters using different electrode holders keeping rest of the assembly unchanged. Electrode assembly is the arrangement which can give two kind of linear movements to the electrode. For this purpose two edge welded bellows have been used.

The system contains two stainless steel pipes of different diameters attached to different end-flanges. Outer and inner pipes have outer diameter ~21.5mm and ~14.0mm. Each pipe is ~2.5mm thick. One pipe controls movement of electrode holder and the second holds and controls the electrode to change its length that is exposed inside the plasma. These two pipes are connected to two bellows (long bellow and short bellow) of same internal diameter (each

bellow having inner diameter ~32mm) and different stroke lengths and can be manoeuvred independently.



1. Inner (SS) tube, 2. Outer (SS) tube, 3. Long bellow, 4. Short bellow, 5. Electrical feed through (insulated with ceramic tubes)



1. Mo Electrode, 2. Copper sleeve, 3. Ceramic sleeve, 4. Inner (SS) tube, 5. Outer (SS) tube (all lengths are given in mm).

Figure 3.1. (a) Cross-sectional view of electrode assembly and (b) electrode holder.

Bellow with higher axial motion (long bellow) controls the electrode tip position inside the plasma as electrode tip position required more movement whereas bellow with lower axial motion (short bellow) controls the length of electrode exposed inside the plasma. The pipe with the larger diameter holds the ceramic sleeve and slides over the pipe of smaller diameter, which holds the Molybdenum (Mo) electrode. To maintain accurate linearity of the bellow movement, they are made to move on four fixed guide rods. In totality, by means of long bellow we can move electrode tip inside the edge of plasma placing it at different radial locations while keeping length of electrode unchanged and using the second bellow we can change the electrode's exposed length by keeping the tip position unchanged. The longer bellow has been used for bringing the whole system out of the tokamak without breaking the vacuum through a gate valve. The sleeve, which slides over the electrode to change its exposed length, is made of machinable ceramic as shown in Fig. 3.1b. It consists of a thin copper cylinder, grounded through the system body, sandwiched between two ceramic cylinders. The copper cylinder acts as a shield to the magnetic field generated by the

electrode current due to the unexposed part of the electrode. This magnetic field must be shielded out; otherwise, it can lead to unwanted local magnetic field perturbation. The maximum variation of the electrode-exposed length is over ~ 50 mm whereas its position can be changed up to ~ 10 cm inside the plasma, with an accuracy of less than 1 mm. Ceramic tubes have been used to isolate the electrode electrically from the inner SS-tube which holds it maintaining an isolation resistance $\sim 2G\Omega$ at 2 kV between the electrode and assembly body. The whole assembly is tested for its UHV compatibility up to 7.0×10^{-9} Torr, achieving a leak rate below (5.0×10^{-9} mbar-l/s) before installation. The temperature rise of Mo electrode placed in the edge region of ADITYA tokamak plasma (electrode diameter 5 mm and exposed length 10 mm sustained for 30 ms, in edge plasma of ADITYA tokamak with density $\sim 3 - 5 \times 10^{18} \text{ m}^{-3}$ and electron temperature 30 – 50 eV) is expected to be $\sim 1200 \text{ C}$, which is much less than the melting point of Mo (2623°C). Cross-sectional view of electrode assembly and electrode holder are shown in Fig.3.1. Picture of electrode assembly is shown in Fig. 3.2.

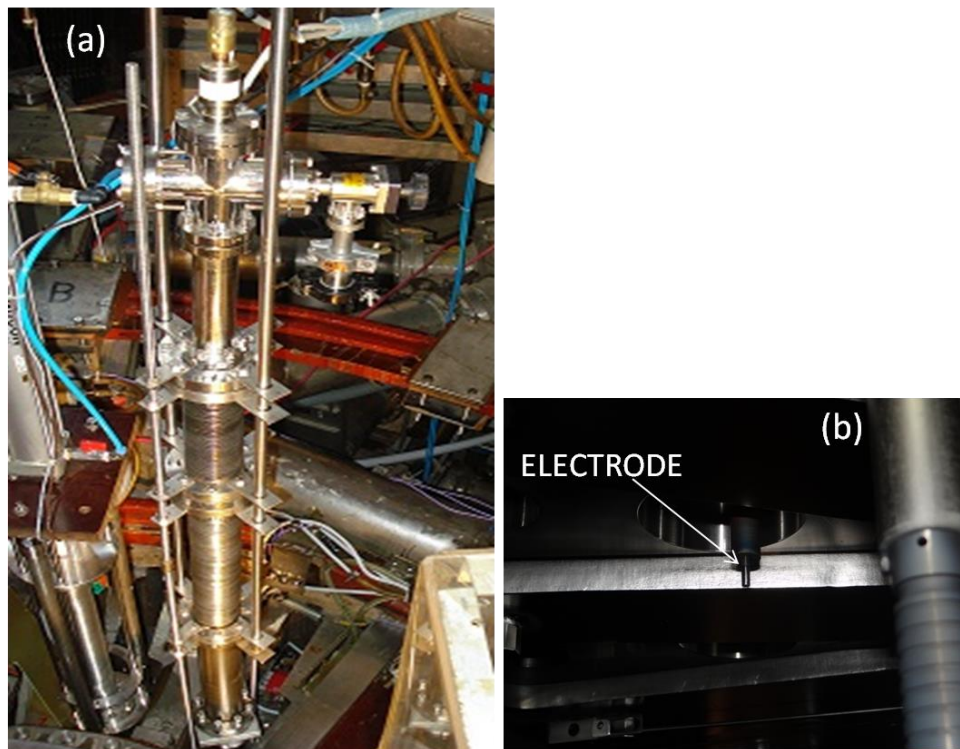


Figure 3.2. (a) Electrode assembly mounted on top of ADITYA tokamak and (b) inner view of ADITYA showing electrode mounted on top of the machine.

3.2 Biasing Pulsed Power Supply

3.2.1 Criteria and philosophy

To apply biasing voltage to the electrode placed inside the Last Closed Flux Surface (LCFS) of ADITYA tokamak, there exist a number of requirements for the power supply. The requirements are derived from the characteristics of the ADITYA tokamak plasma and from the results obtained in similar biasing experiments performed on other tokamaks. As it is evident from previous electrode biasing experiments summarised in Table 1.1, achieving L – H transition required wide range of voltages (50 V – 900 V) to be applied to the electrode and the current drawn by the electrode also varied quite substantially from ~ 20 A to ~ 250 A. Further, the previous experiments in other tokamaks show that the radial current drawn by the electrode significantly exceeds the ion saturation current and are inconsistent with those predicted by neoclassical theory. Furthermore, the application of the bias voltage to the electrode inserted inside the plasma leads to charging of the magnetic surface that is intercepted by the electrode tip. Therefore, the current drawn to the electrode depends on the area of the average magnetic surface, not on the electrode area, and the perpendicular conductivity. The expected value of electrode current, I_{elec} , is estimated ~ 150 A in order to establish an electric field of the order of 5 kV/m with the electrode tip positioned 2 cm inside the LCFS using the equation $I_{elec} = j_r A$, where j_r is the perpendicular current density and A is the area of the average magnetic surface in the electric layer. The perpendicular current density j_r is estimated from the radial momentum equations in terms of radial electric field E_r and the effective collision frequency ν_{ii} and is given by $j_r = n_i m_i \nu_{ii} / B_\phi^2$ [3.1], where n_i is the ion density, m_i is the ion mass and B_ϕ is the toroidal magnetic field using edge plasma parameters of ADITYA tokamak ($n_e = n_i \approx 5 \times 10^{18} \text{ m}^{-3}$ and $T_e \approx 30 \text{ eV}$).

3.2.2 Power Supply

To deliver the biasing voltage at a desired instant into the plasma during current flat top phase, a switching mechanism is required to put on and off the biasing voltage and the start time of the biasing pulse as well as its duration, which must be adjustable. Controllable switches like insulated gate bipolar transistor (IGBT), power bipolar junction transistors ~BJTs, metal–oxide–semiconductor field effect transistors ~MOSFETs, GTO thyristors, or SCRs with forced commutation are all suitable for obtaining a desired bias voltage pulse.

The pulsed power supply (PPS) is consisted of two parts: biasing circuit and force - commutation circuit. Biasing circuit powers the electrode at any time during plateau phase of plasma current and consists of a capacitor bank, thyristor SCR switch (S1) and trigger circuit (T1 or T2). In ON- state electrode current in the SCR flows from anode to cathode. Commutation circuit turns off the SCR by “forcing” a current through the SCR in the direction opposite the electrode current.

We have used a SCR (T150E120) with peak inverse voltage rating of 1200V and continuous DC current 150A from Insel rectifiers (India) for generating the biasing voltage pulse using forced commutation technique due to its rugged performance and low cost. Although the SCR is rated for 150A continuous current, it can deliver a current of nearly 10 times of its rated DC value for a limited time of the order few tens of milliseconds. The main SCR carrying the load current has been turned off using forced commutation technique with another SCR (10RIA120) with a much lower rating of 1200V and 10A DC made by International Rectifier providing the reverse voltage and current from another capacitor of $\sim 8\mu F/1kV$. A separate charging circuit was used to charge this capacitor. The schematic of the power supply circuitry for biasing the electrode is shown in Fig. 3.3. Tokamak vessel is reference ground for PPS. Pulsed Power Supply picture is shown in Fig. 3.4.

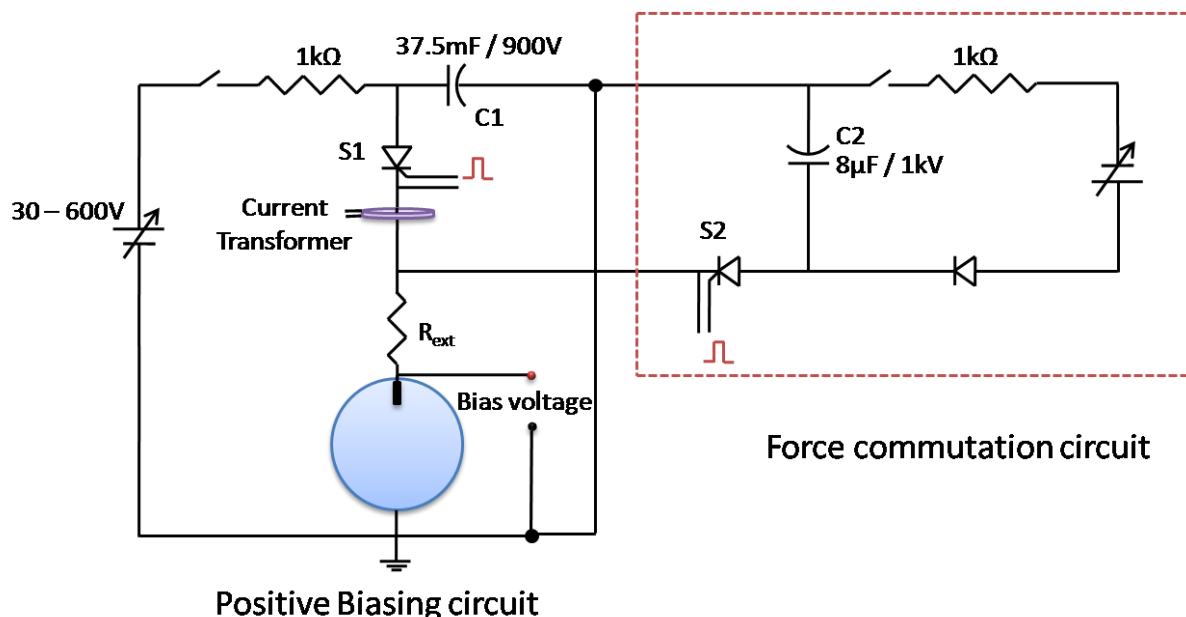


Figure 3.3. Schematic diagram of pulsed power supply depicts positive biasing arrangement

3.2.2.1 Capacitor Bank

Keeping the above mentioned considerations in mind a pulsed power supply based on a capacitor bank consisting of electrolyte capacitors has been designed to bias the electrode in

ADITYA tokamak. Main capacitor bank (C1) consists of a total of 10 electrolyte capacitors which are economical and easy to handle manufactured by Alcon Electronics (India) each having a capacitance of $15mF$ and maximum voltage rating of $450V$ has been used as the power source. The total capacitance of the bank is $\sim 37.5mF$, which can deliver a maximum current $\sim 150A$ at $900V$ for $\sim 30ms$ with a drop of only $\sim 50V$. A $600V$, $1.5A$ power supply has been used to charge the capacitor bank through a charging resistance of $1k\Omega$.

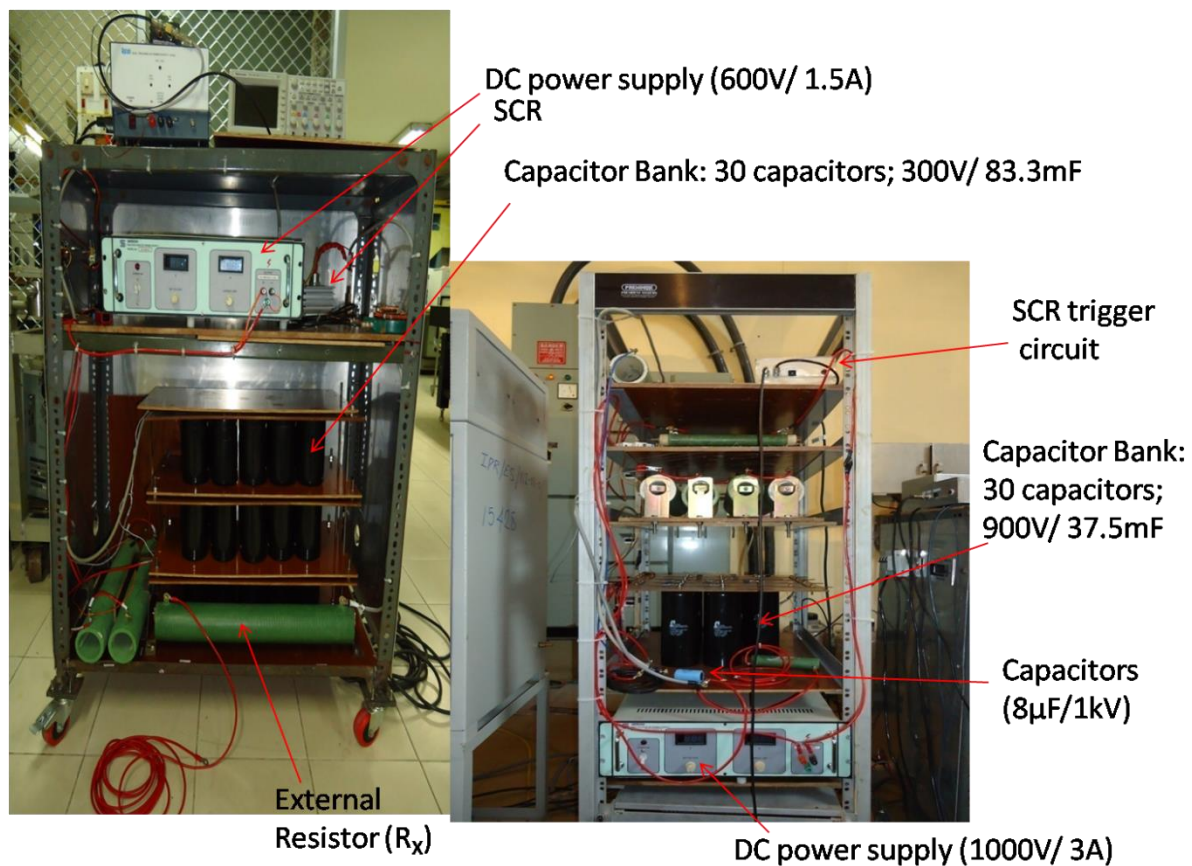


Figure 3.4. Pulsed Power Supply used for biasing experiments

3.2.2.2 Trigger circuits

To switch on and off both the SCRs at desired time loop voltage generated trigger (T1) and MHD signal generated trigger (T2) are designed.

3.2.2.2.1 Loop voltage generated trigger (T1)

Both SCRs are triggered into the on state by applying a pulse of positive gate current for a short duration in their forward blocking states. Fig. 3.5a shows the electronic circuitry for triggering both the SCRs at desired times. A master TTL trigger voltage pulse has been generated by the loop voltage signal, which is measured by single turn loop placed around the

torus of tokamak. During the start of the loop voltage TTL is generated and fed to a PIC18F45J10-I/P micro-controller IC to generate an output pulse of 3V/ 25mA and to introduce selectable time delays to the pulse. The output pulse is then amplified to ~14V and a Darlington pair of transistors has been used to enhance the current up to ~150mA to obtain the trigger pulse required for triggering the SCR. The original trigger from the loop voltage signal is at CAMAC (or digital) ground. Loop voltage trigger signal is electrically isolated using HCNR200-000E opto-coupler before being fed to PIC18F45J10-I/P micro-controller IC, which is at vessel ground. This opto-isolator provides an electrical isolation ~ 5 kV. The output trigger of PIC18F45J10-I/P micro-controller IC is then fed to the gate of the SCR through a 1:1 pulse transformer, which is required for electrically isolating the trigger circuit from the power supply. Out-put pulse (Fig. 3.5b) of 14V delivers required ~150mA current to gate for ~110 microseconds, which is much longer than switch-on time (~ 10 microseconds) of SCR.

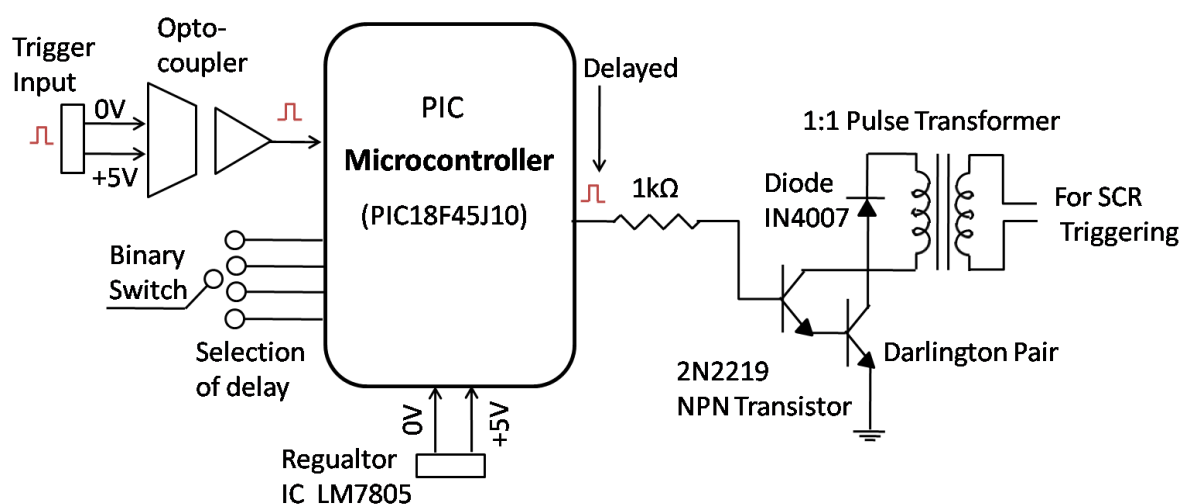


Figure 3.5(a). Block diagram of electronic circuit of SCR trigger circuit (T1)

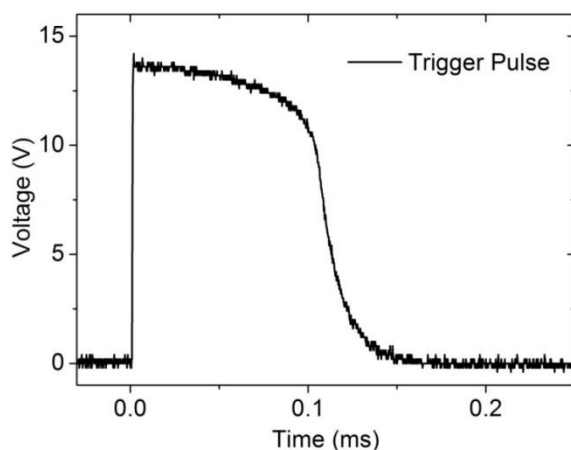


Figure 3.5(b). Output trigger pulse

First the main SCR S1 is triggered into conduction to deliver the voltage of the main capacitor bank (C1) on to the plasma load. Depending upon the requirement of the pulse width, the SCR S2 is triggered using another trigger module to drive a momentary reverse voltage on S1 to turn it off.

3.2.2.2.2 MHD signal generated trigger (T2)

Apart from improving the confinement properties of the plasma using electrode biasing, disruptions are also controlled by applying the bias to the electrode prior to the disruption event in ADITYA tokamak. It is well established that positively biased electrode produces positive sheared radial electric field, which in turn induces positive sheared poloidal flow. This fact can be used as a feasible method to study effect of sheared poloidal flow on stability of resistive tearing modes. In ADITYA biased electrode has been used to study disruption mitigation by stabilizing tearing modes in H₂ gas puff induced disruption.

To perform disruption stretch experiment the rise of MHD oscillations is used as a precursor of disruption event and is monitored by a novel low cost multi-channel Micro-Controller based timing circuit with comparator. Whenever the amplitude of these MHD oscillations induced by injecting H₂ gas overshoot a particular pre-set value, a trigger pulse is generated and delivered to a SCR switch which triggers the voltage on the electrode placed inside the plasma to avoid disruptions. The schematic of this circuit is shown in Fig. 3.5c.

This circuit detects the second MHD oscillations in Mirnov coil signal with a pre-set threshold and to generate trigger pulse output. First large MHD oscillations are generated at ~0ms, when loop voltage signal starts. In ADITYA current flat top starts ~35ms. We puff Hydrogen gas ~40ms to disrupt plasma. Gas puff generates large MHD oscillations. Trigger circuit detects these (second) MHD oscillations in Mirnov coil signal to generate a single pulse to drive the electrode biasing circuit.

Trigger circuit first compares the precursor signals (Mirnov oscillations) fed into it with the pre-set values using a comparator AD790. The other input of the comparator is connected to a variable voltage divider potentiometer and a threshold value is set at this input. Threshold value is set depending upon the MHD signal amplitude which can cause disruption. Set threshold voltage is monitored on the panel. Comparator rejects unwanted oscillations due to noise along with signals lower than threshold and produces a sequence of pulses whenever MHD oscillation rise above the set threshold in the input.

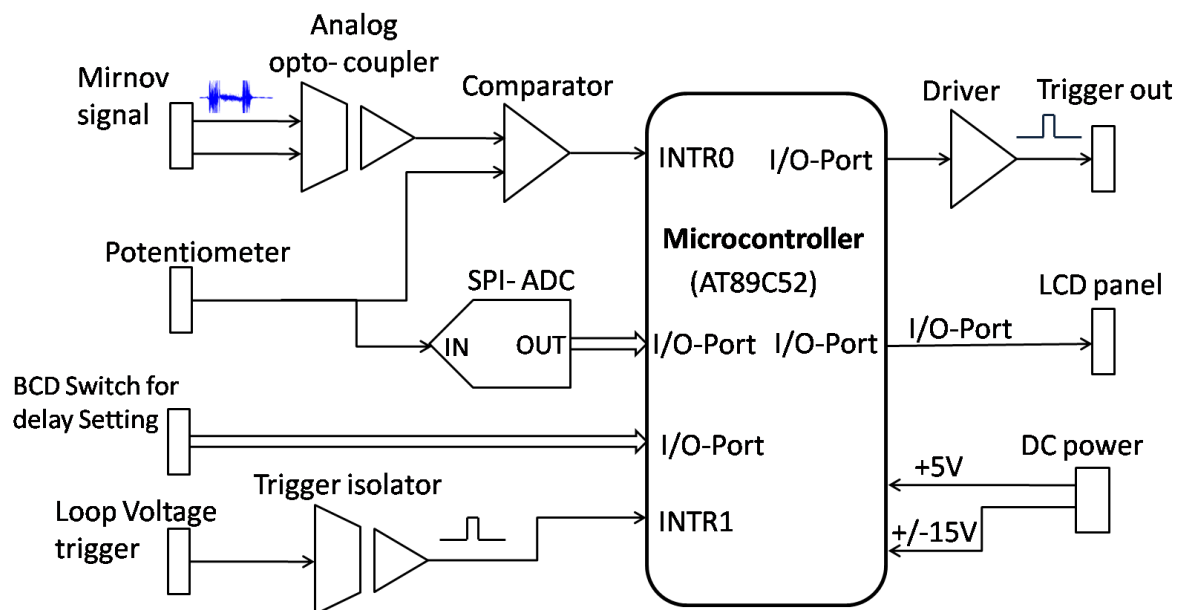


Figure 3.5(c). Block diagram of MHD generated trigger circuit (T2)

The output of this comparator is fed into the interrupt pin of microcontroller which is programmed to generate desired trigger pulse. The process starts with a master trigger from loop voltage at the initiation of every plasma discharge at $t = 0$. First MHD oscillations are detected at this time. The MHD oscillations during the plasma current rise have to be avoided and hence the program will freeze for variable preset time ($\sim 35 - 40$ ms for our experiments) until the plasma current reaches its flat-top. After this, delay program starts comparing the MHD oscillations with the preset values and generates a trigger pulse whenever the MHD signal crosses the preset level.

At the instant of first oscillation of second MHD burst crosses the threshold value set in comparator, the program will generate a trigger pulse. In our experiments second MHD oscillations are generated by puffing gas (generally at ~ 40 ms).

The trigger pulse output is then fed into a buffer circuit. Buffered trigger pulse is used as a master pulse for the trigger circuit (T1) described above, which fires the SCR for application of bias voltage to the electrode. The program stops at the end of the plasma discharge and the microcontroller IC is reset before the start of the next plasma discharge. Fig.3.5d shows the functional flow chart of operation of multi-channel Micro-Controller based timing circuit with comparator.

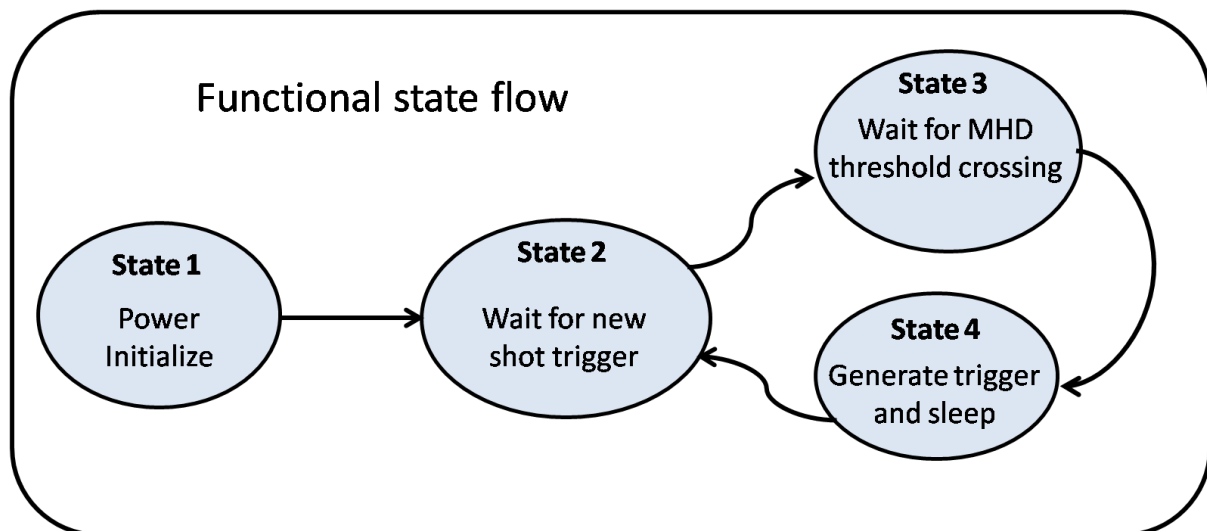


Figure 3.5(d). Functional flow chart of operation of multi-channel Micro-Controller based timing circuit with comparator.

3.2.2.3 Performance of the pulsed power supply

After getting stable and reproducible discharges we inserted the electrode inside the plasma. To test the performance of the biasing power supply we placed the electrode tip 3.0 cm inside the LCFS with an exposed length of 20 mm. Fig. 3.6 shows the plasma current, electrode current and bias voltage in a typical discharge (#26427), where a bias voltage of ~ 190 V was applied to the electrode. A radial current of ~ 80 A is drawn by the electrode without any appreciable drop in the capacitor voltage. The bias voltage, shown in the figure, depicts the local floating potential before the bias is turned on; as soon as the bias is on with triggering the main SCR (S1) at ~ 42 ms, it jumped to the ~ 190 V level in less than ~ 150 - 200μ s. The second SCR (S2) is fired at ~ 57 ms which turns off main SCR (S1), thereby disconnecting the power supply in less than ~ 150 - 200μ s. As soon as the SCR (S1) is turned off, the electrode is seen to come back to the floating potential level.

3.3. Experimental Diagnostics

3.3.1 Radial array of Langmuir probe

It is well known fact that in H-mode plasma edge parameters like electric field and density are modified. An array of Langmuir probe designed and developed to measure the modifications in radial profile of radial electric field and density in radial direction at the edge region of ADITYA tokamak plasma due to biasing. Edge parameters were measured at six radial positions at the plasma edge in typical ADITYA discharges.

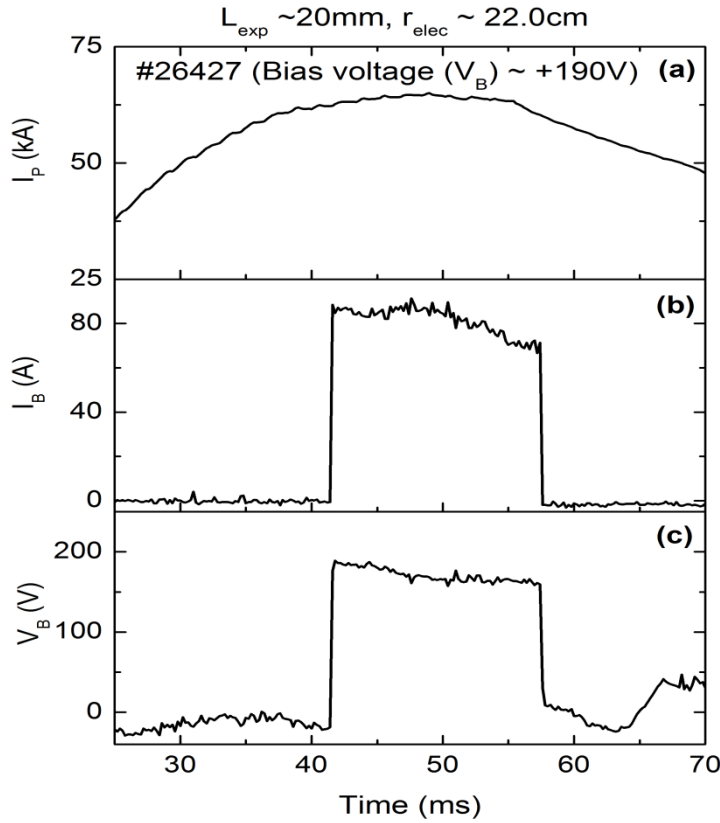


Figure 3.6. Demonstration of pulsed power supply working with the plasma load in shot #26427. Electrode exposed length in plasma and radial position of its tip from plasma center are $L_{exp} \sim 20$ mm and $r_{elec} \sim 22$ cm, respectively. Temporal profile of (a) plasma current (I_P), (b) drawn electrode current (I_B) and (c) biasing voltage (V_B) across electrode and ground. At $t \sim 41$ ms electrode is biased at $V_B \sim 190$ V and electrode draws $I_B \sim 80$ A current. At $t \sim 57$ ms electrode biasing is switched off using commutation circuit in the pulsed power supply. Before the biasing is switched on electrode is at floating potential of plasma and no current is drawn by the electrode.

3.3.1.1 Theory

In tokamaks Langmuir probes are generally used to measure local plasma density, electron temperature and plasma potential at the plasma edge [3.3 – 3.5]. In this technique the current to the probe is monitored as the probe voltage changes.

If the probe is sufficiently negative, it draws only ions and current flowing in Langmuir probe circuit is ion saturation current. As probe voltage Φ becomes less negative with respect to the plasma, energetic electrons from the tail of the distribution are also collected by the probe until, at the floating potential Φ_f . At this point electron and ion currents cancel one another

Chapter 3: Experimental Set-up

and probe draws no current. A further increase in Φ leads to a steep rise in electron current which eventually saturates at space potential, the potential of the plasma Φ_p .

If the probe is sufficiently negative, the potential at the sheath edge $\Phi_s \approx -k_B T_e / 2e$. At the plasma-sheath interface electron and ion density is approximately $n_{is} = n_{es} (= n_0 \exp(e\Phi_s / k_B T_e)) \approx 0.6n_0$, where $n_0 (= n_{i0} = n_{e0})$. n_{i0} and n_{e0} are ion and electron density far from the probe.

For a potential more negative than the floating potential Φ_f the electron contribution to the current drops off until the probe draws only ion current given by $I_{is} = n_{is} \bar{v}_{is} eA / 4$, where A is the surface area of the probe. If in the vicinity of the sheath $\bar{v}_i = C_s = (k_B T_e / m_i)^{1/2}$, ion saturation current is given by

$$I_{is} \approx (0.6n_0) C_s eA / 4 = 0.6n_0 eA (k_B T_e / m_i)^{1/2}. \quad (3.1)$$

In the regime $\Phi_f < \Phi < \Phi_p$, in which electron current is drawn, the electron sheath shields the probe from electrons of low energy and electrons with sufficient energy overcome this potential barrier. In thermal equilibrium the electron current to the probe is then the random current, reduced by the Boltzmann factor, i.e.,

$$I_e = \frac{n_0 eA}{2} (2k_B T_e / \pi m_e)^{1/2} \exp(e\Phi / k_B T_e) \quad (3.2)$$

The floating potential is defined by $I_i = I_e$, i.e., when no current flows in the Langmuir probe circuit. This is given by the expression

$$\Phi_f = \frac{T_e}{2e} \left[\ln \left(2\pi \frac{m_e}{m_i} \right) - 1 \right] \quad (3.3)$$

Plasma potential is given by the relation

$$\Phi_p = \Phi_f + \frac{k_B T_e}{2e} \ln \left(\frac{2m_i}{\pi m_e} \right) \quad (3.4)$$

For hydrogen plasma $\frac{k_B T_e}{2e} \ln \left(\frac{2m_i}{\pi m_e} \right) \sim 3.5T_e (eV)$.

Electric field between two Langmuir probes can be estimated by measuring floating potentials and electron temperatures by the two probes as $E = -(\Phi_{p1} - \Phi_{p2}) / d$, where d is the separation between the two probes, Φ_{p1} and Φ_{p2} are estimated plasma potential by the two probes.

3.3.1.2 Probe construction and installation

The radial profile of floating potential has been measured using a radial array of six single Langmuir probes mounted on top port toroidally ~ 180 degree away from electrode location (Fig.3.7). All the components inside Langmuir probe assembly were fastened with screws and by making threads. Pumping holes have been provided in different components to minimize trapping of gas. Assembly was tested for ultra-high vacuum (UHV) condition up to 3×10^{-9} Torr.

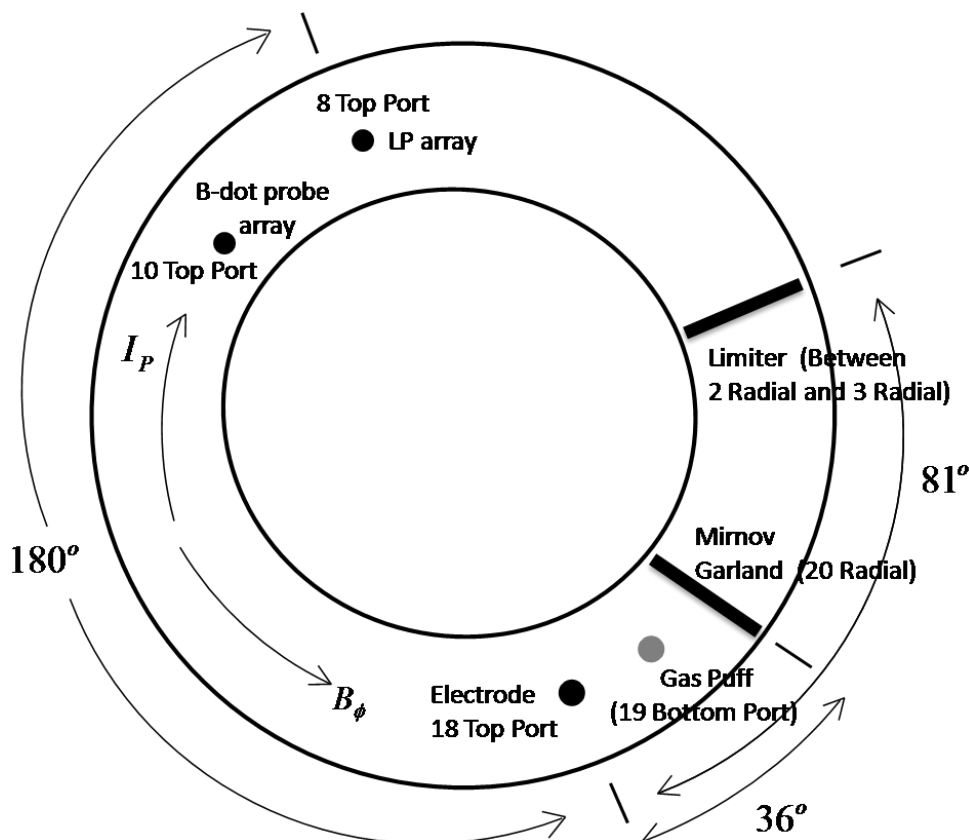


Figure 3.7. Top view of ADITYA tokamak shows location of electrode assembly, Langmuir probe array, B-dot probe array, Gas puffing system, Mirnov garland and limiter

These cylindrical shaped Langmuir probes were used to measure radial profiles of floating potential and density near edge during biasing. The probe tips are made of Molybdenum and each cylindrical probe has length and diameter 2mm and 3mm , respectively. The centre to centre distance between two adjacent probes is $\sim 7\text{mm}$. Each probe's cylindrical neck is covered with ceramic sleeve. The picture of the probe array is shown in Fig.3.8.

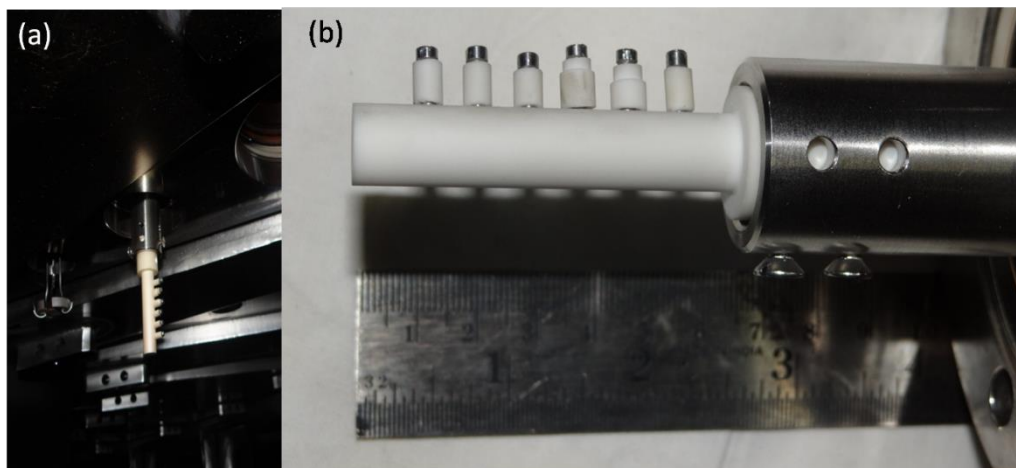


Figure 3.8. (a) Inner view of ADITYA showing Langmuir probe array mounted on top of machine and (b) Langmuir probe array. Each probe's neck is covered with ceramic sleeve.

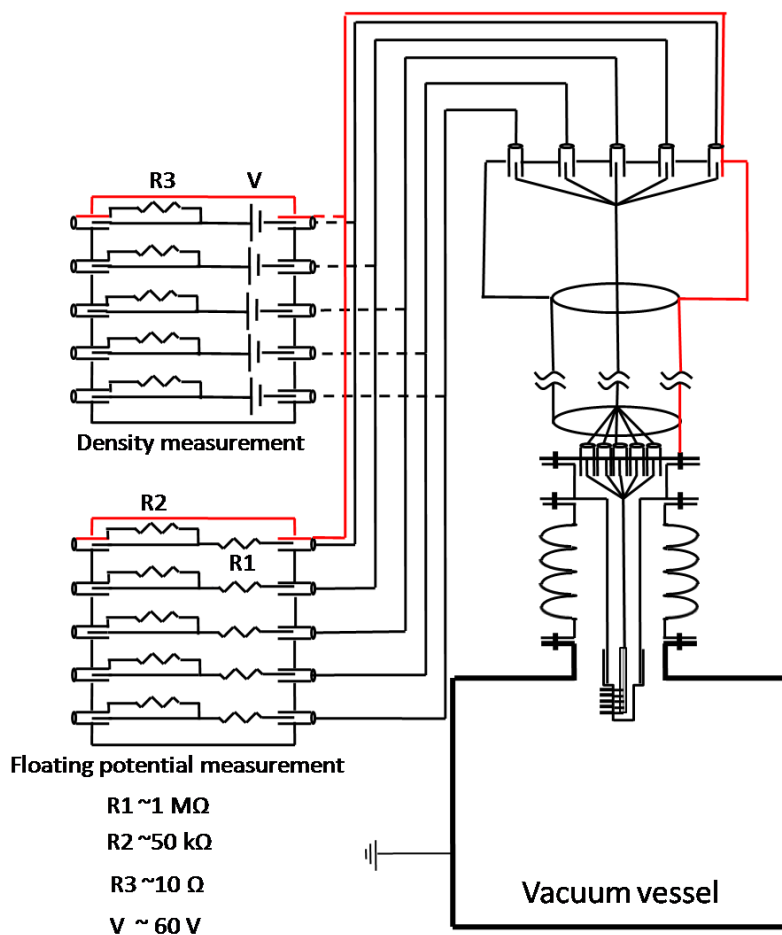


Figure 3.9. Circuit descriptions of plasma floating potential and density measurements by Langmuir probe array. A floating power supply was used to measure plasma density. Red coloured lines show grounding scheme for the measurements.

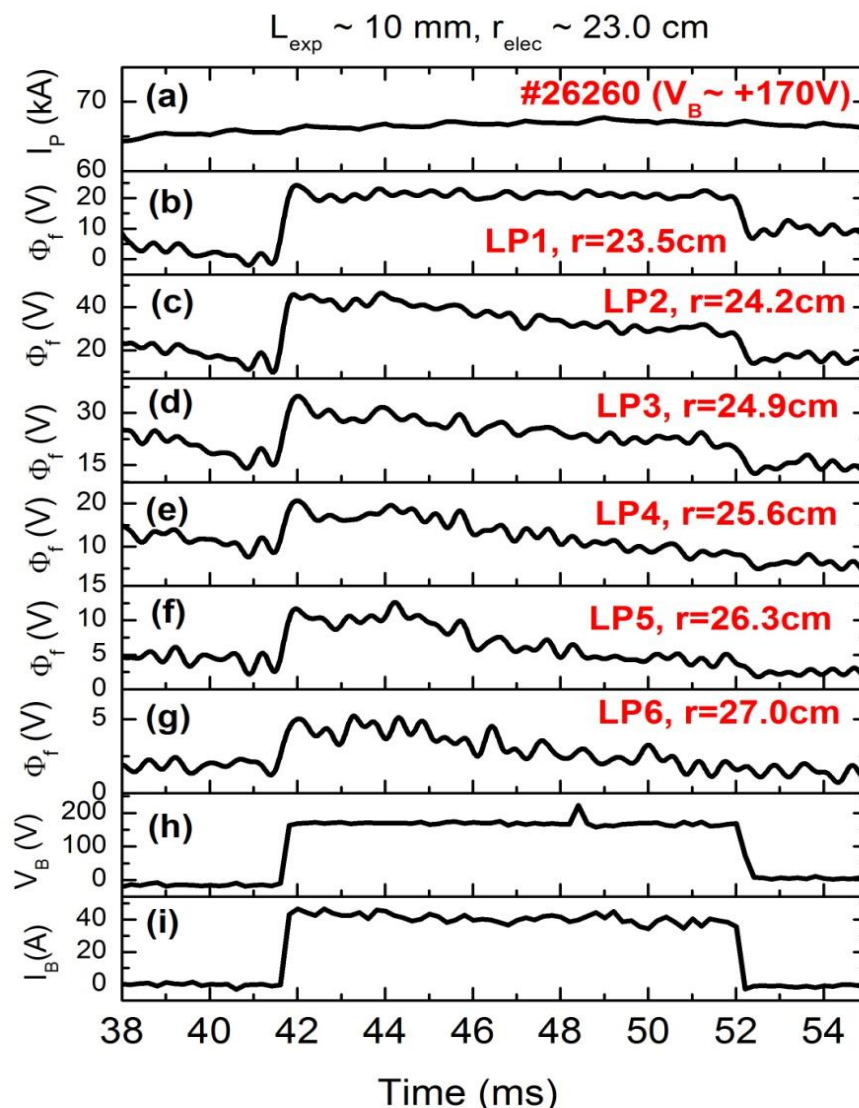


Figure 3.10. (a) Plasma current, (b - g) floating potential (Φ_f) measured by 6 Langmuir probes, (h) electrode voltage, and (i) electrode current for shot no #26260.

3.3.1.3 Measurements

Floating potential measurements have been carried out by directly connecting the probes to the data acquisition through a resistive voltage divider (1:20) and an opto-isolator. For density measurements, the probes were biased by floating power supplies at $\sim -60\text{V}$ and the probe current is measured by measuring voltage drop across $\sim 10\Omega$ resistance. Fig.3.9 shows the block circuit diagram of both the measurements. Both floating potential and density signals are digitized at a frequency $\sim 100 \text{ kHz}$. The change in floating potential at various radial locations during the biasing is clearly seen in Fig. 3.10, which shows temporal evolution of plasma current, floating potential measured at six radial positions, bias voltage

and electrode current. Fig. 3.11 compares the radial profile of floating potential (Φ_f) in discharge #26260 prior to biasing (~ 40 ms) and during biasing (~ 42 ms). It is clear from the figure that during biasing the profile (profile refers to radial profile throughout the text) of floating potential steepens near the edge region of plasma in between electrode location and the limiter as observed previously in other biasing experiments [3.1, 3.2, 3.6, 3.7]. In this discharge $d\Phi_f/dr$ changes to 1.3×10^3 V/m after biasing (~ 42 ms) from its value -0.43×10^3 V/m before electrode biasing (~ 40 ms). Application of positive biasing voltage to electrode results in the extraction of electrons from the plasma. To prevent an indefinite charge build-up, the plasma reacts by setting up a increased plasma potential to generate radial electric field E_r capable of driving out ions to the wall. More, the biasing voltage, more electrons are drawn from the plasma, higher the plasma potential develops to set up larger electric field. As the relation between the plasma potential (Φ_p) and floating potential is given by $\phi_p = \phi_f + 3\nabla T_e / e$, the plasma potential will vary in the same way as floating potential varies if the temperature (T_e) remains constant. Assuming the biasing does not change the electron temperature significantly in this region the steepening of floating potential profile reflects the steepening of plasma potential profile which indicates the setting up off sheared radial electric field (E_r) in this region due to application of bias voltage to the electrode.

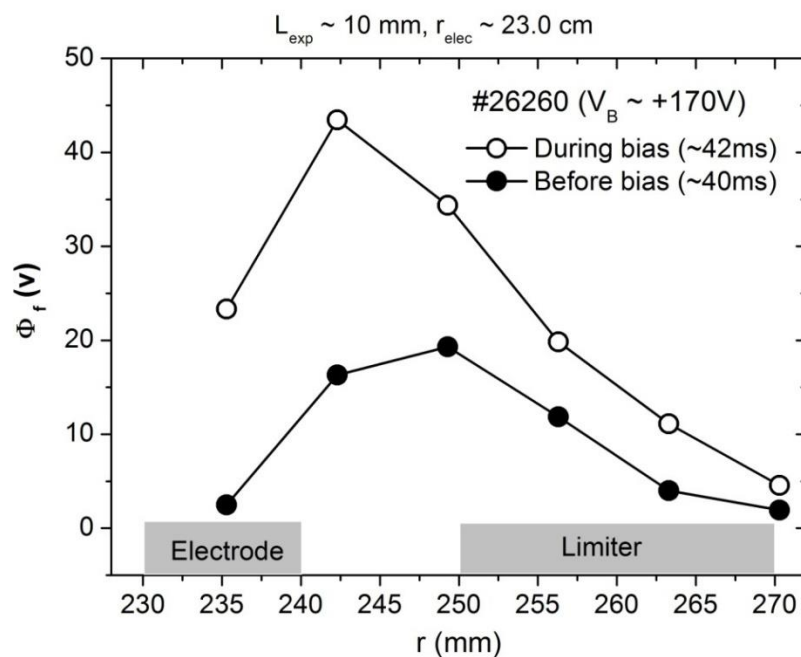


Figure 3.11. Radial profile of floating potential (Φ_f) for discharge #26260 measured by Langmuir probe prior to biasing (~ 40 ms) and after biasing (~ 42 ms).

3.3.2 Radial array of radial and poloidal magnetic probes

A radial array of radial and poloidal magnetic probes array were used to measure change in radial profile of toroidal current density at the plasma edge due to bias voltage.

3.3.2.1 Theory

Plasma current density measurements using magnetic probes

The Maxwell's equation $\nabla \times B = \mu_0 J$ can be written in cylindrical geometry as

$$\frac{1}{r} \frac{d}{dr} (rB_\theta(r,t)) - \frac{1}{r} \frac{d}{d\theta} (rB_r(r,t)) = \mu_0 J_z(r,t) \quad (3.5)$$

Assuming magnetic surfaces are concentric, the components of B_r may be ignored and hence we have

$$\frac{1}{r} \frac{d}{dr} (rB_\theta(r,t)) = \mu_0 J_z(r,t) \quad (3.6)$$

Now let us assume a current profile

$$J_z = J_0 \left(1 - \left(\frac{r^2}{a^2} \right) \right)^n \quad (3.7)$$

where a is the plasma radius and n is a parameter to be determined experimentally. Replacing J_z of eqn. 3.6 by eqn.3.7 and then integrating with boundary condition, at $r=0$, $B_\theta = 0$, we have

$$1 - \left(1 - \frac{r^2}{a^2} \right)^{n+1} = \frac{2(n+1)}{\mu_0 J_0 a^2} r B_\theta \quad (3.8)$$

Now the eqn. 3.8 can be fitted with the experimental values of $B_\theta(r)$ measured using magnetic probes at different r treating n as a fitting parameter. Once n is known the current density distribution can easily be deduced from eqn. 3.7.

3.3.2.2 Probe construction and installation

A radial array of B-dot coils was employed in this experiment on ADITYA in toroidal direction $\sim 216^\circ$ away from electrode counter-clock wise as seen from top (Fig. 3.7) to measure poloidal and radial magnetic field. The array has five poloidal field sensing probes and five radial field sensing probes placed alternately (Fig. 3.12). Poloidal and radial coil consists of ~ 125 and ~ 400 turns of 40AWG kapton enamelled copper wire wound around macor ceramic rod. Radial coils have inner diameter 5mm and outer diameter ~ 9 mm.

Poloidal coils have inner diameter $\sim 5\text{mm}$ and outer diameter $\sim 11\text{mm}$. Separation between radial and poloidal coil is $\sim 9.5\text{mm}$. Length of radial and poloidal coils is $\sim 4\text{mm}$ and $\sim 3\text{mm}$ respectively. Coils were covered with grounded (with vessel) $25\mu\text{m}$ Al foil to shield electrostatic fluctuations to avoid capacitive pickup by electric fields. The probes are inserted into a ceramic tube of 14mm diameter for particle shielding. Magnetic probe array assembly is shown in Fig. 3.13.

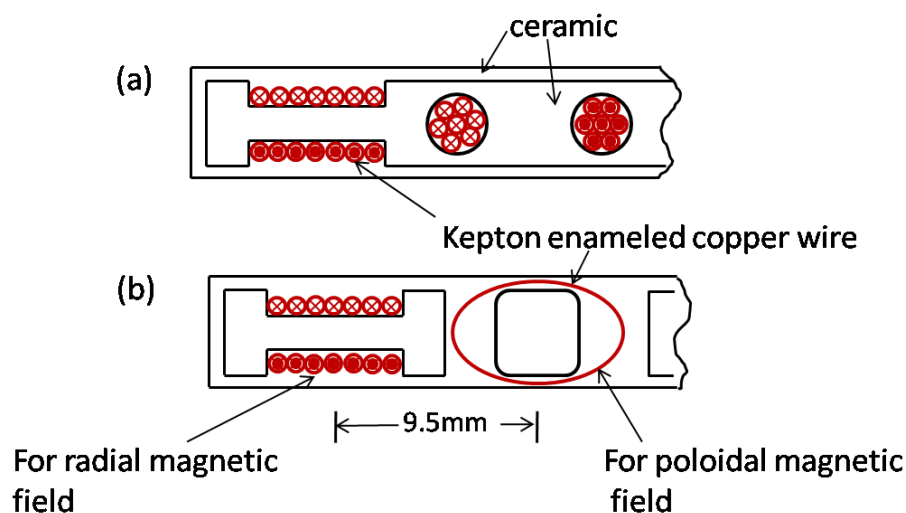


Figure 3.12. Schematic drawing of a section of B-dot probe array. There are five such sections in the array, which measure radial profiles of radial and poloidal magnetic field. Figure (a) shows cross-section of the two B-dot probes measuring radial and poloidal magnetic field. Figure (b) is another cross-sectional view of same section of the B-dot probe at 90° angle of the figure (a).

3.3.2.3 Calibration of probes

Magnetic probes were calibrated for sensitivity and frequency response before use in the actual experiments.

(a) **Calibration for sensitivity:** Sensitivity is simply proportional to the area-turns product of the coil, i.e., $na = V / (dB / dt)$ [3.4], where V is the coil voltage before integration, n is the number of turns, a is the area per turn in m^2 , and dB / dt is the rate of field change in T/s . To calibrate magnetic field sensors a Helmholtz coil was used as a magnetic field generator. All the probes were calibrated for sensitivity by 50Hz current in Helmholtz coil. Let us first discuss Helmholtz coil which we used for calibration.

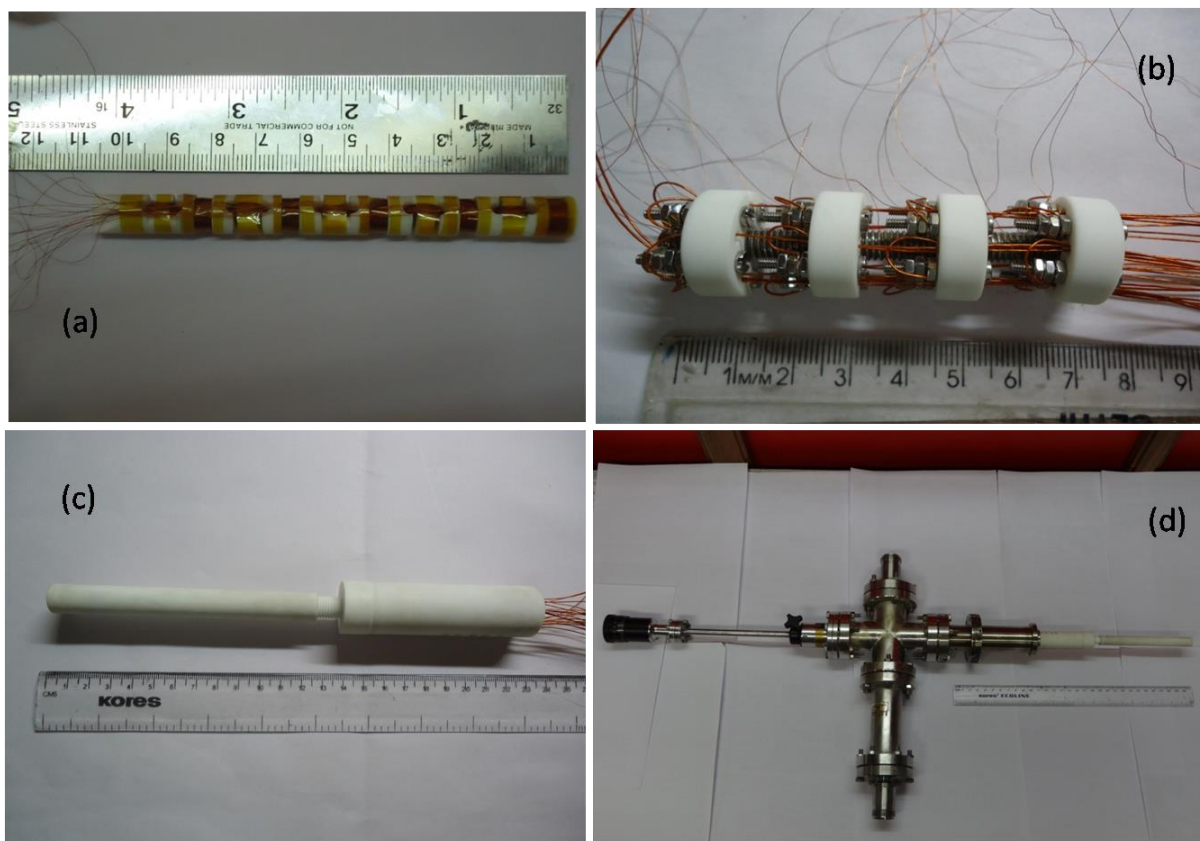


Figure 3.13. Construction of magnetic probe array: (a) array of magnetic probes to measure radial and poloidal magnetic fields, (b) electric connections of the probes, (c) probes covered with ceramic and (d) magnetic probe assembly.

Helmholtz coil

Helmholtz coil (Fig. 3.14) pair consists of two identical coils, each of radius $R= (225\text{mm})$, separated by the same distance R and carrying current $I = \sim 0\text{-}22 A_{p-p}$. The axial field due to Helmholtz coil is given by

$$B_z(z) = \frac{\mu_0 N I R^2}{2} \left[\left(z + \frac{R}{2} \right)^{-3/2} + \left(z - \frac{R}{2} \right)^{-3/2} \right], \quad (3.9)$$

where number of turns in each coil is $N = 50$. Magnetic field in a half-way between the

Helmholtz coils, i.e., $z = R/2$, is very homogeneous and given by $B_z = \frac{8N}{5\sqrt{5}} \frac{I\mu_0}{R} \text{Tesla}$

Effective area (na) for each B-dot probe in B_z field of Helmholtz coil,

$$na = V / \left(\frac{8N}{5\sqrt{5}} \frac{\mu_0}{R} \frac{dI}{dt} \right) = V / \left(\frac{8N}{5\sqrt{5}} \frac{\mu_0}{R} (2\pi f) I \right). \quad (3.10)$$

Again, for $f = 50\text{Hz}$ current I in Helmholtz coil, slope of V vs I gives effective area for each coil. Measured effective area of radial and poloidal probes are $na \sim 0.0068\text{-}0.0076 \text{ m}^2\text{-turns}$ and $na \sim 0.0020\text{-}0.0027 \text{ m}^2\text{-turns}$, respectively.

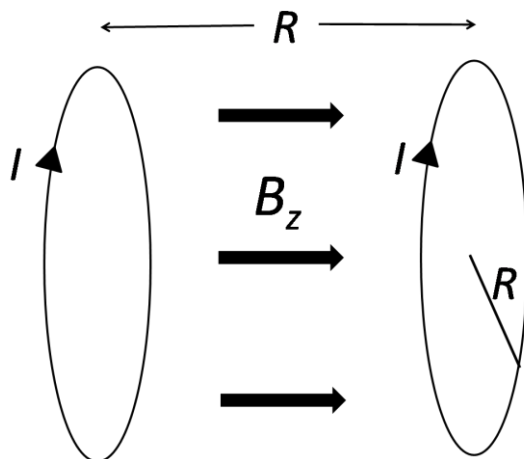


Figure 3.14. Helmholtz coil arrangement

(b) Frequency response: The frequency response of the coil is determined by the time constant $\tau = L/R$, which is the shortest field –fluctuation time the coil will respond to with adequate sensitivity. L is the inductance of the coil and R is the resistance connected across its output. Inductance and resistance of the probes was measured using LCR meter. Inductance, resistance and frequency response for these probes are shown in Table 3.1.

(c) In-situ calibration of probes

Sensitivity of magnetic probes may get affected because of misalignment during the installation on vacuum vessel. Therefore, in-situ calibration was carried out to identify toroidal magnetic field direction after the installation of the probes on the tokamak. For this toroidal magnetic field coils were energized without plasma.

	Radial probes	Poloidal probes
Resistance	$\sim 39\Omega$	$\sim 18\Omega$
Inductance (at 120Hz)	$\sim 900\mu\text{H}$	$\sim 125\mu\text{H}$
Frequency response (R/L)	$\sim 43\text{kHz}$	$\sim 144\text{kHz}$

Table 3.1. Frequency response measurement of radial and poloidal probes

3.3.2.4 Measurements

As the poloidal magnetic field is generated by toroidal plasma current, integrated signal follows temporal profile same as the plasma current. Fig. 3.15 shows the poloidal magnetic field measured using five poloidal probes in the array at five radial locations for discharge #26332.

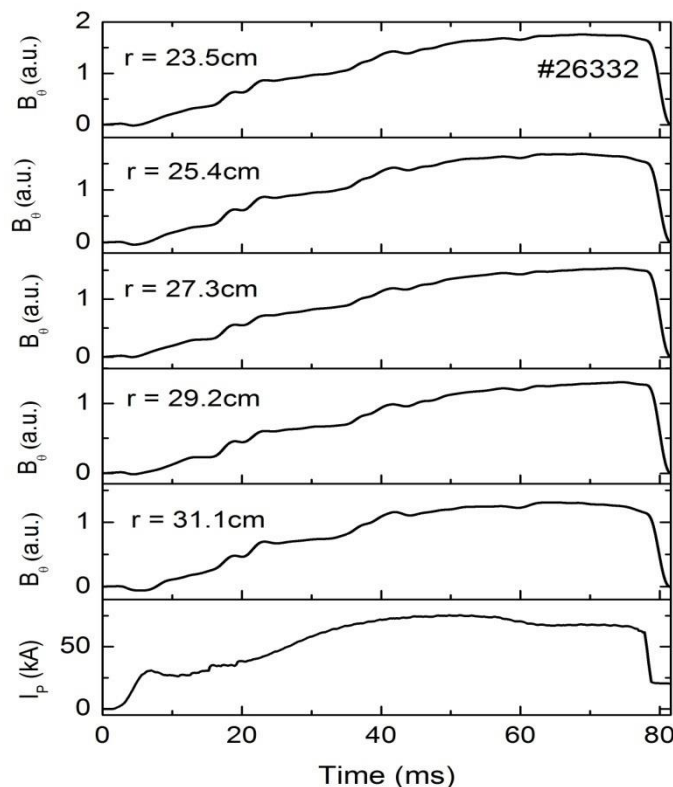


Figure 3.15. Poloidal magnetic field measurement by magnetic probe array at different radial locations for discharge #26332

3.4 Techniques for MHD island identification and island width calculations

3.4.1 Singular Value Decomposition (SVD) method

In present thesis to estimate tearing mode number and their island size Singular Value Decomposition (SVD) technique [3.8] has been used. Tearing mode number is depicted from poloidal structure of the mode, which is calculated by poloidal array of magnetic probes measuring \dot{B}_θ fluctuations.

The method is based on a theorem from linear algebra which says that a rectangular matrix X can be broken into the product of three matrices- an orthogonal matrix V , a diagonal matrix S , and the transpose of an orthogonal matrix U . The theorem is usually presented something like this:

$$X_{nm} = V_{nm} S_{nm} U_{nm}^T \quad (3.11)$$

where $V^T V = I$, $U^T U = I$; the columns of V are orthonormal eigenvectors of XX^T , the columns of U are orthonormal eigenvectors of $X^T X$, and S is a diagonal matrix containing the square roots of eigen values from V or U in descending order (putting the largest in s_{11} , the next largest in s_{22} and so on until the smallest value ends up in s_{nm}).

By SVD technique coherent overall structure can be extracted by the Mirnov coil signals which can be considered as a collection of oscillating time series. In this method Mirnov garland data obtained in M channels of one discharge is expressed as a matrix. All channels are sampled at same frequency. Matrix possesses the i -th time sample of the j -th channel as its (i, j) element.

Consider time series of M -channels of \dot{B}_θ oscillations simultaneously measured at different poloidal positions are arranged as a M -dimensional vectors $x(t) = [x_1(t), x_2(t), \dots, x_M(t)]$. Each channel data is a time series sampled every t_s seconds leads to a set of N vectors $x(0), x(t_s), \dots, x((N-1)t_s)$. A $N \times M$ rectangular matrix can be written as

$$X = \frac{1}{\sqrt{N}} \begin{pmatrix} x(0) \\ x(t_s) \\ \dots \\ x((N-1)t_s) \end{pmatrix} = \begin{pmatrix} x_1(0) & \dots & x_m(0) \\ \dots & \dots & \dots \\ x_1((N-1)t_s) & \dots & x_m((N-1)t_s) \end{pmatrix} \quad (3.12)$$

Singular Value Decomposition of above matrix is a product of three matrices as given by (3.11). The vectors $u^{(j)}$, called *principal axes*, form an orthonormal basis on which the signal decomposed. Since this basis diagonalizes the covariance matrix, it is expected that it describes better the features of the whole signal. In Matrix 'S' Diagonal elements are called *singular values*. Matrix 'U' is the *principal axis* and depicts about spatial structure of \dot{B}_θ fluctuations for a mode. Matrix V is the *principal component* and gives temporal profile of \dot{B}_θ fluctuation for a mode.

3.4.2 Soft X-ray tomographic reconstruction

Sawtooth oscillations (internal disruptions) and major disruptions are routinely observed in Ohmically heated ADITYA tokamak discharges. Soft x-ray (SXR) tomography is used as the main tool to analyse the instabilities in the tokamak discharges along with other supportive diagnostics. From chord-integrated measurements, a 2-D X-ray image of the plasma cross-

section can be derived. This can provide much information on the plasma structure and the evolution of the image with time is useful for studying MHD instabilities.

In analytical method [3.9], using the polar coordinate system (r, θ) as shown in Fig. 3.16, the signal from each detector is proportional to the x-ray chord brightness, $f(p, \phi)(W/m^2/sr)$, and it is related to the local emissivity $g(r, \theta)(W/m^3)$ through $f(p, \phi) = \int_{L(p, \phi)} g(r, \theta) dl$ with the integration performed along a line of sight $L(p, \phi)$ of a detector through the plasma. If the emissivity is circularly symmetric, i.e., $g(r, \theta) \equiv g(r)$ the equation would reduce to 1-D integral commonly known as Abel transform. Cormak [3.10, 3.11] derived an analytic solution to the tomography problem and demonstrated its application to imaging which was free from any assumption with regards to plasma rotation, position and symmetry.

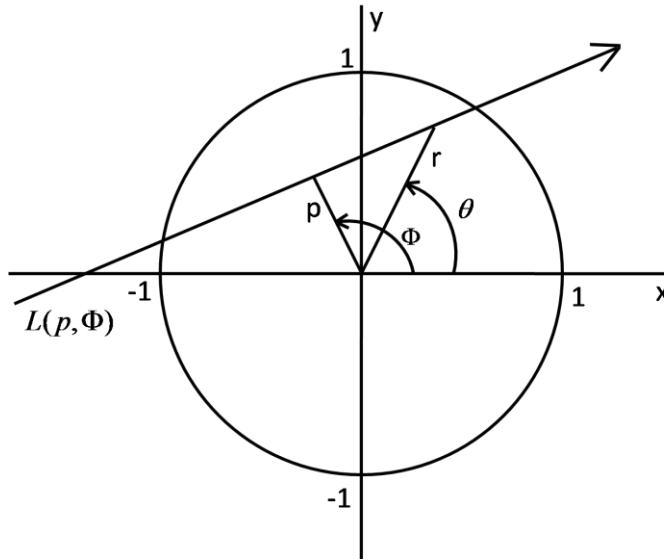


Figure 3.16. Detectors integrate the local emission, $g(r, \theta)$ along lines-of-sight, L , defined by (p, ϕ) . The emitting region must be completely contained within the circular region.

SXR tomography analysis [3.12, 3.13] presented in this thesis has been done with the help of a single array of detectors assuming rigid rotation of the modes to analyse the mode structure of internal disruption. The dominant frequencies obtained by the fast Fourier transform (FFT) analysis of the signal at the time of internal disruption are the harmonics of the same mode which are common in toroidal system. Singular value decomposition (SVD) method has been used to analyse the time series of tomographic reconstructions to identify the $m/n=1/1$ modes magnetohydrodynamic modes and to show different features of the spatio-temporal evolution of the emissivity distribution. Fourier-Bessel function [3.14] used as the base function for radial distribution, which is consistent with the boundary condition that

polynomial should have a value of zero at the boundary because there is no x-ray emission from the cool boundary region.

3.5 References

- [3.1] R. J. Taylor, et al., *Phys. Rev. Lett.* **63**, 2365 (1989)
- [3.2] L. G. Askinazi, et al., *Nucl. Fusion* **32**, 271 (1992)
- [3.3] T. J. M. Boyd and J. J. Sanderson, *The Physics of Plasmas*, Cambridge University Press, 2003
- [3.4] I. H. Hutchinson, *Principles of Plasma Diagnostics* (second edition), Cambridge University Press, 2002
- [3.5] F. F. Chen, *Introduction to Plasma Physics and Controlled Fusion* (second edition, **Vol 1: Plasma Physics**) Springer Science, 2006
- [3.6] R. R. Weynants, et al., *Nucl. Fusion* **32**, 837 (1992)
- [3.7] E. Y. Wang, et al., *Nucl. Fusion* **35**, 467 (1995)
- [3.8] C. Nardone, *Plasma Phys. Control. Fusion* **34**, 1447 (1992)
- [3.9] R. S. Granetz, P. Smeulders, *Nucl. Fusion* **28**, 457 (1988)
- [3.10] A. M. Cormack, *J. Appl. Phys.* **34**, 2722 (1963)
- [3.11] A. M. Cormack, *J. Appl. Phys.* **35**, 2908 (1964)
- [3.12] A. K. Chattopadhyay, C. V. S. Rao, S. K. Mattoo and R. Srivatsan, Institute for Plasma Research Technical Report, **IPR/TR-88/2002** (2002)
- [3.13] A. K. Chattopadhyay et al., *Indian J. Pure Appl. Phys.* **44**, 826 (2006)
- [3.14] A. K. Chattopadhyay and C.V.S. Rao, *Pramana- Journal of Physics* **Vol. 61, No. 1, July**, 141 (2003)

Chapter 4

Disruption Mitigation Using Biased Electrode in ADITYA Tokamak

4.1 Introduction

In tokamaks, sometimes plasma current is lost abruptly resulting in plasma disruptions [4.1, 4.2]. Plasma disruptions in tokamaks result not only in complete loss of plasma current but also in unacceptable large power and force loads on surrounding structures having potential to damage the machine itself. This is of great concern to fusion community for successful operation of magnetically confined fusion reactors and it must be avoided. Lot of efforts have been devoted over the years to explore various ways to avoid disruptions. Stabilisation of magnetohydrodynamic (MHD) modes or suppression of magnetic islands is a key ingredient to the solution of this problem. Depending upon the device and the disruption mechanism successful avoidance of disruption using electron-cyclotron-resonance heating (ECRH) has been obtained in many tokamaks such as FTU [4.3], JFT-2M [4.4], RTP [4.5] and T-10 [4.6]. In FTU it has been shown that MHD mode coupling plays an important role during disruptions, which can be exploited for disruption avoidance through localised ECRH injection. Other than ECRH, electron-cyclotron current drive (ECCD) [4.7], and neutral beam (NB) heating [4.8] has also been successfully attempted to avoid disruptions in DIII- D and TEXTOR tokamaks respectively through MHD mode stabilization. Spontaneous disruptions occurring naturally during the end phase of the SINP- tokamak discharges are also found to be significantly influenced by electrode biasing [4.9].

In this chapter a set of experiments performed in the ADITYA tokamak [4.10] is presented, in which the deliberately incited disruptions using H₂ gas-puff are successfully mitigated through application of positive bias voltage on a Molybdenum (Mo) electrode placed inside the LCFS. The injection of H₂ gas-puff instigate MHD perturbations that grow in amplitude and stop rotating by being locked through coupling between different modes and causing

disruption of the plasma. By applying positive bias voltage larger than some threshold value to the electrode placed inside the LCFS prior to the gas injection leads to substantial reduction in the growth of magnetic islands corresponding to $m/n = 3/1, 2/1$ MHD modes, which in turn prevents them from locking and delays or avoids the current quench. The stabilisation of MHD-modes or suppression of magnetic islands by plasma rotation has been established both experimentally [4.11] and theoretically [4.12, 4.13] with flows arising from variety of causes such as unbalanced neutral beam injection, radio frequency heating or as a by-product of micro-turbulence. It has been shown analytically as well as numerically that sheared plasma toroidal or poloidal flow can change the linear stability of resistive tearing modes, hence suppressing the magnetic islands. In TCABR tokamak, MHD mode suppression was observed with electrode biasing and sheared plasma rotation was conjectured as possible explanation [4.14]. In this work, the sheared (shear refers to the radial gradient) poloidal plasma rotation through $J_r \times B_\phi$ force generated by biased electrode has been exploited to linearly stabilize the conventional tearing modes leading to suppression of magnetic island growth and delaying or avoidance of disruptions. Increasing the poloidal plasma rotation and its shear in the vicinity of $m/n = 3/1$ island location by biased electrode prevents the growth of both $m/n = 2/1, m/n = 3/1$ MHD modes indicating these modes are toroidal sidebands of each other and leads to delay or avoidance in current quench.

4.2 Observations of suppression of MHD fluctuations with bias

Experiments reported in this thesis were performed by inserting the Molybdenum electrode of 5 mm diameter from the top port of the ADITYA tokamak. Fig. 4.1 shows a schematic diagram of the whole set-up for biasing the electrode positively. First we intend to find most effective electrode exposed length (L_{exp}) along with its position (r_{elec}) responsible for the L-H transition and disruption avoidance, by moving specially designed electrode-holding assembly in-situ. After obtaining stable and reproducible plasma discharges the electrode tip is placed at different radial locations inside the LCFS until the presence of the electrode disturbs the plasma. No noticeable change in discharges regarding its reproducibility in terms of achieving same plasma current, density and temperature compared to typical ADITYA discharges without the electrode is observed by placing the electrode up to 3.5 cm inside the LCFS with an exposed length of ~ 20 mm. When the electrode tip (5 mm diameter) is placed beyond ~ 3.5 cm inside the plasma with an exposed length of ~ 20 mm, the insulating ceramic sleeve, which is ~ 20 mm in diameter moves beyond ~ 2.0 cm inside the LCFS and

causes significant reduction in overall plasma density and temperature compared to those of a typical ADITYA discharge. Further, in this case the reproducibility of plasma discharges is lost and frequent disruptions of plasma current are also observed. Keeping the insulating sleeve below 2.0 cm inside the LCFS, the electrode tip position can be moved beyond 3.5 cm inside the LCFS, however, then the electrode exposed length becomes more than 20 mm, which draws higher currents at low voltages in typical discharges of ADITYA tokamak causing frequent minor disruptions leading to major disruptions on many occasions. Fig. 4.2(a) compares the plasma currents in two discharges, one without bias and one with the application of ~ 110 Volts to the electrode placed at $r_{elec} \sim 21.5$ cm with an exposed length ~ 25 mm. In this case the electrode draws ~ 80 A at ~ 110 V of electrode voltage [Fig.4.2 (b, c)] and the biased discharge disrupts as the current falls abruptly after the application of bias. Hence, the electrode tip has been varied from 1 cm to 3.5 cm inside LCFS with its exposed length varied from 10 mm – 25 mm.

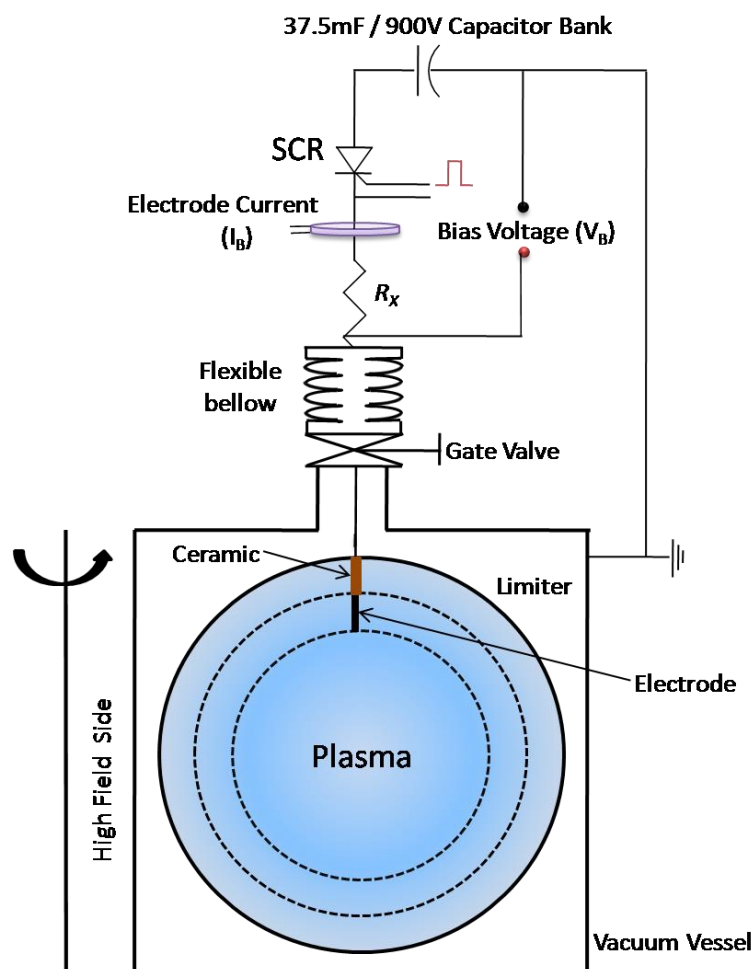


Figure 4.1. Schematic diagram of electrode biasing set-up for positive biasing.

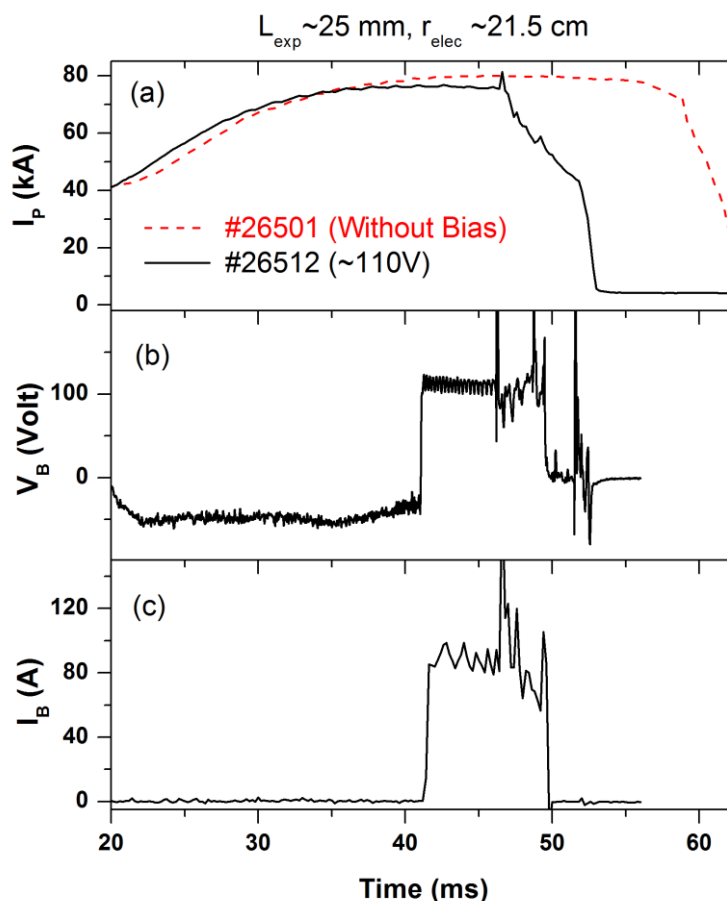


Figure 4.2. (a) Comparison of plasma current from two discharges (#26501 without bias in red dashed line and #26512 with bias in black solid line) with electrode placed at $r_{elec} \sim 21.5$ cm with an exposed length $L_{exp} \sim 25$ mm in the biased discharge. (b) Electrode voltage, V_B and (c) electrode current, I_B in biased discharge # 26512.

Fig. 4.3 shows the variation of current drawn by the electrode as a function of biasing voltage for electrode tip kept at 2 cm – 3.5 cm inside the LCFS with various electrode exposed lengths (10 mm – 25 mm) in plasma. With the electrode tip kept at $r_{elec} = 23$ cm, the variation of electrode exposed length from 10 to 15 mm does not change the electrode currents drawn with different biasing voltages and in all these cases the current saturates ~ 40 A after ~ 150 Volts. Similar trend of electrode current variation with different biasing voltages has been observed by moving the tip further inside to $r_{elec} = 22.5$ cm with electrode exposed length of 10 mm. However, changing the exposed length to 15 mm keeping the electrode tip at $r_{elec} = 22.5$ cm the electrode current increases and saturates at ~ 60 A after ~ 150 Volts. Increasing the exposed length further to ~ 20 mm, higher currents are drawn to the electrode which do not saturate reaching up to 100 A at ~ 250 V. Further increase in electrode exposed length leads to disruptions as higher currents ~ 80 A are drawn at 100 Volt as shown in Fig.4.2.

Investigating further the influence of electrode exposed length on the plasma performance it has been observed that the improvement in confinement and disruption mitigation are obtained with keeping the electrode tip at $r_{elec} = 22$ cm with an exposed length of 20 mm in typical ADITYA discharges.

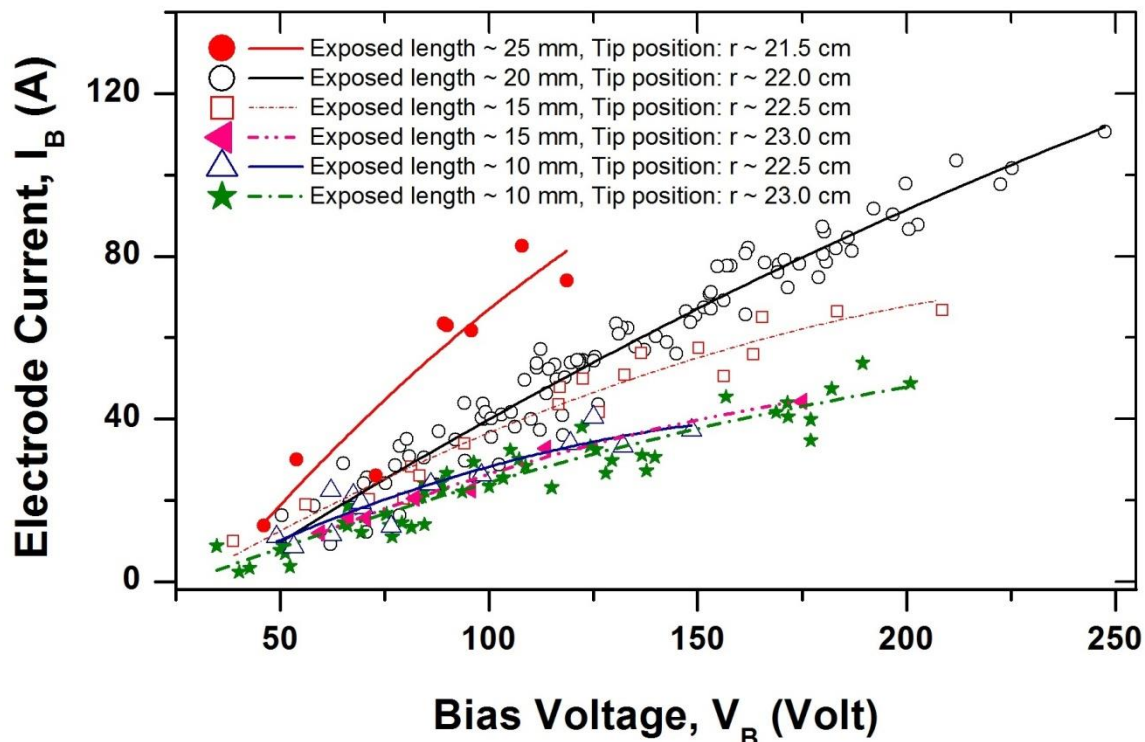


Figure 4.3. Variation of electrode current (I_B) as a function of biasing voltage (V_B) for different electrode tip positions (r_{elec}) of 2 cm – 3.5 cm inside the LCFS with various electrode exposed lengths (L_{exp}) of 10 mm – 25 mm.

Fig. 4.4 presents the temporal evolution of electrode current for different electrode exposed lengths of 10, 15, and 20 mm. Although similar electrode currents are drawn with all three exposed lengths initially after the application of bias voltage, the electrode current decreases after ~ 5 ms of application of bias voltage in case of electrode-exposed length of 20 mm placed at $r_{elec} = 22$ cm whereas it remains almost constant in other two cases. This decrease in the electrode current with the biasing voltage remains constant known as bifurcation in the electrode current, is a signature of increased perpendicular resistivity leading to improved confinement. Thus, the improvement in confinement as well as disruption mitigation has been observed mainly with electrode-exposed length of 20 mm placed at $r_{elec} = 22$ cm in typical discharges of ADITYA tokamak.

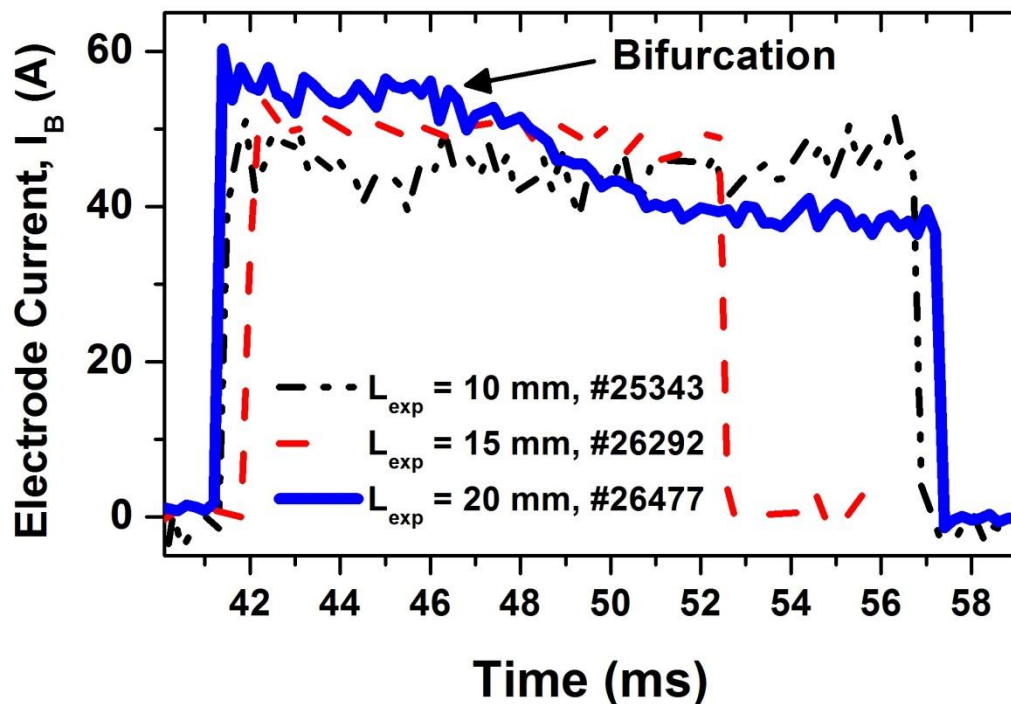


Figure 4.4. Comparison of temporal evolution of electrode current for three electrode exposed lengths of 10 mm (#25343, black dot-dash line), 15 mm (#26292, red dash line), and 20 mm (#26477, blue solid line).

The biasing experiments were carried out in the typical discharges of ADITYA tokamak by applying 20–40 ms biasing voltage pulses at the plasma current flat-top. The positive biasing of the electrode improved the energy and particle confinement of typical ADITYA discharges consistent with the previous experiments of biasing in other tokamaks [4.14-4.20]. Further investigation revealed that the biasing had a substantial effect on the MHD fluctuations along with affecting the electrostatic fluctuations, which again was in agreement to similar observations in few tokamaks [4.14, 4.21]. Suppression of MHD instabilities during different phases of discharges such as current flat-top, current ramp-down and disruptions by electrode [4.22] or limiter [4.23] biasing has been reported earlier. However, the new and important observation in our experiments was that the changes in MHD fluctuations occurred prior in time compared to the changes in the electrostatic (ES) fluctuations. Fig.4.5 shows temporal evolutions of MHD fluctuations measured by Mirnov coil, ES fluctuations in density signal measured by Langmuir probe, electrode current and bias voltage. It can be clearly seen from the figure that after the onset of the bias voltage the MHD fluctuations decreased immediately, whereas the reduction in the ES fluctuations occurred after ~ 5 ms. These observations of MHD fluctuation suppression with biasing propelled us to investigate

whether this technique can be used to mitigate the plasma disruption initiated by growth in MHD instabilities. We found the answer in affirmative and in the following we present the description of a novel approach towards controlling the tokamak disruptions by electrode biasing which is demonstrated for the first time.

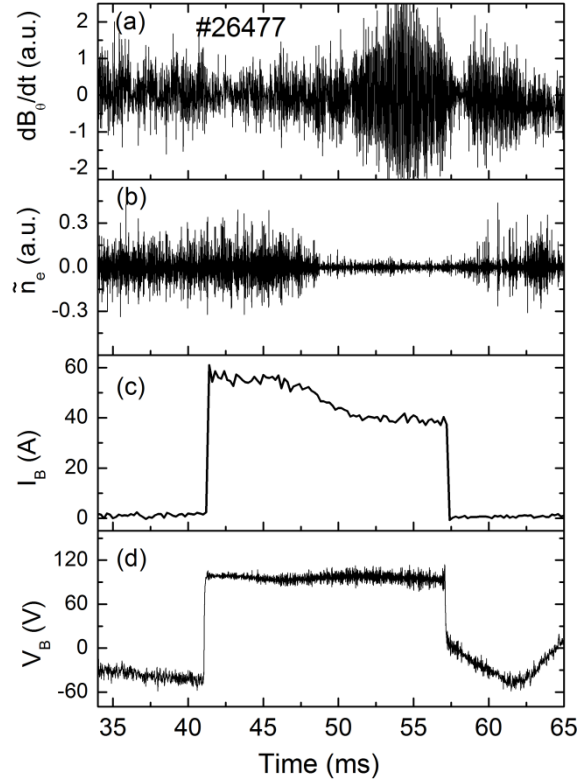


Figure 4.5. Time evolution of (a) \dot{B}_θ fluctuation at high field side, (b) density fluctuation (\tilde{n}_e), (c) Bias voltage (V_B) and (d) electrode current (I_B)

4.3 Control of MHD triggered disruption

The experiments were carried out at toroidal field $B_\phi = 0.75$ T, maximum $I_p \sim 65 - 70$ kA with electron density $\sim 1.0 - 1.5 \times 10^{19} \text{m}^{-3}$ and electron temperature $T_e \sim 350 - 450$ eV. Possibility of density limit disruption by gas puff can be ruled out because density is much lower than the Greenwald limit [4.24] $n_G = 10^{20} I(\text{MA}) / (\pi a^2) \text{m}^{-3}$ ($\sim 3.6 \times 10^{19} \text{m}^{-3}$) for ADITYA tokamak. Moreover, plasma current during experiment was ~ 70 kA which is much below the current

limit disruption [4.16] $I_p = \frac{2\pi a^2 B_\phi}{\mu_0 R q_a} \sim 100$ kA for $q_a \sim 3.5$ operation in ADITYA tokamak.

Therefore, possibility of current limit disruption is also discarded. The electrode is introduced

from the top port of the machine. These values of I_P and B_ϕ have been chosen so as to keep the island spread of $q = 3$ rational surface within the electrode exposed length or near (~ 1 cm) to the radial position of the electrode. In these discharges, the maximum input power of the bias circuit ($\sim 200V \times 75A$) is less than 10% of the flat-top Ohmic input power in ADITYA tokamak. The best results of suppression of MHD activities and disruption avoidance are obtained at electrode current of 0.1% plasma current.

After obtaining normal repetitive discharges of 70 – 80ms durations, hydrogen gas is puffed in sufficient amount during the I_P plateau phase (from 40 to 45ms) to obtain disruptive discharges. A typical gas-puff induced disruptive discharge (shot#26570) along with a discharge with disruption evasion using biased electrode (shot#26571) is shown in Fig. 4.6. Plasma current (I_P) and loop voltage (LV) for both the discharges are shown in Fig. 4.6(a). For these two discharge conditions Figs. 4.6(b) to 4.6(e) give an expanded display, covering the 40-55 ms period of the electron density (measured with microwave interferometry [4.25]), the electron temperature (measured with the transmission ratios of soft X-ray flux through two different absorber foils of 25 μm and 70 μm thickness), the soft X-ray flux and the plasma stored energy (measured by diamagnetic loop [4.26]). Corresponding time evolutions of gas-puff pulse, bias voltage and electrode current are shown in Figs. 4.6(f), 4.6(g) and 4.6(h), respectively.

The time evolution of H_α line intensity is shown in Fig. 4.6(i), which shows an increase just after the gas injection in both the discharges, confirming the presence of gas-puff in both the discharges. The avoidance of the disruption by applying a bias voltage of +190 V to the electrode is clearly demonstrated from the Figs. 4.6(a) – 4.6(e) where the plasma parameters are shown to continue unchanged unlike suffering abrupt changes in without bias case.

Further investigation in an another set of similar without-bias (shot #26714) and with-bias discharges (shot #26719) reveals that the influx of H_2 gas causes the abrupt growth of MHD modes which destroy magnetic flux surfaces creating stochastic magnetic field lines, which fill the whole plasma in a stochastic manner and leads to current quench and termination of the discharge #26714, very similar to those observed in many tokamaks during gas-puff induced density-limit disruptions [4.27, 4.28]. These modes clearly subside in the discharge with applied bias voltage of $\sim +220$ V (Fig. 4.7) and thereby avoid current disruption as shown in Fig. 4.7(a). The comparison of \dot{B}_θ oscillations measured with Mirnov coil located at the mid-plane in the low-field side for disruptive discharge and one in which the disruption is avoided is shown in Fig. 4.7b and 4.7c, respectively. Their time-frequency analysis using

short-time FFT is shown in Fig. 4.7d and 4.7e respectively. The island width of $m = 2$ and $m = 3$ islands between the disruptive discharge and one in which the disruption is avoided is shown in Fig. 4.7f and 4.7g respectively.

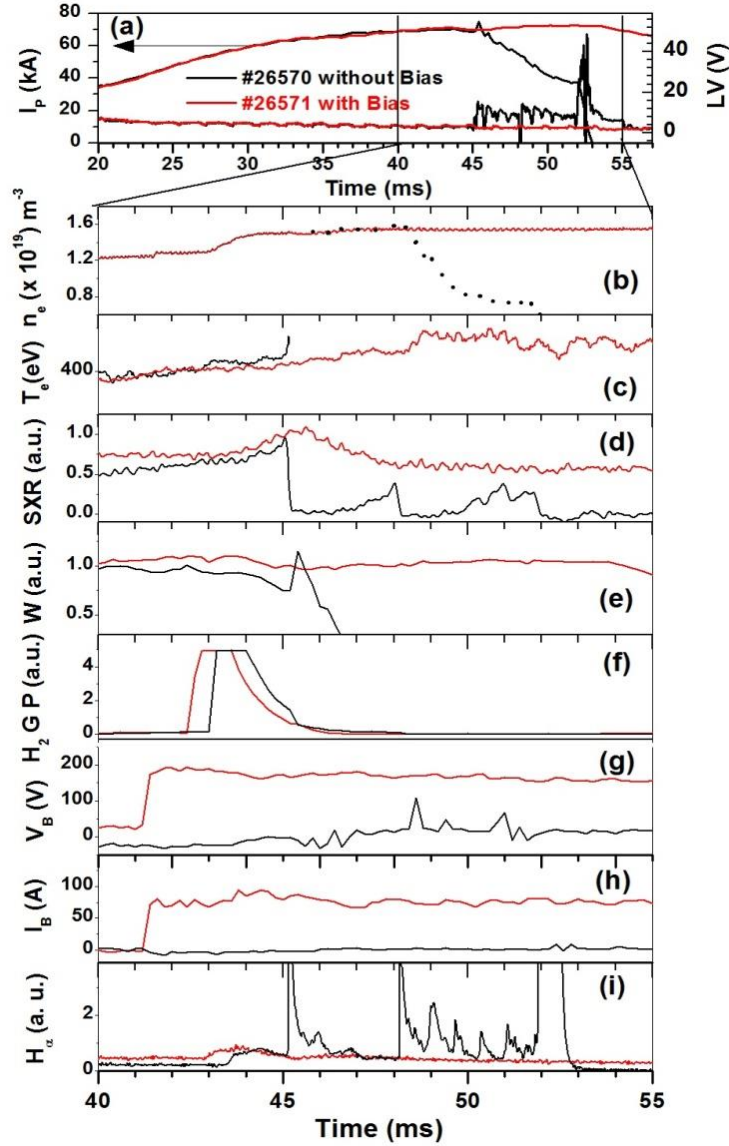


Figure 4.6. Comparison of without bias (#26570 black) and with bias (#26571 red) discharges with H_2 gas injection: (a) plasma current (I_P), loop voltage (LV), (b) plasma density (n_e), (c) electron temperature (T_e), (d) SXR emission, (e) stored energy, (f) H_2 gas-puff pulse (g) biasing voltage (V_B), (h) bias current (I_B) and (i) H_α emission. Disruption is avoided in #26571 with application of bias. The dotted line in (b) represents the density measurements and temperature measurements with uncertainties during the disruption phase respectively. $L_{exp} \sim 20$ mm and $r_{elec} \sim 22$ cm.

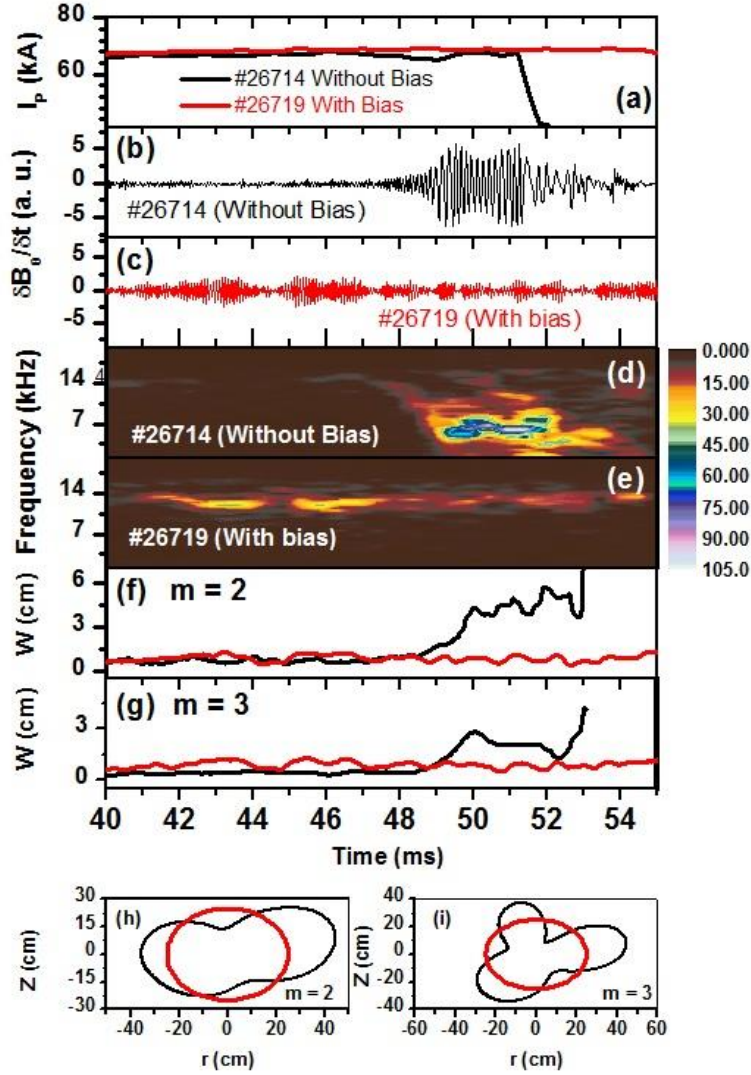


Figure 4.7. Comparison of without bias (#26714 black) and with bias (#26719 red) with H_2 gas injection: (a) I_p , (b, c) \dot{B}_θ at midplane, low field side (d, e) Time-frequency spectrum of \dot{B}_θ , (f, g) Island width of $m = 2, 3$ modes, (h, i) spatial structures of $m = 2, 3$ modes. Disruption (by gas puffing at $t \sim 42$ ms) is avoided in #26719 with application of bias at $t \sim 41$ ms.

The MHD modes $m = 2$ and 3 are identified from the temporal evolution of perturbations in the poloidal magnetic field that is measured using 12 magnetic coils placed equidistant in the azimuthal direction using singular value decomposition (SVD) technique. The island widths are estimated from the measured amplitudes of $\tilde{B}_\theta / B_\theta$ by using the formula [4.29, 4.30]

$$W / r_S = 2 \left[(2/m) (r_c / r_S)^m (\tilde{B}_\theta / B_\theta) \right]^{1/2}, \quad (4.1)$$

where W is the island width, m is poloidal mode number, r_s is the radius of the mode resonant surface and r_c is the radius of the Mirnov probe location. The radii of the mode resonant surfaces, r_s , are deduced from reconstructed radial current density profile of the form

$$j(r) = j_0 [1 - (r^2 / a^2)]^\nu \quad (4.2)$$

In large aspect-ratio circular plasma safety factor at the centre (q_0) and at the edge (q_{edge}) are related as [4.31]

$$\frac{q(a)}{q(0)} = \nu + 1 . \quad (4.3)$$

The exponent $\nu \sim 4$ is obtained from fitting the q profile incorporating the values of q at the plasma boundary ($q_{edge} \sim 3.8$) and the radius of $q = 1$ surface, $r_{q=1} = r_{inv} \sim 7\text{cm}$, obtained from tomographic reconstruction of SXR emission [4.32] and taking central $q_{r=0} \sim 0.8$. Position of $r_{q=1}$ (inversion radius) can also be calculated from the empirical law, $r_{inv} = 0.5a / \sqrt{q_{edge}}$ [4.33]. Reconstructed radial profiles of current density and edge safety factor are shown in the Fig. 4.8.

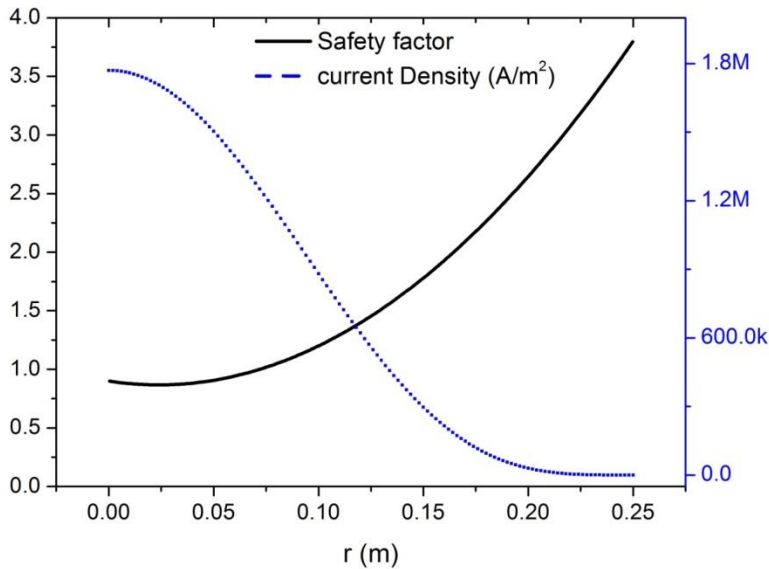


Figure 4.8. Reconstructed radial profiles of toroidal current density and safety factor

It is clear from signals of three magnetic coils of Mirnov garland separated by $\Delta\theta = 24^\circ$ (Fig. 4.9) measuring poloidal magnetic fluctuations that in these repeatable discharges islands $m/n=3/1$ and $m/n=2/1$ rotate in ion diamagnetic direction, i.e., modes rotate from high field side to low field side in lower half of poloidal plane.

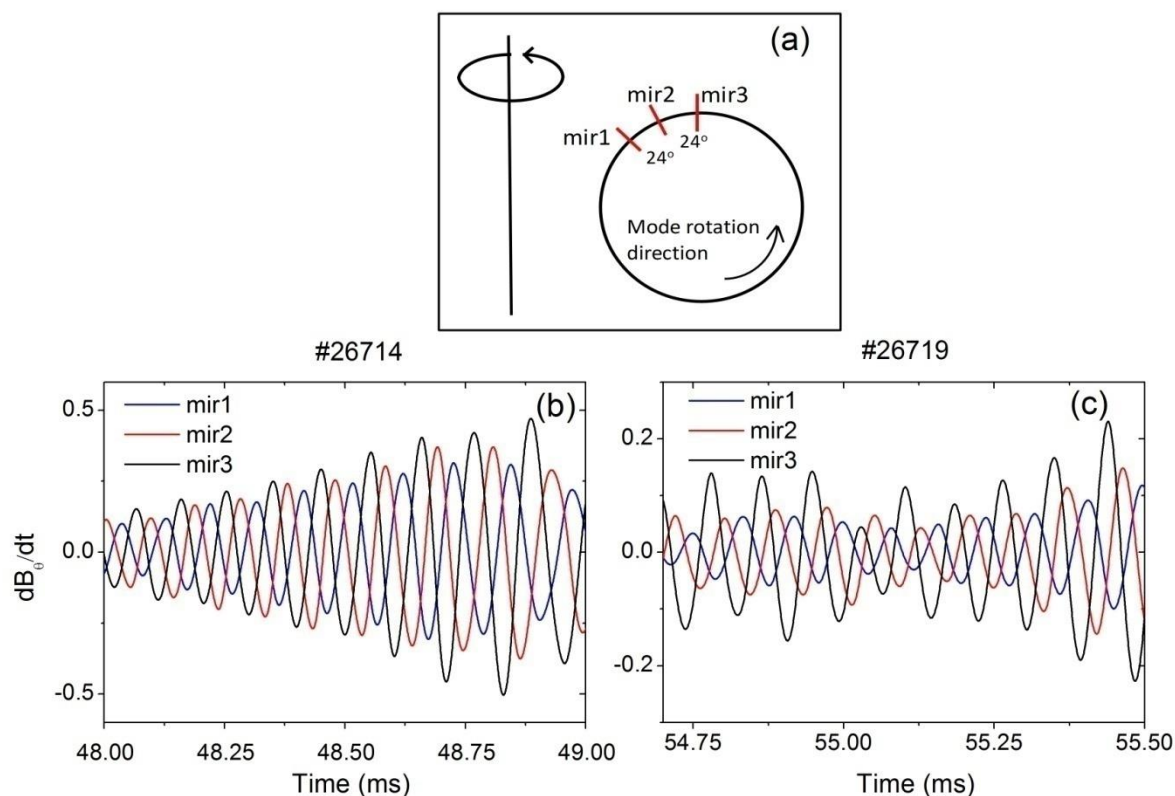


Figure 4.9. (a) Position of three magnetic probes of Mirnov garland in a poloidal plane used to detect mode rotation direction. (b) and (c) show time evolution of magnetic fluctuations of the three probes shown in (a) indicate that modes rotate in the ion diamagnetic direction in discharge #26714 and #25719, respectively.

Investigating further the effect of biasing on $m = 1$ mode using SXR tomography, it was found that biasing did influence the $m = 1$ mode too. Fig.4.10 shows the sequence of tomographic images depicting the time evolution of SXR emissivity contours in both with and without bias discharges. As soon as the gas is injected into both the disruptive (#26714 at ~ 42 ms) and disruption-avoided (#26719 at ~ 42 ms) discharges, an expansion of region of $m/n = 1/1$ mode localization occurs which is visible in soft x-ray reconstruction shown in Figs. 4.10a(i) and 4.10b(i) obtained at $t \sim 47$ ms. The tomographic reconstruction is performed using Bessel function as a base function for radial expansion coefficients [4.32, 4.34, 4.35] assuming rigid rotation of mode [4.36 – 4.38]. In the disruptive discharge (#26714), the expansion of $m/n = 1/1$ mode continued with time and after the abrupt growth of $m = 2$ and $m = 3$ perturbations at $t \sim 49$ ms, the soft X-ray contours degraded further at $t \sim 50$ ms (Fig. 4.10a(ii)) and complete destruction of the $q = 1$ magnetic surfaces occurred at $t \sim 51$ ms as shown in Fig. 4.10a(iii) leading to the fatal major disruption terminating the plasma current

completely at ~ 51 ms. The scenario is contrastingly different in the discharge where bias is applied to electrode ~ 1 ms prior to the gas puff. In this case too, the $m/n = 1/1$ mode localization region starts extending after the onset of the gas-puff, however, the $m = 2$ and $m = 3$ islands do not grow (Fig.4.7f, 4.7g). The $m/n = 1/1$ mode localization region also saturates (Figs. 4.10b (ii), (iii), (iv)), and no disruption event takes place and plasma current lives on. Although the reduction in \dot{B}_θ fluctuations corresponding to $m/n = 2/1, 3/1$ fluctuations starts with an application of $V_B \sim 120$ V, the complete disruption avoidance in discharges with $I_p \sim 65$ -70 kA of ADITYA tokamak has been obtained with biasing voltage of more than ~ 180 -190V.

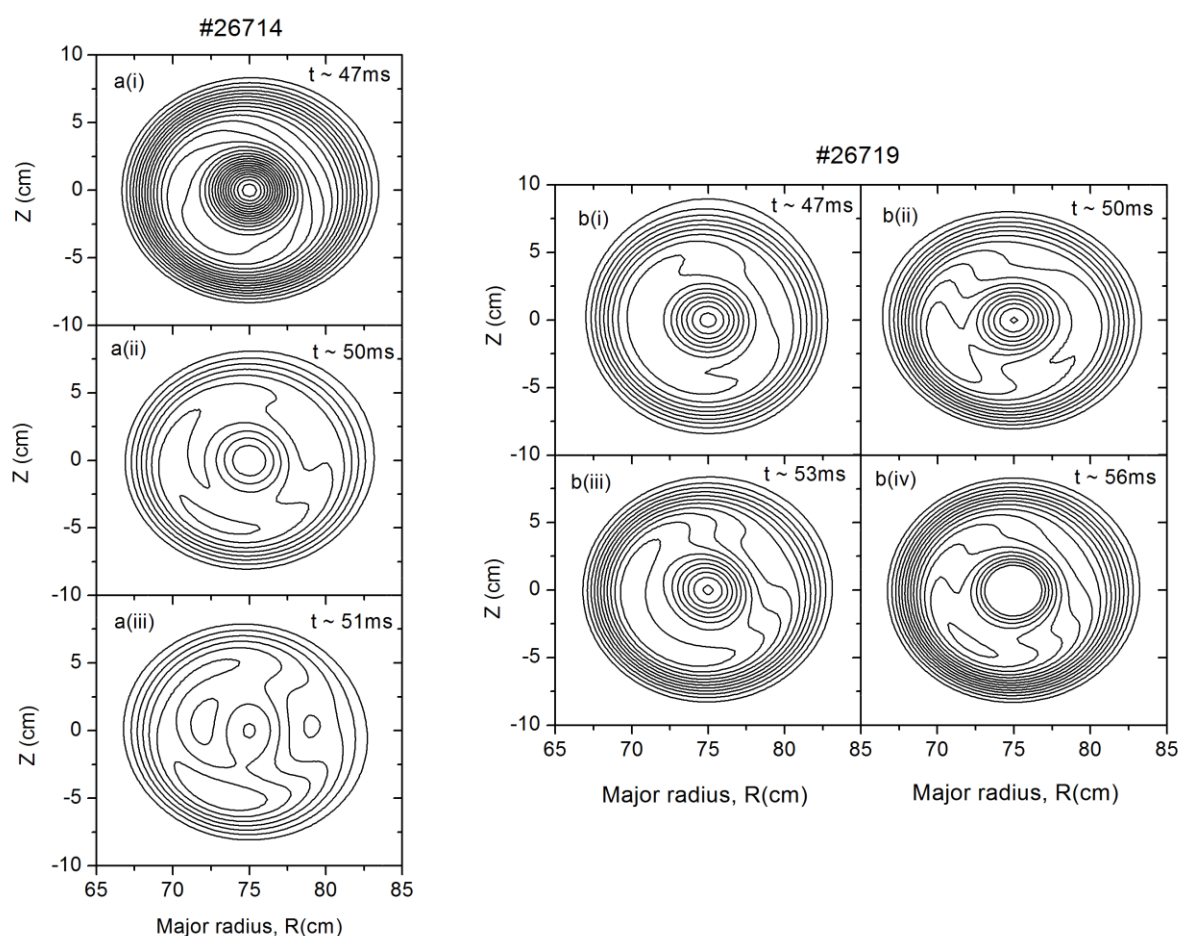


Figure 4.10. Tomographic results using SVD analysis of the reconstructed SXR emissivity in ADITYA Tokamak of (a) shot # 26714 and (b) #26719 in different time interval. Spatial eigen modes (topos) show time evolution of $m/n=1/1$ island for both the discharges.

4.4 Discussion

It is quite a well known fact that the positively biased electrode placed inside the LCFS creates positive radial electric fields [4.23]. This radial electric field induces a thin layer of

$E_r \times B_\phi$ driven poloidal flows with high shear near the separatrix. Further, many theoretical investigations reported that the sheared flows can influence the linear stability of resistive tearing modes [4.13, 4.39, 4.40]. We explore the possibility of shear poloidal rotation generated by biased electrode restricting the MHD island growth through decrease in the linear stability parameter Δ' and thereby avoiding disruptions in our experiments.

The radial profile of poloidal velocity (v_θ) is obtained by measuring radial profile of plasma potential with a rack Langmuir probe. The radial profile of plasma potential (Φ_p) is obtained using the relation $\Phi_p = \Phi_f + 3k_B T_e$ (k_B is Boltzmann constant) by separately measuring the floating potential (Φ_f) and electron temperature (T_e) using a Langmuir probe. To avoid the disturbances in Φ_f measurements during gas-puffs and subsequent disruptions, we measured the variations of radial profile of plasma potential at different biasing voltage in similar discharges by keeping the electrode location and exposed length same. Application of positive bias voltage builds up positive plasma potential leading to an increase in the positive radial electric field and its shear in the region between electrode and last closed flux surface (LCFS). At $r \sim 25$ cm the positive radial electric field reaches up to ~ 5 kV/m at ~ 210 V biasing voltage from ~ 2.5 kV/m in the without bias case. The radial profile of plasma potential without bias and with different bias voltages measured at ~ 2 ms after the application of bias is shown in Fig. 4.11(a). With the toroidal magnetic field in the anticlockwise B_ϕ direction as viewed from top in the reported set of discharges the biased induced $E_r \times B_\phi$ rotation increase in the ion-diamagnetic drift direction and its shear through $E_r \times B_\phi$ drift. The poloidal velocity ($v_{E \times B} = E_r / B_\phi$) increases from ~ 3.3 km/s in the without bias discharges to ~ 6.7 km/s at $r = 25$ cm with ~ 210 V biasing.

From SVD analysis it is found that both the modes rotate with same frequency (angular velocity) (Fig.4.12). It is also clear from the short time fast Fourier transformation (FFT) of \dot{B}_θ oscillations measured with Mirnov coil located at the mid-plane in the low-field side (Fig. 4.7d, e) that modes rotates at the frequency ~ 11 -14 kHz. It is possible to speculate on why the mode frequency remains same for both the modes. The cause of the island rotation might be due to diamagnetic effect (so called drift tearing mode [4.41]) or the radial electric field, E_r , giving rise to $E_r \times B_\phi$ drift. Due to edge biasing radial electric field is enhanced, which causes high rotation of drift tearing modes. Experiments and theory suggest that in $E_r \times B_\phi$ rest frame propagation frequency of the mode is equal to the electron diamagnetic

frequency, i.e., $\omega \sim mT_e / rB_\phi L_{pe}$, which is local electron drift frequency for mode m with the electron pressure gradient scale length $L_{pe} = -p_e / (dp_e / dr)$. Electron temperature and pressure length scale at both the rational surfaces is different. For $m=2$ at $r_s \sim 17$ cm, electron pressure scale length is larger than that for $m=3$ at $r_s \sim 21$ cm, giving the same frequency to both the modes.

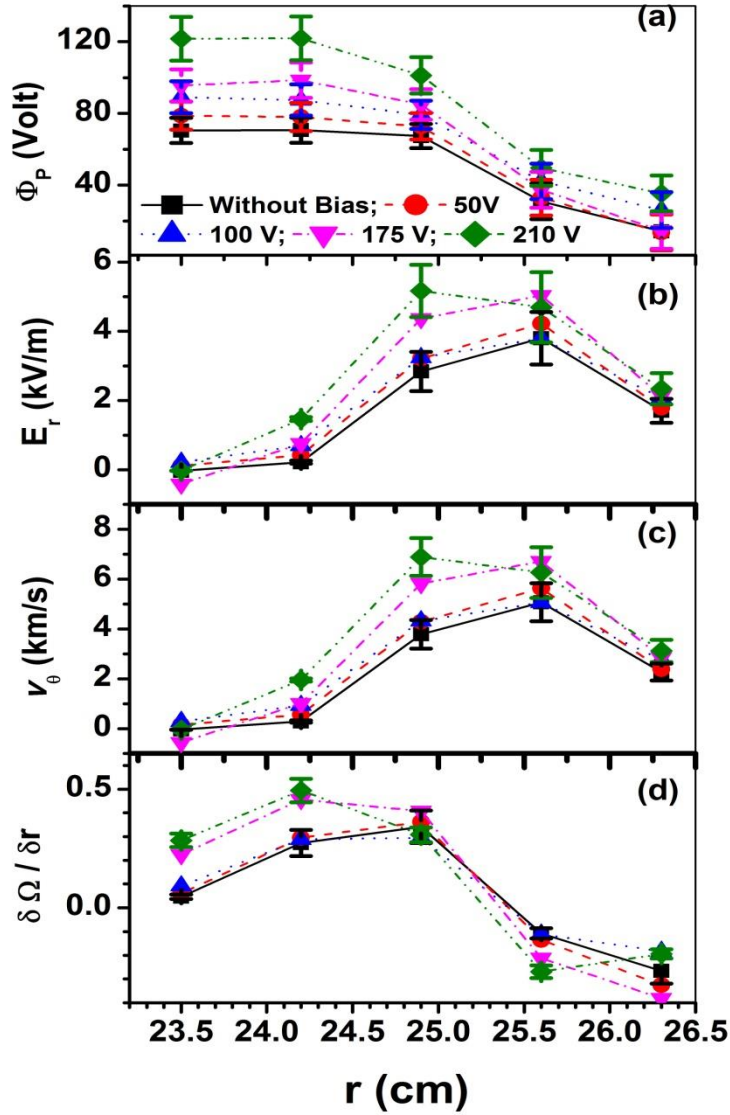


Figure 4.11. Radial profiles of (a) plasma potential (b) radial electric field (c) poloidal flow velocity and (d) radial shear in normalised poloidal flow, with and without bias.

Fig.4.13 shows the comparison of time evolution of island rotation speed in both the with- and without-bias discharges measured by phase difference of fluctuations of two Mirnov coils separated by $\Delta\theta = 24^\circ$. In the disruptive discharge (#26714) the island rotation speed

decreases soon after the gas injection whereas the islands continue to rotate in the ion diamagnetic direction with biasing (#26719) suggesting that modes do not overlap and lock here.

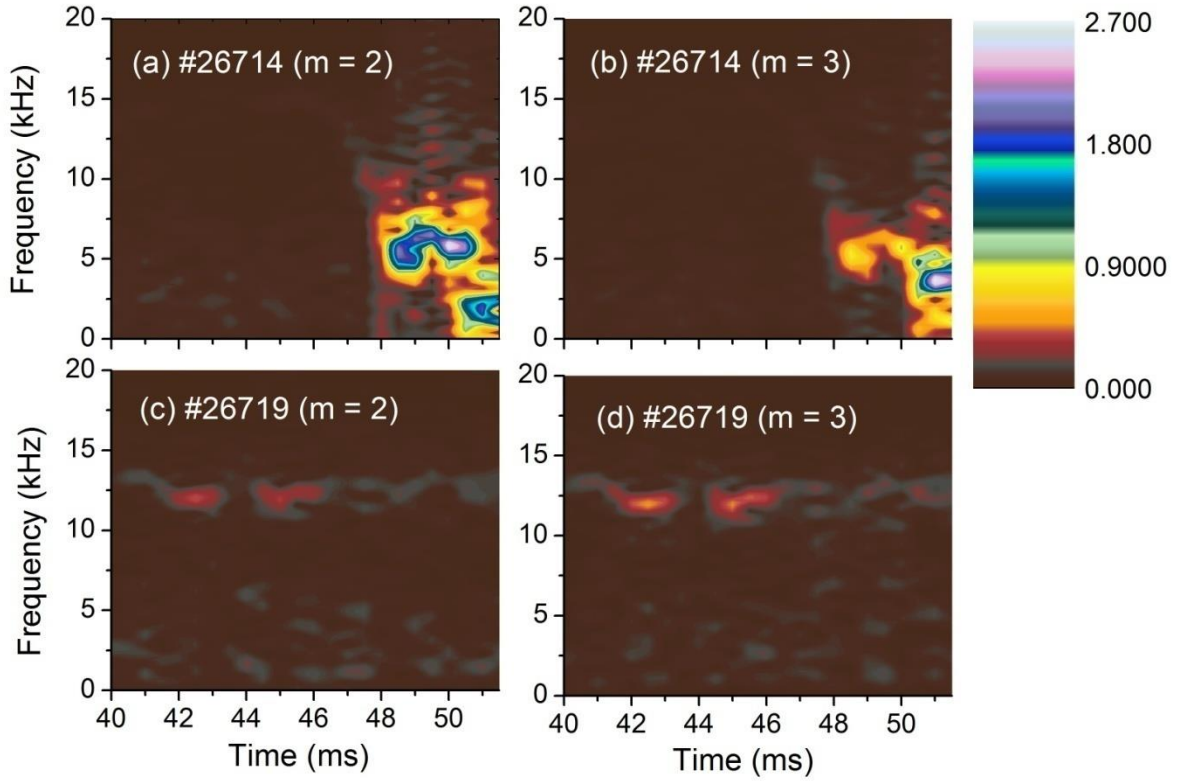


Figure 4.12. Short Time FFT analysis of $m=2$ and $m=3$ fluctuations computed by SVD analysis shows that modes $m/n = 3/1$ and $2/1$ rotate with same frequency in #26714 ((a) and (b)) and #26719 ((c) and (d)).

The evolution of magnetic islands in tokamaks are defined by the linear stability parameter Δ' and hence we looked for the variation in the linear stability parameter Δ' with the sheared poloidal flows generated by different bias voltages. In order to obtain the variation in the linear stability parameter Δ' with the sheared poloidal flows generated by different bias voltages, we deduced Δ' from the linear tearing mode growth rate [4.43],

$$\gamma \approx 0.55 \tau_R^{-3/5} \tau_A^{-2/5} (\Delta' a)^{4/5} \left(\frac{a}{R} n \frac{aq'}{q} \right)^{2/5}, \quad (4.4)$$

where $\tau_R = a^2 \mu_0 / \eta$ is resistive diffusion time and $\tau_A = a / v_{A\theta}$ is Alfvén transit time, with γ being obtained by fitting an exponential function ($W = W_0 + W_1 e^{\gamma t}$) to the time evolution of W

after the gas-puff, η is Spitzer resistivity, $v_{A\theta} = B_\theta / \sqrt{\mu_0 m_i n_i}$ is poloidal Alfvén velocity. A typical fit is shown in Fig. 4.14(a) for $m = 2$ mode in the disruptive discharge #26714. ($\Delta'a$)

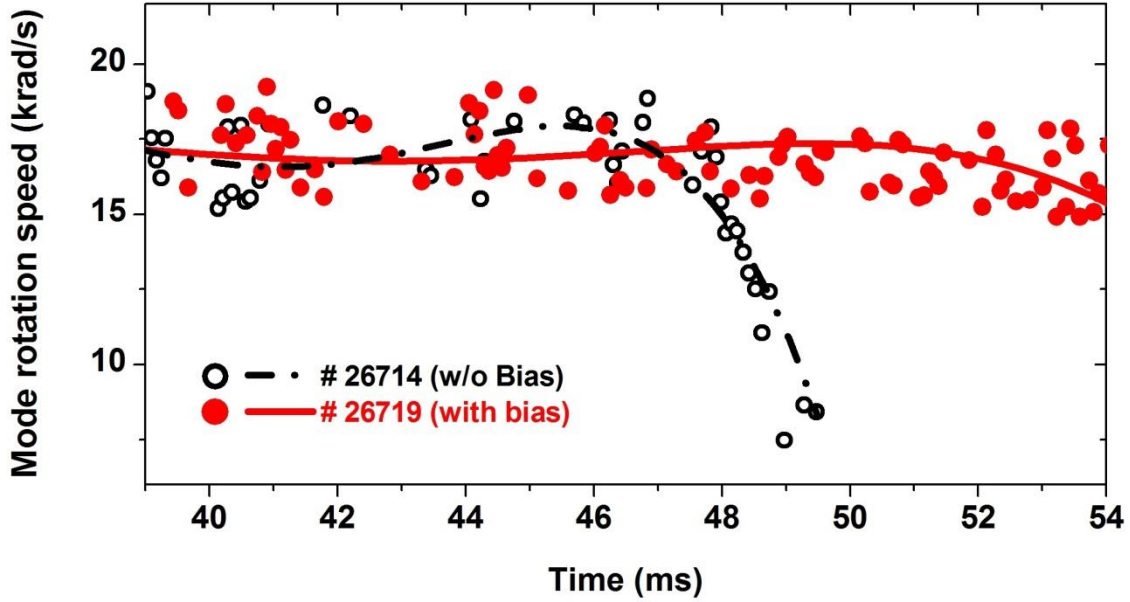


Figure 4.13. Time evolution of island rotation speed in without bias discharge (#26714) and with bias discharge (#26719) measured by phase difference of two \dot{B}_θ coils separated $\Delta\theta = 24^\circ$ from each other.

is further estimated using the island evolution equation for a tearing mode close to saturation given by [4.44]

$$\frac{dW}{dt} = 1.66\Delta' \frac{\eta}{\mu_0} \left[1 - \frac{W}{W_S} \right], \quad (4.5)$$

where W_S is the saturation island width. Close to island width saturation dW/dt is linear with $1 - (W/W_S)$. With measured values of island width, its time derivative and saturated island width, the value of Δ' have been evaluated from the slope of the fitted linear curve close to saturation. ‘Temporal profile of dW/dt ’ and ‘ dW/dt versus $(1 - W/W_S)$ ’ close to saturation for $m = 2$ mode in the disruptive discharge #26714 are plotted in Figs. 4.14(b) and 4.14(c), respectively. The slope of the linear fit in Fig. 4.14(c) gives the value of $1.66\Delta'\eta/\mu_0$ and hence Δ' . The value of ($\Delta'a$) estimated using both the methods matches to within a factor of 2.

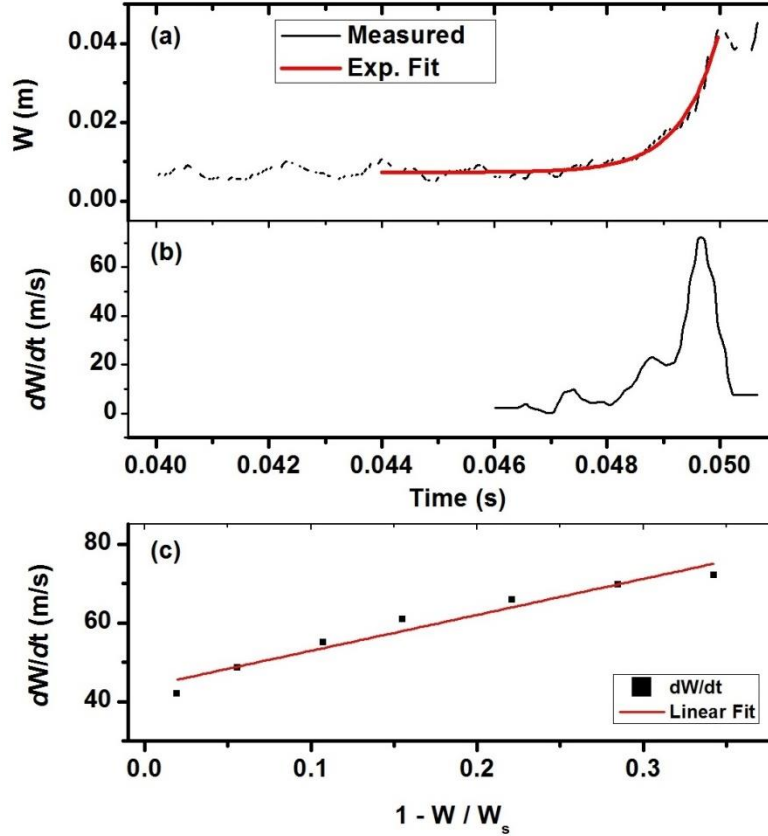


Figure 4.14. (a) Time evolution of island width of $m = 2$ mode, W (black) with an exponential fit (red) in the disruptive discharge #26714 after the gas-puff and (b) dW/dt of (a). (c) dW/dt versus $(1 - W/W_s)$ close to saturation and linear fit (red solid line).

Fig.4.15 (a, b, c) shows the variation of saturated island width and Δa as a function of flow shear for both $m = 2$ and $m = 3$ modes. Normalized flow shear ($d\Omega/dr$) has been calculated as

$$\frac{d\Omega}{dr} = r \times \left[\frac{d}{dr} \left(\frac{E_r}{rB_\phi} \right) \right] / v_{A\theta}. \quad (4.6)$$

The figure clearly shows that increase of positive poloidal flow shear has a stabilizing effect on the stability index as well as on the saturation island width. Without biasing the normalized flow shear (with plasma radius) normalized with poloidal Alfvén velocity ($\sim 240 \text{ km/sec}$) remains ~ 0.25 at $r \sim 24 \text{ cm}$ in the without bias case. With $\sim 220 \text{ V}$ biasing the normalized flow shear becomes to ~ 0.5 leading to stabilization of the modes and hence avoidance of disruption [4.40]. Although, the flow shear is generated in the edge region near to $q = 3$ surface, the increased flow shear also influences the $m = 2$ mode which remains quite far from the increased shear location. The reason for this is still unclear; however, this may be due to coupling between the modes as they may be the toroidal sidebands of each other and

their harmonics. This effect is analogous to what is reported in [4.3, 4.42], where direct heating by ECRH of one of the magnetic islands (either, 2/1 or 3/1) stabilizing other mode.

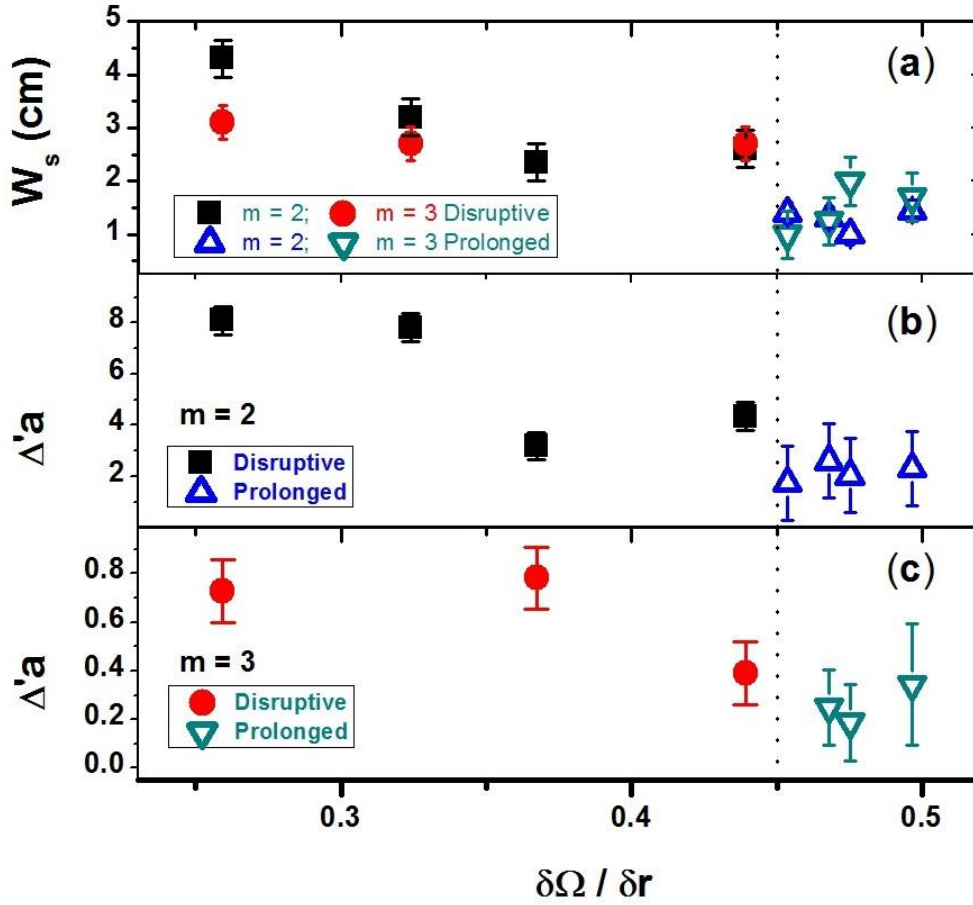


Figure 4.15. Variation of saturation island width (W_s) and ($\Delta'a$) as a function of poloidal flow shear for $m = 2$ and $m = 3$ modes.

The positive values of Δ' confirm the conventional tearing modes are unstable after the gas puff. The data points in Fig. 4.15 are average of minimum two discharges for each point and the error bars also include the uncertainty in estimated locations of the modes using the current profile form mentioned earlier in the text. The saturated island width as well as the value of ($\Delta'a$) for both the modes decreases slowly with the increase in poloidal flow shear, however, the disruption is avoided only when the flow shear reaches a value of ~ 0.45 (vertical dotted line in Fig. 4.15) near the vicinity of $q = 3$ surface at $r \sim 24$ cm. At this shear value the ratio of normalized flow shear and the normalised magnetic shear ($a \frac{\partial}{\partial r} \frac{1}{q}$) (Normalized magnetic shear) [4.45] approaches to one.

The boundary layer theory of the resistive tearing mode in presence of shear flow suggests that the presence of flow shear affects both the internal resistive region as well as the external ideal region significantly by changing the value of Δ' [4.40]. It is shown that complete stabilization of tearing modes occurs when $|G'/F'| > 1$ and the marginal stability occurs at $|G'/F'| \approx 1$, where G' and F' are the flow and magnetic shears respectively. In our experiments the criteria $|G'/F'| \approx 1$ gets satisfied in the vicinity of $q = 3$ surface within experimental limits of identification of the location of $q = 3$ surface in the discharges in which the disruptions are successfully mitigated. Furthermore, it is observed that the increased flow shear also influences the $m = 2$ and $m = 1$ mode although their resonant surface lies quite far from the increased shear location. As the ADITYA tokamak has not very large aspect ratio, the toroidal coupling of the modes $m = 3, 2, 1$ is quite possible which may be the reason for the modifications in the $m = 2$ and $m = 1$ modes.

In the above-mentioned experiments we have applied the bias voltage at a pre-determined time prior to the gas-puff as we know that the gas puff is going to disrupt the plasma. However, naturally occurring disruptions in tokamaks are random phenomena, which can occur at any time. Hence to mitigate them in real time using biasing, the biasing voltage should be applied prior to these disruptions by identifying any precursor of such disruptions. For real time control of the gas-puff induced disruptions in ADITYA tokamak, we used the growth of the MHD modes due to gas-puff as precursor for disruption. The bias voltage on electrode is automatically triggered when the Mirnov probe signal exceeds a preset threshold (usually 0.1-0.5 V) using the electronic circuit described in chapter 3. Fig.4.16 shows two repeatable discharges #25362 and #25367 each with $I_p \sim 60\text{kA}$. Discharge #25362 has been disrupted deliberately using H_2 gas puff at $\sim 53.6\text{ms}$. Just after the gas is puffed the Mirnov oscillations start growing reaching to saturation prior to current disruption. In discharge #25367 we fed one of Mirnov coil signal to the circuit described in chapter 3 and set a threshold of 0.5V. In this discharge when the gas is puffed at $\sim 51\text{ms}$ the MHD oscillations start growing and as soon as its magnitude grows more than the set threshold, the circuit generate a trigger which enables application of bias voltage on the electrode. It is clearly evident from Fig. 4.16 that with the application of the bias voltage the growth of MHD oscillations subsides and current quench time increases. In these experiments we are only able to delay the current quench and not completely mitigate the disruptions. This may be due to the delay in application of bias voltage and demands further reduction of set threshold

voltage in the circuit for bias trigger generation. But the threshold voltage cannot be reduced less than the variation in the Mirnov oscillation present prior to gas puff.

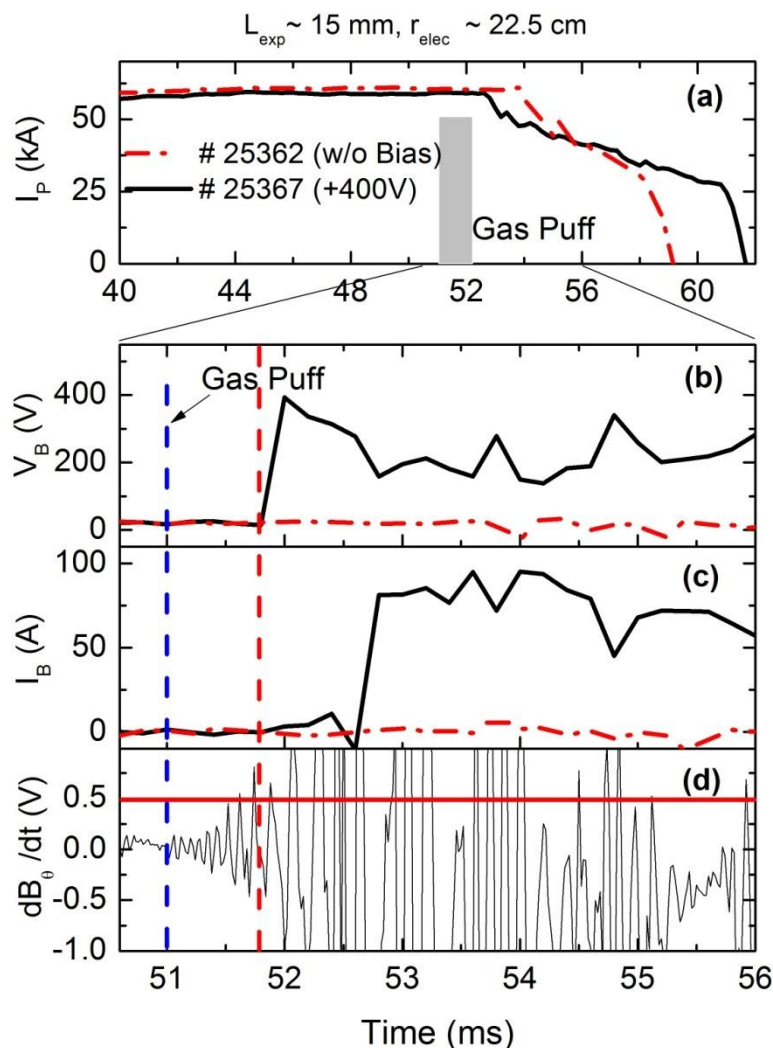


Figure 4.16. Synchronization of bias application with Mirnov signal: (a) Comparison of two repeatable plasma discharges (#25362 without bias in red and #25367 with bias in black. H_2 Gas is puffed at 51ms (also shown in (b), (c) and (d) by vertical blue dotted line). (d) On puffing gas MHD oscillation amplitude crosses a set threshold value (0.5V in #25367, shown by horizontal red line) in trigger circuit, triggers SCR and thereby switch on the bias voltage on the electrode (shown in (b), (c) and (d) by vertical red dotted line). $L_{exp} \sim 15 \text{ mm}$ and $r_{elec} \sim 22.5 \text{ cm}$.

4.5 Summary

In summary, The influence of electrode exposed length on plasma performance has been extensively studied and most of results related to the improved confinement and disruption mitigation are obtained in case of the electrode tip being kept at $\sim 3 \text{ cm}$ inside the last closed flux surface (LCFS) with an exposed length of $\sim 20 \text{ mm}$ in typical discharges of ADITYA

tokamak. Further, disruption avoidance and complete recovery of the discharge has been obtained in ADITYA tokamak by stabilization of MHD modes by means of electrode biasing in the H₂ gas puff induced disruptions. The magnetic islands corresponding to $m/n = 2/1, 3/1$ perturbation do not grow with the application of positive bias voltage to an electrode placed inside the LCFS of ADITYA tokamak leading to disruption avoidance. A threshold value ~ 180-190 volt has been found to be required at $I_p = 65 - 70$ kA for avoidance. The bias voltage induced sheared poloidal rotation profoundly influences the magnitude of Δ' and consequently the stability of tearing modes. More systematic electrode position, electrode exposed length and biasing voltage scans along with reciprocating electrode system are envisaged for best optimisation of above three parameters and also for its use in bigger tokamaks for disruption avoidance. This technique may have advantage over the disruption avoidances using ECRH or NBI as in those cases real time changes of deposition locations will be difficult whereas the reciprocating electrode can easily be placed at any desired locations in the extreme edge region. The real time control of disruptions is also attempted with triggering the bias voltage automatically when the Mirnov probe signal exceeds a preset threshold value using a uniquely designed electronic comparator circuit.

4.6 References

- [4.1] ITER Physics Expert Group on Disruptions, Plasma Control and MHD and ITER Physics Basis Editors, *Nucl. Fusion* **39**, 2251 (1999)
- [4.2] J. A. Wesson, et al., *Nucl. Fusion* **29**, 641(1989)
- [4.3] B. Esposito, et al., *Phys. Rev. Lett.* **100**, 045006 (2008)
- [4.4] K. Hoshino, et al., *Phys. Rev. Lett.* **69**, 2208 (1992)
- [4.5] F. Salzedas, et al., *Nucl. Fusion* **42**, 881 (2002)
- [4.6] D. A. Kislov, et al., *Nucl. Fusion* **37**, 339(1997)
- [4.7] F. Volpe, et al., *34th EPS Conference on Plasma Phys. Warsaw, 2 - 6 July 2007 ECA Vol. 31F*, P-1.132 (2007)
- [4.8] P. C. de Vries, et. al., *Plasma Phys. Control. Fusion* **38**, 467(1996)
- [4.9] D. Basu, et al., *Phys. Plasmas* **20**, 052502 (2013)
- [4.10] S. B. Bhatt, et al., *Indian Journal of Pure and Applied Physics*, **Vol. 27 September-October**, 710 (1989)
- [4.11] Y. Narushima, et al., *Nucl. Fusion* **51**, 083030(2011)
- [4.12] C. C. Hegna, *Nucl. Fusion* **51**, 113017(2011)
- [4.13] D. Chandra, et al., *Nucl. Fusion* **47**, 1238(2007)

- [4.14] I. C. Nascimento, et al., *Nucl. Fusion* **47**, 1570 (2007)
- [4.15] R. R. Weynants, et al., *Nucl. Fusion* **32**, 837 (1992)
- [4.16] L. G. Askinazi, et al., *Nucl. Fusion* **32**, 271 (1992)
- [4.17] E. Y. Wang, et al., *Nucl. Fusion* **35**, 467 (1995)
- [4.18] C. Silva, et al., *Nucl. Fusion* **44**, 799 (2004)
- [4.19] Joydeep Ghosh, et al., *Nucl. Fusion* **47**, 331 (2007)
- [4.20] R. J. Taylor, et al., *Phys. Rev. Lett.* **63**, 2365 (1989)
- [4.21] Debjyoti Basu, et al., *Phys. Plasma* **19**, 072510 (2012)
- [4.22] H. Biglari, P. H. Diamond and P. W. Terry, *Phys. Fluids B* **2**, 1 (1990)
- [4.23] I. Shesterikov, et al., *Phys. Rev. Lett.* **111**, 055006 (2013)
- [4.24] M. Greenwald, J. L. Terry, S. M. Wolfe, et al., *Nucl. Fusion* **28**, 2199 (1988)
- [4.25] P. K. Atrey, S. B. Bhatt, D. Bora et al., *Indian J. Phys.* **66B (5 & 6)**, 489 (1992)
- [4.26] S. Kumar, et al., *Rev. Sci. Instrum.* **81**, 123505 (2010)
- [4.27] K. H. Finken, et al., *Nuclear Fusion* **41**, 1651(2001)
- [4.28] R. R. Weynants, et al.,(*Proc. 17th Eur. Conf. Amsterdam, 1990*), *European Physical Society Journal* **1**, 287 (1990)
- [4.29] TFR GROUP, 'Major and Minor Disruptions in TFR', Rep. No.EUR-CEA-FC-1151.
- [4.30] A. D. Cheetham et al., *Nucl. Fusion* **27**, 843 (1987)
- [4.31] J. Wesson, Tokamaks, Third edition, Oxford University Press, 2004
- [4.32] A. K. Chattopadhyay, et al., *Indian Journal of Pure & Applied Physics*, **44**, **November**, 826 (2006)
- [4.33] Equipe TFR, *Proceedings of 6th International conference on plasma physics and controlled nuclear fusion research, IAEA, Vienna* **1**, (1977)
- [4.34] A. K. Chattopadhyay, et. al., *Pramana- Journal of Physics* **Vol. 61, No. 1, July**, 141 (2003)
- [4.35] A. K. Chattopadhyay, C. V. S. Rao, S. K. Mattoo and R. Srivatsan, *Institute for Plasma Research Technical Report, IPR/TR-88/2002* (2002)
- [4.36] R. S. Granetz and J. F. Camacho, *Nucl Fusion* **25**, 727 (1985)
- [4.37] Y. Nagayama, S Tsuji, K. Kawahata, N. Noda and S. Tanahasi, *Jpn. J. Appl. Phys.* **20**, L779 (1981)
- [4.38] R. S. Granetz and J. F. Camacho, *Rev. Sci. Instrum.* **57**, 417 (1986)
- [4.39] A. I. Smolyakov, et al., *Plasma Phys. Control. Fusion* **43**, 1661 (2001)
- [4.40] X. L. Chen, et al., *Phys. Fluids B* **2**, 495 (1990)
- [4.41] D. Biskamp, *Nucl. Fusion* **19**, 777 (1979)

Chapter 4: Disruption Mitigation Using Biased Electrode in ADITYA Tokamak

[4.42] E. Lazzaro, et al., *Phys. Rev. Lett.* **84**, 6038 (2000)

[4.43] G. Bateman, *MHD Instabilities*, MIT press, 1980

[4.44] R. B. White, *Phys. Fluids* **20**, 800 (1977)

[4.45] R. J. La Haye, et al., *Nucl. Fusion* **Vol 37, No. 3**, 397 (1997)

Chapter 5

Effect on Electrostatic and Magnetic Fluctuations Due to Biased Electrode in ADITYA Tokamak

5.1 Introduction

Suppression of electrostatic fluctuations [5.1 - 5.3] has been observed in many fusion devices during L-H transition, considered to be due to sheared $E_r \times B_\phi$ drift flow. Stabilization of $E_r \times B_\phi$ flow shear due to large sheared radial electric field has been repeatedly emphasized to explain L-H transition in magnetically confined fusion devices [5.4]. Many theoretical models [5.5 – 5.8] have been given to explain cause of generation of radial electric field. Role of current density profile modification is also considered a candidate for the observation of precursor magnetic oscillations in the H- mode transition [5.9, 5.10]. Experimental work done in TCABR [5.11], HT-7 [5.12] tokamaks have shown influence on MHD fluctuation amplitude during transition. In ASDEX [5.9] change in current density profile at the edge was found to trigger high confinement mode. Recently done biased electrode experiments in SINP tokamak [5.10] have shown that edge toroidal current density profile modifies prior to increment in radial electric field during transition to improved confined regime. Some theoretical models [5.13 – 5.16] suggested that current-density profile with finite j_{edge} may trigger the H-mode transition. These theories predict suppression of edge turbulence due to increased edge magnetic shear in the divertor configuration. Another theory [5.17] predicted that the stabilization of the ideal ballooning mode due to finite j_{edge} in divertor plasma may cause transition. However, until now there is no clear picture exists which is capable of interpret the temporal chronology of all the L-H transition events, i.e., which event is the cause and which one is the effect. One of the most important problems, a possible mutual influence

of island evolution, radial electric field and plasma confinement, is still not understood fully. Coupling of electrostatic turbulence and magnetic fluctuations in TCABR tokamak has been reported during onset of high MHD activity with and without biasing [5.11, 5.18]. In this chapter experimental observations on ADITYA tokamak discharges, in which onset of electrode biasing reduces coupling of electrostatic turbulence and magnetic fluctuations via current profile modification giving rise to improved confinement regimes have been discussed.

In the next section we describe the experimental parameters. Typical temporal profile of rise time of bias voltage and electrode current has been discussed in section 5.3. Behavior of electrostatic and magnetic fluctuations during biasing has been discussed in section 5.4. Analysis and discussion have been presented in section 5.5. Summary of the results has been presented in section 5.6.

5.2 Experimental parameters

For the experiments reported in this chapter plasma current is kept at $I_p \sim 65-70kA$ and central electron density (n_{e0}) is kept at $\sim (1-1.5) \times 10^{19} m^{-3}$. Toroidal magnetic field is $B_\phi \sim 0.75T$. For the discharges presented in this chapter electrode tip is positioned at 3cm inside the limiter and its exposed length in the plasma is kept constant at 20mm. Floating potential and plasma density data at the plasma edge recorded at sampling rate 100kHz.

5.3 Time evolution of biasing voltage and electrode current

In this section we intend to understand the rise time and temporal profile of biasing voltage and electrode current on the basis of leaky capacitor model of magnetically confined toroidal plasma. We found that using this model, steady state values of electrode current in different confinement regimes (Fig. 5.1) by taking two different values of the cross-field plasma resistance along with rise time of electrode voltage and drawn current can be explained.

A rotating magnetized plasma subject to static perpendicular magnetic and electric fields can be described as electrically equivalent to a parallel combination of a capacitor (C_p) and a resistor (R_p) [5.19], shown in Fig. 5.2.

In tokamak plasma cross-field dielectric constant for poloidal flow is given by [5.20]

$$k_\perp = 1 + \frac{c^2}{v_A^2} (1 + 2q^2), \quad (5.1)$$

where $v_A = B_\phi / \sqrt{m_i n_i \mu_0}$ is Alfvén velocity, c is speed of light, q is safety factor near electrode position.

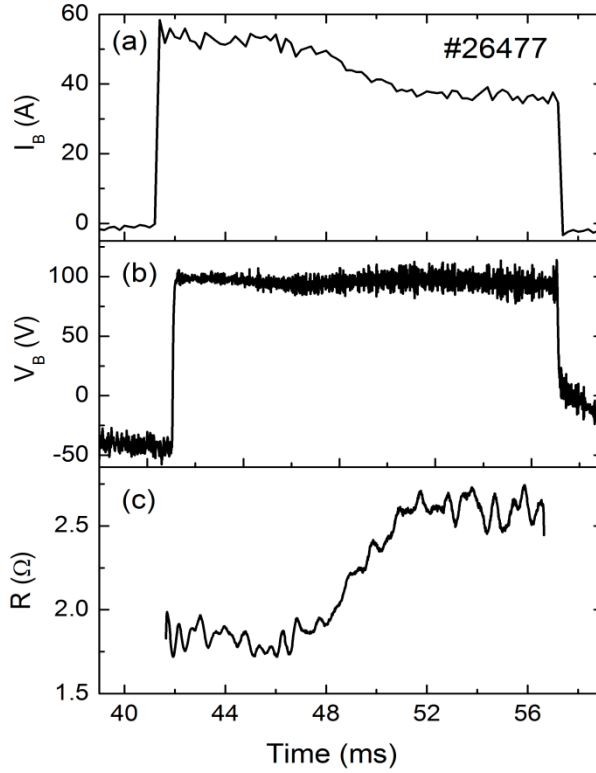


Figure 5.1. Temporal evolution of (a) electrode current (I_B), (b) bias voltage (V_B) and (c) cross – field plasma resistance calculated as V_B/I_B . Figure depicts that after ~ 46.5 ms electrode current decreases indicating increase in cross – field plasma resistance.

Fig. 5.2 shows a RLC-circuit with a constant current DC power supply (V_E). R_x is the external current limiting resistor in series with plasma load, which is modelled as an inductor (L_p) in series with parallel capacitor (C_p) and resistor (R_p). When plasma load is biased, electrode current $I_B (= i_1 + i_2)$ flows in the biasing circuit. When a positive biased applied between electrode and limiter, the path of electrode current is: power supply \rightarrow external resistor \rightarrow electrode \rightarrow plasma \rightarrow limiter (limiter is at vessel ground) \rightarrow power supply. In our model we assume that current flowing in the capacitor (C_p) and resistor (R_p) are i_1 and i_2 , respectively, as shown in Fig. 5.2.

Initially biasing circuit is open and no current flows in the circuit and electrode is at floating potential (V_f). Therefore, when electrode biasing is switched on, the initial conditions for total current, I_B , flowing in the circuit and voltage at electrode, V_B , are given by

$$I_B = 0 \text{ and } V_B = V_f, \quad (5.5)$$

where V_f is the floating potential of the plasma at electrode position.

Applying Kirchoff's voltage law to the circuit, we get-

$$V_E - I_B R_X - L_P (dI_B / dt) - \int i_1 dt / C_P = 0 \quad (5.6)$$

$$\int i_1 dt / C_P = i_2 R_P \quad (5.7)$$

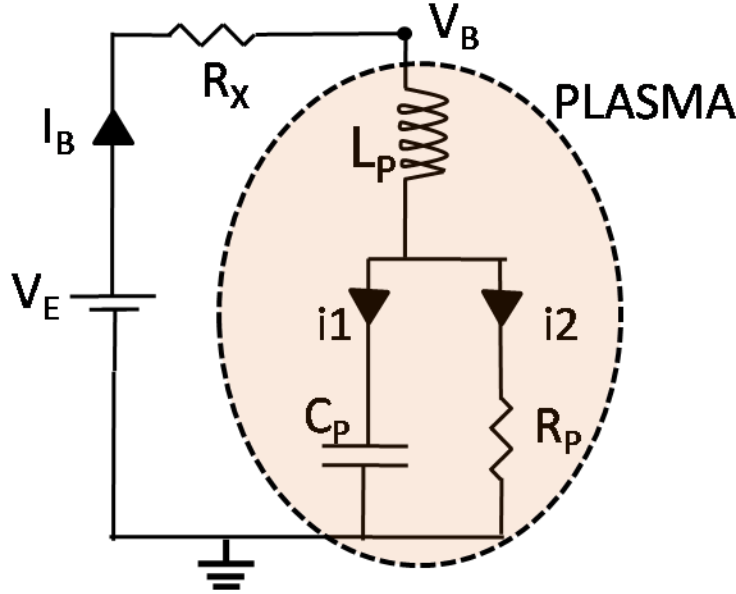


Figure 5.2. Leaky capacitor model of the rotating plasma along with biasing circuit. V_E is biasing power supply voltage and R_X is current limiting resistor. Voltage at electrode is V_B . Rotating plasma under influence of toroidal magnetic field and radial electric field is modelled as parallel combination of plasma capacitance and cross-field plasma resistance in series with plasma inductance.

Using initial conditions and applying Laplace transform technique; we find solution for i_1 as follows-

$$i_1 = (P \exp(s_1 t) + Q \exp(s_2 t)) / L_P, \quad (5.8)$$

where $P = (s_1(a_2 B_1 - b_2) + (a_2 C_1 - c_2)) / (s_2 - s_1)$, $Q = (s_2(b_2 - a_2 B_1) + (c_2 - a_2 C_1)) / (s_2 - s_1)$,

$$s_1 = (-B_1 + \sqrt{B_1^2 - 4A_1 C_1}) / 2A_1, \quad s_2 = (-B_1 - \sqrt{B_1^2 - 4A_1 C_1}) / 2A_1, \quad \text{where } A_1 = 1, B_1 = b_1 / a_1,$$

$$B_2 = b_2 / a_2, \quad C_1 = c_1 / a_1, \quad C_2 = c_2 / a_2, \quad \text{where } a_1 = L_P C_P R_P, a_2 = L_P C_P V_f,$$

$$b_1 = L_P + (C_P R_P R_X), \quad b_2 = (L_P i_0) + (C_P R_X V_f), \quad c_1 = R_X + R_P, \quad c_2 = V_E$$

Solution for i_2 is as follows-

$$i_2 = A + (B \exp(s_1 t) + C \exp(s_2 t)), \quad (5.9)$$

where $A = V_E / L_P C_P R_P s_1 s_2$, $C = (T_1 - T_2 - T_3) / (s_1 - s_2)$, $B = (V_f / R_P) - A - C$, where $T_1 = -V_f s_2 / R_P$, $T_2 = V_E / (L_P C_P R_P s_2)$, $T_3 = (L_P i_0 + C_P R_X V_f) / L_P C_P R_P$, where s_1 and s_2 are same as above.

Total current I_B flowing in the circuit is given by

$$I_B = i_1 + i_2. \quad (5.10)$$

Voltage across the electrode is given by

$$V_B = V_E - I_B R_X. \quad (5.11)$$

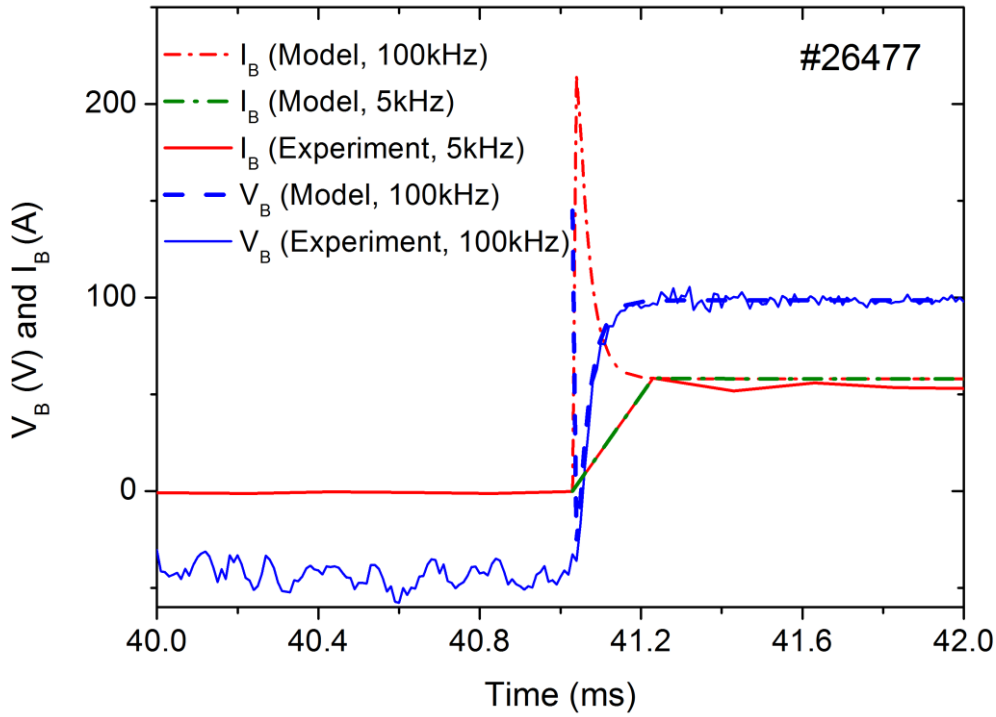


Figure 5.3. Comparison of electrode voltage (V_B) and electrode current (I_B) calculated from leaky capacitor model with those of experimentally measured for plasma shot #26477.

In Fig. 5.3 temporal profile electrode voltage and electrode current calculated from leaky capacitor model has been compared with profiles for discharge #26477. In this discharge power supply is charged at voltage $V_E \sim 145V$. Initially when bias is switch on electrode is at floating potential $V_f \sim -50V$ and no current flows in the circuit. After the bias is switched on electrode draws $\sim 58A$ current. External current limiting resistor $R_X \sim 0.8\Omega$ is connected in

series with electrode in the circuit (Fig. 5.2). Electrode current data was digitized at 5kHz. Biasing voltage data was digitized at 100kHz and 5kHz in different shots depending upon availability of digitizers. We take $R_p \sim 1.7\Omega$ as calculated using experimentally measured electrode voltage and drawn current. Taking $V_E \sim 145V$ (capacitor bank charging voltage for shot #26477), $L_p \sim 3 \times 10^{-6} H$, $C_p \sim 6 \times 10^{-5} F$, and $V_f \sim -60V$ temporal profiles of electrode current and electrode voltage calculated on the basis of above discussed model are also shown in the Fig. 5.3. This figure shows electrode current calculated at 5kHz and 100kHz both. Calculated wave form results and experimentally measured ones have same trend at 5kHz. V_B and I_B both reach steady state in $\sim 150\mu\text{sec}$. During biasing electrode voltage gradually decreases to a value $\sim 90V$. Later on bias voltage again increases and electrode current decreases so that cross-field plasma resistance (R_\perp) linearly increases to $\sim 2.7\Omega$ (Fig.5.1) during transition regime (regime C). In this regime, plasma resistance, R_\perp , changes linearly at the rate $\sim 0.25\Omega/ms$.

The electrode current showed a clear decrease for an increase in the electrode voltage indicates an increase in cross- field resistance measured by electrode characteristics. The increase in cross-field resistance value suggests an improvement in the radial particle transport. This may be due to the nonlinearity of ion viscosity, which plays an important role in the bifurcation phenomena of the L–H transition [5.6, 5.22 – 5.28] and has been observed in tokamaks and stellarators [5.29 – 5.35]. A simultaneous and remarkable suppression of density fluctuations corresponds to the transition to improved confinement mode.

On setting $V_B = 140V$, $R_x = 0.8\Omega$, $L_p \sim 3 \times 10^{-6} H$, $C_p \sim 6 \times 10^{-5} F$, $R_p \sim 2.7\Omega$ and $V_f \sim 90V$ in the above described model, we get new steady state value of the electrode current, which is $I_B \sim 35A$. During transition regime slow decrease of electrode current cannot be explained by taking a constant cross-field plasma resistance. This can only be explained by taking slowly increasing resistance in the model. Hence, leaky capacitor model discussed above is found to be in good agreement with ADITYA plasma discharges.

5.4 Electrostatic and magnetic fluctuation behaviour during electrode biasing

Fig. 5.4 shows temporal profile of (a) plasma current (I_p), (b) density fluctuations (\tilde{n}_e) (c) \dot{B}_θ signal measured by one of Mirnov coil at high field side, (d) $|\tilde{B}_\theta|/B_\theta$, (e) H_α line

intensity, (f) CIII signal, (g) SXR signal, (h) cross field plasma resistance calculated using (i) electrode current and (j) electrode voltage signal. Applied bias voltage reaches to its maximum value in $\sim 150\mu s$ and electrode draws $\sim 58A$ current. Simultaneously, reduction in MHD fluctuations is observed. After $\sim 5ms$ of the application of bias voltage, electrode current decreased spontaneously to $I_B \sim 35A$. At this moment the electrostatic turbulence starts subsiding and following this, magnetic fluctuations starts increasing again. After the biasing voltage is switched off, both magnetic and electrostatic fluctuation levels return to their respective values of before biasing. In the discharges presented here, the observed MHD oscillations level remains typically $\tilde{B}_\theta / B_\theta \sim 0.3\%$ before biasing. Soon after onset of the biasing it reduces to $\tilde{B}_\theta / B_\theta \sim 0.1\%$ and again increases up to $\tilde{B}_\theta / B_\theta \geq 1\%$ after 10 ms into the biasing period.

For the analysis purpose we have divided the observed electrode current into five time zones, named as A, B, C, D and E, depending upon the characteristic behaviour of electrostatic and magnetic fluctuations. These fluctuation characteristics are compared with those prevailing before the bias (time zone A) and those existing after biasing (time zone E). All time zones are marked in Fig. 5.4 by dotted lines. In time zone B, i.e. just after the application of bias voltage \dot{B}_θ fluctuations are reduced in comparison to that of before bias (Fig. 5.4 (c)) and SXR signal (Fig. 5.4 (g)) starts increasing, which after $\sim 3ms$ saturates. In the beginning of time zone C, at $t \sim 46ms$ electrode current starts decreasing spontaneously with the bias voltage remaining constant which indicates a linear increase of cross – field plasma resistance as described in earlier section. In this time zone nature of electrostatic (Fig. 5.4 (b)) and magnetic (Fig. 5.4 (c)) fluctuations changes slowly with electrostatic fluctuations starts decreasing while the magnetic fluctuations starts increasing and SXR signal rises again. We call this time zone of increasing resistivity and decreasing ES fluctuations as ‘transition regime’. After this, in time zone D the electrostatic turbulence gets suppressed considerably at the plasma edge and magnetic fluctuation amplitude further increases. At the end of time zone D, electrode current reaches to its steady state value ($I_B \sim 35A$). A simultaneous and remarkable suppression of density fluctuations corresponds to the transition to improved confinement mode. After the biasing is switched off (time zone E), both the electrostatic and magnetic fluctuations attain their respective value of before biasing.

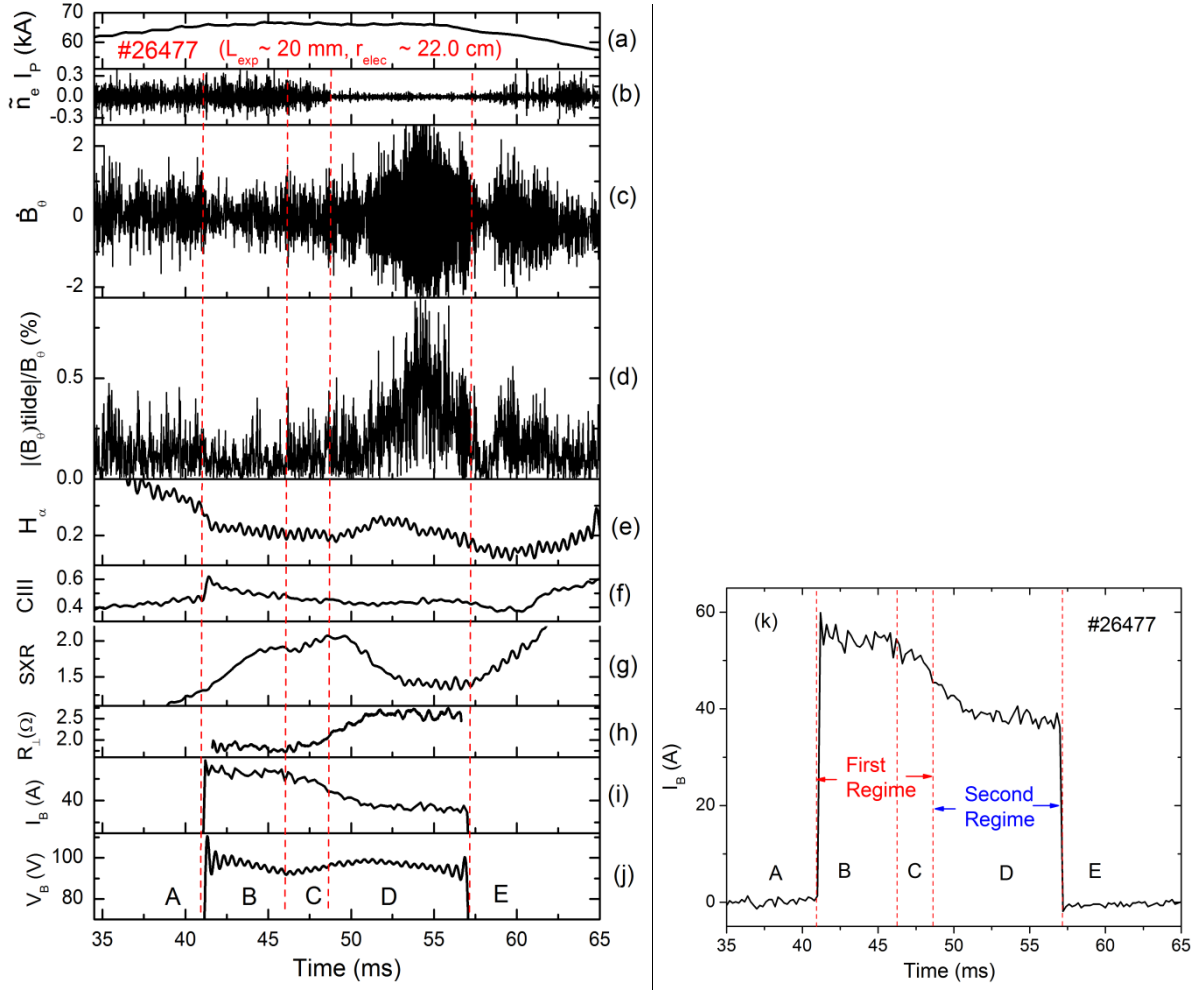


Figure 5.4. Temporal profile of (a) plasma current (I_p), (b) density fluctuations (\tilde{n}_e), (c) \dot{B}_θ signal (in A.U.) measured by one of Mirnov coil at the high field side, (d) $|\tilde{B}_\theta|/B_\theta$, (e) H_α line intensity, (f) CIII signal, (g) SXR signal (A.U.), (h) cross field plasma resistance (R_\perp) calculated using (i) electrode current and (j) electrode voltage signal. Discharge has been divided into time zones A-E based on behaviour of electrostatic and magnetic fluctuations. (k) Reduced H_α intensity time zones B and C together have been defined as first regime of improved confinement. Time zone D of higher H_α intensity has also been termed as second regime of improved confinement.

It can be seen in Fig. 5.4 that at the time of onset of biasing when magnetic fluctuations decrease (time zone B), H_α signal (Fig. 5.4(e)) reduces indicating less recycling and particles are more confined. Low H_α signal indicates rise in global density. A rise in SXR signal indicates higher energy confinement and plasma reaches to a regime (first regime) of improved confinement. During transition regime (time zone C), the electrostatic fluctuations

starts decreasing and the magnetic fluctuations begin to increase again and H_α remains at reduced level like in time zone B. Thereafter in the second regime (time zone D) the electrostatic fluctuations decreased further to its minimum level and remained low till the end of biasing pulse, although the magnetic fluctuations increased to its maximum. In this regime of improved confinement higher cross-field plasma resistance ($\sim 2.7\Omega$) is obtained as discussed in previous section. Observed high H_α emission is due to increase transport caused by large MHD fluctuations due to growth of 2/1 and 3/1 tearing modes.

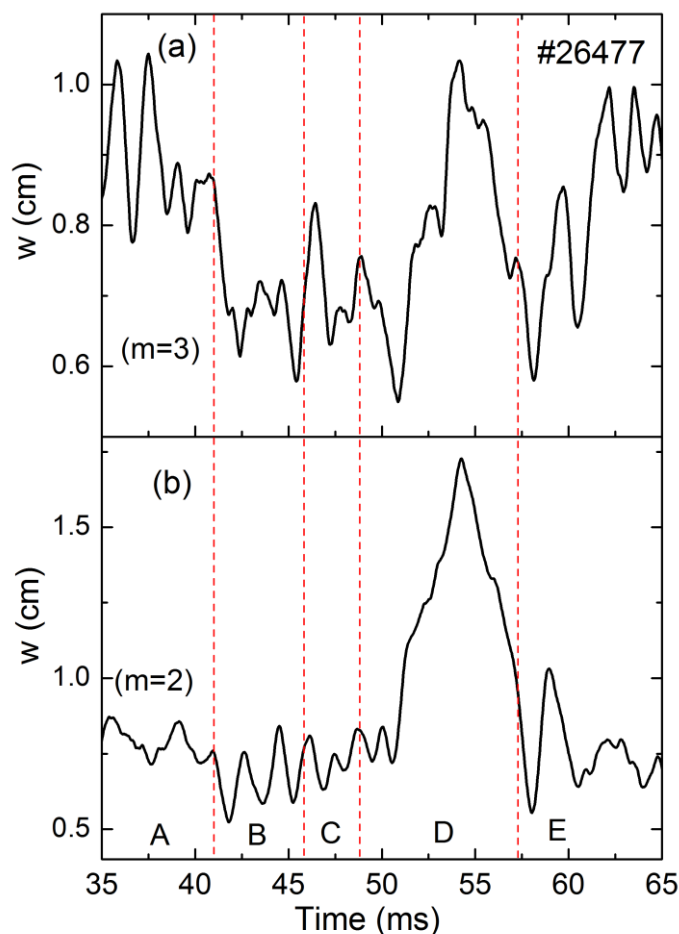


Figure 5.5. Time behaviour of MHD modes, $m/n=3/1$ and $2/1$, in discharge #26477. During first regime of improved confinement (time zone B and C) island size of $m/n=3/1$ tearing mode reduce. No effect on island size of $m/n=2/1$ tearing mode observed during this regime. In second regime of improved confinement island width of $m/n=2/1$ mode increase significantly, triggering larger recycling at the edge.

Before biasing $|\tilde{B}_\theta|/B_\theta$ is approximately $\sim 0.3\%$ (figure 5.4d). As soon as biasing is switched on, level of decrease to $\sim 0.1\%$ in time zone B. During transition regime (time zone C) $|\tilde{B}_\theta|/B_\theta$ signal starts increasing again and grow up to $\sim 0.9\%$ in time zone D for discharge #26477.

Singular value decomposition (SVD) analysis of B_θ fluctuations measured by 12 coils of Mirnov garland reveals that in the first regime of improved confinement (time zone B), width of magnetic island corresponding to mode $m/n = 3/1$ and $2/1$ reduced with considerable reduction in $3/1$ mode (Fig. 5.5). However after the transition, in second improved confinement regime (time zone D), island width of both the $m/n = 3/1$ and $2/1$ mode increased significantly with growth in $2/1$ mode more than in $3/1$ mode.

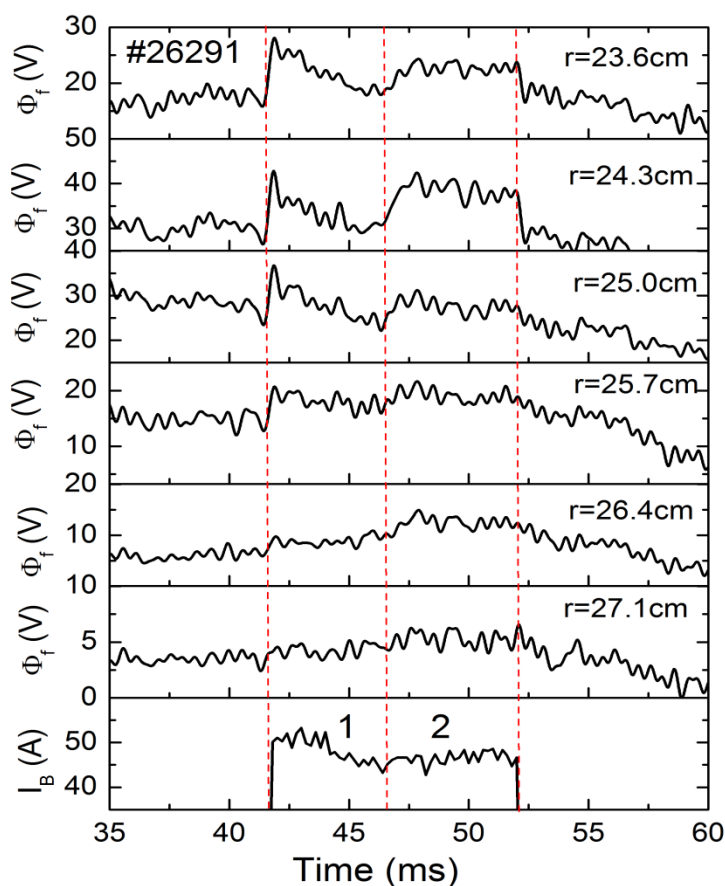


Figure 5.6. Effect of biased electrode on floating potential at the plasma edge measured by radial array of six Langmuir probes.

Further analysis revealed that the radial profile of plasma potential also steepens twice during the application of bias voltage pulse. Once in the start of time zone B and once in D. Fig. 5.6 shows temporal profiles of floating potential measured at six radial locations using radial

array of Langmuir probes in another discharge (#26291) with similar parameters showing similar characteristic of electrode current. Analysis of floating potential data shows that floating potential of plasma increases with the onset of the bias voltage and decreases slowly to almost its value prior to the biasing in ~ 5 ms. However, it suddenly rises again in second regime and persists until biasing is switched off. The second rise of floating potential coincides with the time zone D. Assuming the edge plasma temperature does not change with biasing, the change in floating potential reflects the change in plasma potential. We investigated the behaviour of radial electric field and its shear at specific times during the biasing pulse covering all the time zones.

The average radial electric field, shown in Fig. 5.7a, is obtained by taking the gradient of the plasma potentials ($\Phi_p = \Phi_f + 3T_e$) measured by the single Langmuir probes for similar shot #26291. Radial profile of radial electric field shows that in the first regime the radial profile of electric field gets steep and then flatten again (Fig. 5.7 (a)), whereas during second regime of improved confinement a stronger electric field and its shear develops (Fig. 5.7b), which persists during whole biasing. The radial profile of electric field and its shear is presented in Fig. 5.7a and 5.7b, respectively.

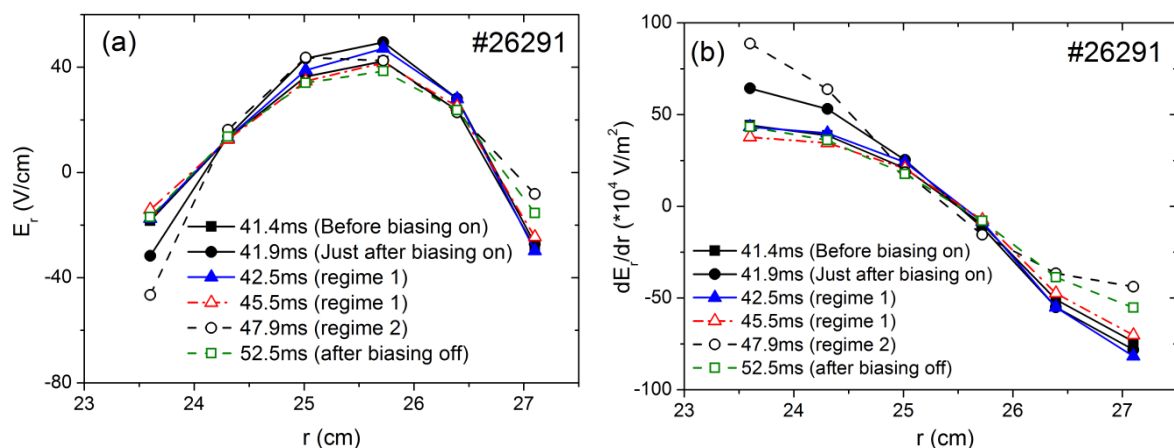


Figure 5.7. Modification in radial profile of (a) radial electric field and (b) its shear during first and second improved confinement regimes. As soon as the biasing is switched on electric field and its shear increase at the beginning of first regime ($t \sim 41.9$ ms). Afterwards both the parameters reduce to previous value during first regime ($t \sim 42.5$ ms and ~ 45.5 ms). During second regime ($t \sim 47.9$ ms) a stronger electric field and shear again develops, which persists during throughout the biasing pulse. After biasing is switched off ($t \sim 52.5$ ms), E_r and its shear (dE_r/dr) achieve their respective values before bias.

The above mentioned observations can be described by similar analogy as being put forward in case of disruption control in previous chapter. In the second regime the increased shear in the radial electric field leads to increased shear in plasma poloidal rotation, which in turn suppresses the ES fluctuations.

In first (time zone B) and second (time zone D) regime radial electric field increase due to biased electrode but only in second regime electric fluctuations suppressed. This can be explained by the threshold poloidal flow shear required for the electrostatic fluctuation suppression. Turbulence is stabilised when shear rate $\omega_{E \times B}$ in the $E \times B$ flow ($v_{E \times B}$) induced by E_r exceeds the turbulence decorrelation rate. Turbulence decorrelation rate is approximated to linear growth rate, which in turn scales with diamagnetic frequency. Mathematically, if $dv_\theta/dr > \gamma_{MAX}$, electrostatic fluctuations suppressed, where γ_{MAX} is the maximum linear growth rate of all the unstable modes in the plasma.

More precisely, $dv_\theta/dr > k_\theta \rho_s C_s / L_n$ [5.36], where C_s is the ion sound speed, $\rho_s = \sqrt{m_i T_i / q_i B_\phi}$ is ion sound Larmor radius, k_θ is the poloidal wave number and L_n is the density length scale. $k_\theta^{-1} \sim$ ion poloidal Larmor radius. So, $k_\theta \rho_s \sim 1$. So, condition for the suppression of turbulence becomes

$$dv_\theta/dr > C_s / L_n. \quad (5.12)$$

In the following discussion we show that in the first regime (time zone B), dv_θ/dr is just below the threshold and in second regime condition (5.12) is satisfied. Taking $T_e \sim 25\text{eV}$ near plasma edge, $C_s \sim 5.0 \times 10^4 \text{ m/s}$ and $L_n \sim 4\text{cm}$. So, $C_s / L_n \sim 1.2 \times 10^6 \text{ s}^{-1}$. In the time zone B electric field increases ($|E_r| \sim 3.5 \times 10^3 \text{ V/m}$) and its shear increases to $\sim dE_r/dr \sim 6 \times 10^5 \text{ V/m}^2$. So, $dv_\theta/dr \sim 0.8 \times 10^6 \text{ s}^{-1}$ and condition (5.12) is not satisfied. A transport barrier in the second regime (time zone D) is formed by strong radial electric field ($|E_r| \sim 5 \times 10^3 \text{ V/m}$) and its shear ($dE_r/dr \sim 9 \times 10^5 \text{ V/m}^2$). So, $dv_\theta/dr \sim 1.16 \times 10^6 \text{ s}^{-1}$ and the condition for electrostatic fluctuations suppression is nearly satisfied.

Suppression of ES fluctuations triggers second confinement regime. Cross-field plasma resistance increases and causes electrode current to reduce. In our experiments, second transport barrier is formed when charging of flux surfaces takes place by biased electrode. Generally, magnetic flux surface charging occurs in 4-8 ms after the onset of electrode biasing.

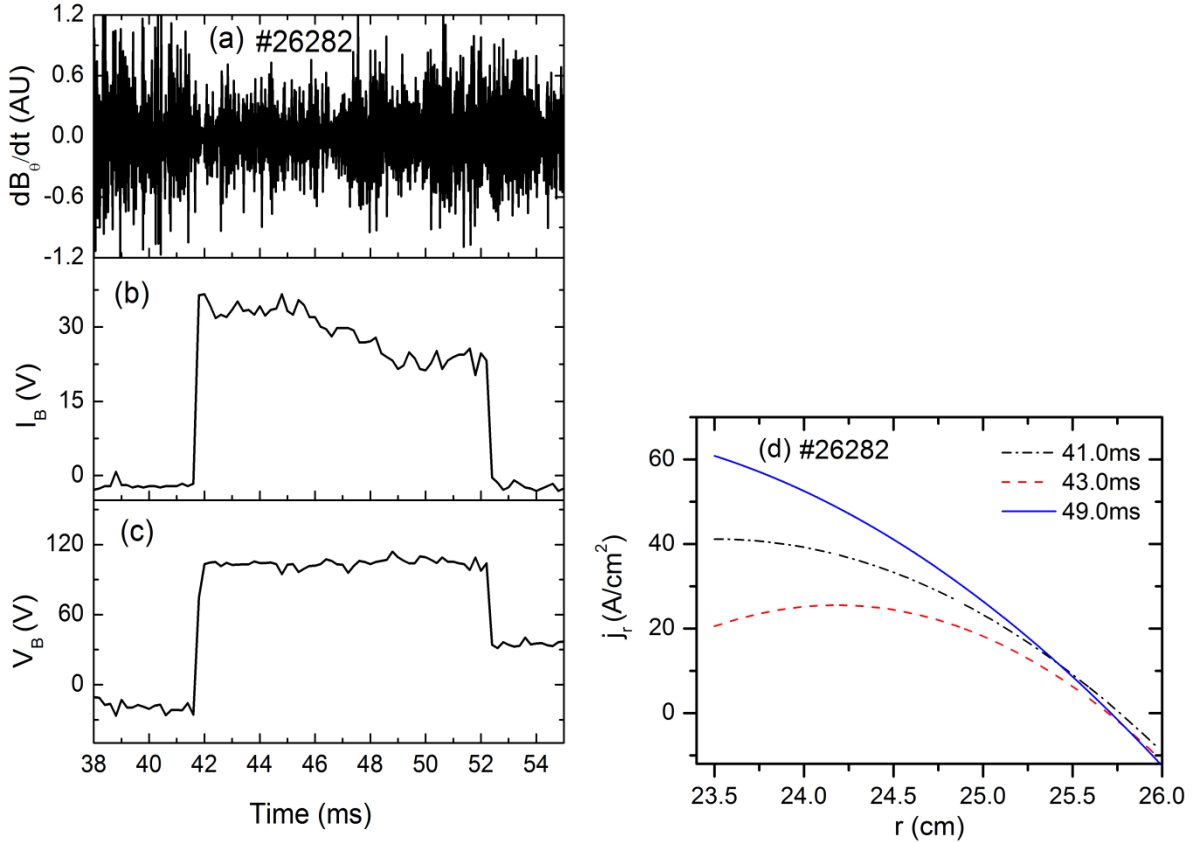


Figure 5.8. (a) \dot{B}_θ signal measured by one of Mirnov coil, (b) electrode current, (c) bias voltage for shot #26282 and (d) radial profile of toroidal current density modifies at the plasma edge before biasing ($t \sim 41\text{ms}$), during first regime ($t \sim 43\text{ms}$) and second regime ($t \sim 49\text{ms}$) of improved confinement for #26282. In first confinement regime current density profile flattens, stabilising $m=3$ tearing mode. Steepening of current density profile causes growth in both $m=3$ and $m=2$ modes during second improved confinement regime.

Further investigation reveals effect of biasing on current density profile at the edge of plasma in a similar discharge (shot #26282). It is clear from the radial profile of toroidal current density at the edge (Fig. 5.8), measured by magnetic probe array (described in chapter 3) that soon after the biasing switch on, the current density profile becomes flatter (at $t \sim 43\text{ms}$) and stabilizes the $m=3$ mode in the first regime. During second regime j_ϕ -profile becomes steep, modes $3/1$ and $2/1$ become less stable and grow.

Chronology of events in transition regime (time zone C) and second confinement regime (time zone D) can be explained by the transport equation of plasma energy

$$n_e \frac{dT_e}{dt} = P + P_{OH} - n_e \chi \nabla^2 T_e \quad [5.37],$$

where P is externally deposit power, P_{OH} is Ohmic power

and χ is thermal conductivity. In transition regime drift modes start suppressing, less loss of

heat occurs, which leads to increase in dT_e/dt because χ decreases (which mean energy confinement time increases ($\tau_E = a^2 / \langle \chi \rangle$)[5.37], which is observed as increase in SXR signal) and thereby ∇T_e sharpens at the edge ($\nabla T_e = -q/n_e \chi$ [5.37], where q is heat flux). So at the edge $j_\phi (\sim E_r / \eta \sim E_r / T_e^{-3/2})$ becomes more peaked and ∇j_ϕ becomes sharp, which in turn induces the MHD modes (3/1 and 2/1) to grow and region of stochastic magnetic field forms near $q=2$ and $q=3$ surfaces and which enhances the transport, in turn H_α intensity increases. Loss of particles and energy due to enhanced transport causes SXR intensity decrease in the second region.

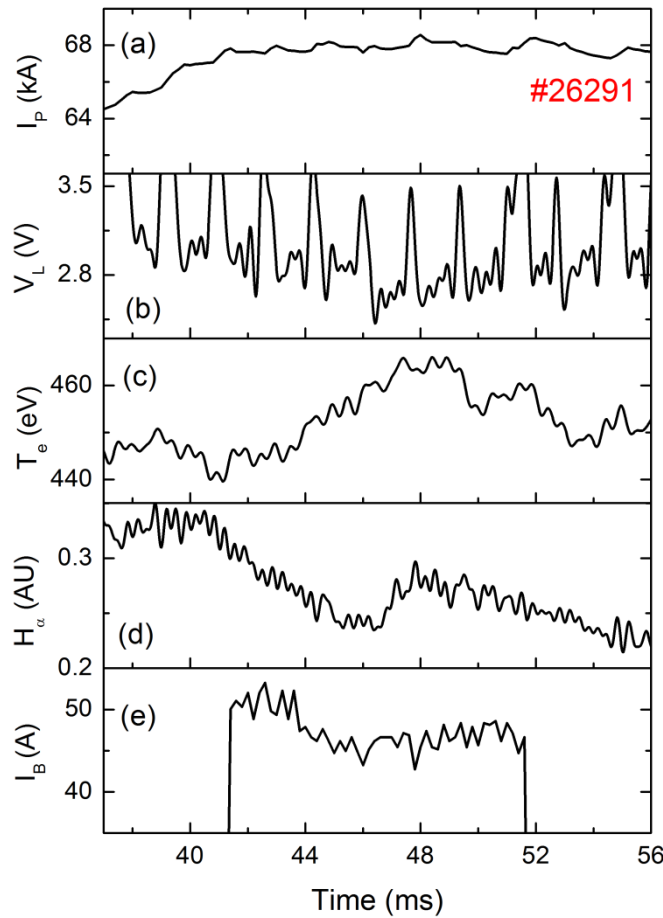


Figure 5.9. Temporal profile of (a) plasma current (I_P), (b) loop voltage (V_L), (c) central electron temperature (T_e), (d) H_α line intensity and (e) electrode current (I_B). In second regime at $t \sim 46$ ms loop voltage decreases due to electron temperature rise.

Figure 5.9 shows temporal profile of plasma current (I_P), loop voltage (V_L), central electron temperature (T_e), H_α line intensity and electrode current (I_B) (Fig. 5.9(a-e)) for shot #26291.

During the onset of biasing (regime B) electron temperature measured by SXR signal increases. At the beginning of the second regime (regime D) temperature again rises by ~3-5%. A ~0.3V drop of loop voltage also observed during in this regime. This can be interpreted as follows- Loop voltage is given by $V_L = I_p R_{\parallel} + L_p (dI_p / dt)$, where R_{\parallel} is parallel plasma resistance and L_p is plasma inductance. Although current density profile steepens during this phase of biasing, internal inductance of plasma increases. However, high confinement triggers electron temperature rise, which indicates lowering of parallel resistivity and hence loop voltage decreases.

The simultaneous observation of development of sheared radial electric field and current density profile modification makes it difficult to predict which one leads to the suppression of magnetic fluctuations. However, it is quite clear that the suppression of magnetic fluctuations occurs prior to the electrostatic fluctuations, which is thought to be the possible cause for transition to improved confinements in tokamaks.

5.5 Discussion

We further investigate the reason behind the two improved confinement regimes with distinct nature by analysing frequency spectra of magnetic oscillations (measured by magnetic coil of Mirnov garland) and electrostatic fluctuations (in density measured by Langmuir probe). In tokamaks density and magnetic fluctuations arise due to pressure gradient and current density gradient, respectively. Fig. 5.9 shows comparison of frequency spectra of magnetic (Fig. 5.9(a)) and electrostatic fluctuations (Fig. 5.9(b)) averaged over eight similar discharges in different time zones described in Fig. 5.4. In the frequency spectra of MHD oscillations and electrostatic fluctuations similar synchronized peak observed before biasing (time zone A). Observations show that before biasing these fluctuations in density and poloidal magnetic field have well-defined peak at $f \sim 12-14$ kHz in the frequency spectra. Soon after the biasing is switched on these peaks disappear in both the electrostatic and MHD fluctuations and no dominant peak in the frequency spectra is observed in time zone B. During transition region (time zone C) magnetic fluctuations starts growing again. In the time zone D, the power spectra of MHD fluctuations show a dominant peak at ~ 11 kHz owing to the growth of $m/n = 2/1$ and $3/1$ islands, however no pronounced peak have been observed in the frequency spectra of the electrostatic fluctuations. After the termination of the biasing pulse (time zone E) (Fig. 5.9(E)), dominant peaks with a common frequency of 14-15 kHz in the frequency spectra of both density and MHD fluctuations reappear, but their power is low.

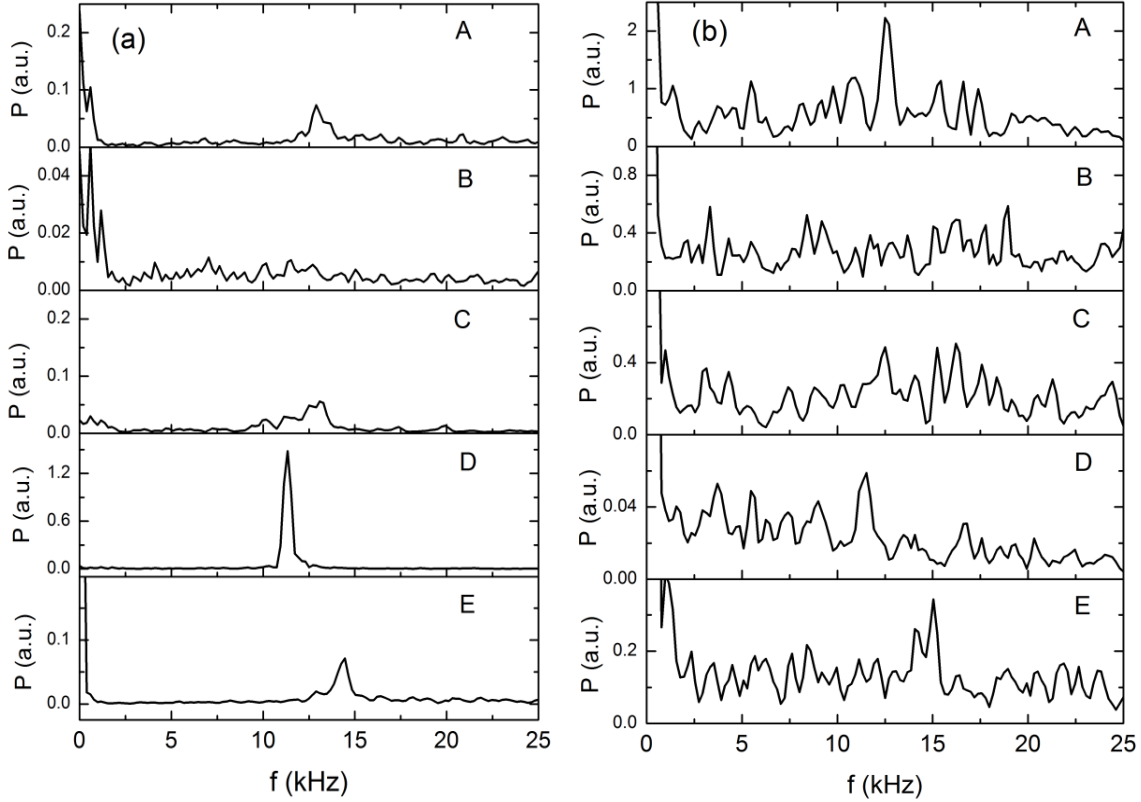


Figure 5.10. Comparison of power spectral properties of (a) magnetic fluctuations measured by Mirnov coil and (b) electrostatic fluctuations measured by Langmuir probes for time zones A - E. Shown power spectrum is average over eight similar discharges.

The observation of coherent peaks in the frequency spectra of electrostatic and magnetic fluctuations at a common frequency of $\sim 12-14$ kHz in time zone A, i.e., before biasing, strongly suggest the presence of a coherent electromagnetic mode and may be arising due to the coupling of drift modes with the Alfvén modes. Presence of Drift-Alfvén modes in typical ADITYA discharges have been reported [5.38] and they are also observed in other tokamaks [5.39]. Drift waves commonly observed in tokamaks, propagate at electron diamagnetic drift velocities, perpendicular to the magnetic field and the pressure gradient. However, when the parallel drift wave velocity becomes comparable to the Alfvén velocity [5.40], i.e., $\omega/k_{\parallel} \sim v_A$, the drift waves also propagate parallel to the magnetic field with substantial magnetic fluctuations having $k_{\parallel} \ll k_{\perp}$. Taking $f \sim 13$ kHz and $k_{\parallel}^{-1} \sim qR \sim 3$ m in our experiments, ω/k_{\parallel} comes out to be $\sim 0.25 \times 10^6$ m/s, which is not very far from the Alfvén velocity $v_A \sim 4 \times 10^6$ m/s. Hence, drift-Alfvén oscillations are possibly present in the above analysed discharges before the biasing (time zone A). The measure of coupling of drift waves to the Alfvén waves

is given by the ratio [5.41] of the inductive and the electrostatic components of the parallel electric field, i.e., $\omega\tilde{A}/(ck_{\parallel}\Phi_0)$, where \tilde{A} is the amplitude of parallel vector potential of \tilde{B}_{θ} .

The strength of the coupling is given by $f_{CF} = \omega\tilde{B}_{\theta}/[k_{\parallel}(|\partial\Phi_0/\partial r|)]$. For pure electrostatic drift mode $f=0$. In our experiments before bias (time zone A) we observe $\tilde{B}_{\theta}/B_{\theta} \sim 0.3\%$. Taking $|\partial\Phi_0/\partial r| \sim 2.0 \times 10^2 \text{V/m}$ at $r \sim 24 \text{cm}$ from the measured values shown in Fig. 5.7a, we obtained the coupling factor $f_{CF} \sim 0.37$, which is reasonably strong. These waves are known to cause cross-field particle transport [5.42]. At the onset of biasing (time zone B) (Fig. 5.9(B)) the radial electric field increases to $|\partial\Phi_0/\partial r| \sim 7.0 \times 10^2 \text{V/m}$ and the magnetic fluctuations reduce to $\tilde{B}_{\theta}/B_{\theta} \sim 0.1\%$, leading to decoupling of these fluctuations with the value of coupling factor reducing by an order to $f_{CF} \sim 0.03$. Consequently, ES and magnetic oscillations are no more coupled and remain uncoupled in time zone C (Fig. 5.9(C)) also. Latter on during the time zone D (Fig. 5.9(D)), although the magnetic fluctuations level increases to $\tilde{B}_{\theta}/B_{\theta} \sim 1\%$ in presence of bias voltage, the electric field further increases to $|\partial\Phi_0/\partial r| \sim 1.0 \times 10^3 \text{V/m}$ and the coupling factor still remains low $f_{CF} \sim 0.06$. This strongly suggests that that Drift-Alfven waves existing in typical discharges of ADITYA tokamak prior to biasing get suppressed due to biasing and leads to improvement in confinement by reducing transport related to these waves along with the reduced transport due to the suppression of electrostatic fluctuations in the edge region.

5.6 Summary

In this chapter we focused on understanding the effect of biasing on electrostatic and magnetic fluctuations and chronology of events. Typical temporal profile of rise time of bias voltage and electrode current has been modelled assuming the poloidally rotating tokamak plasma a leaky capacitor. It is shown by the model that during biasing decrease in electrode current after $\sim 4 - 8 \text{ms}$ into the biasing pulse is due to an increase in cross – field plasma resistance in the transition regime. With the application of bias voltage above some threshold voltage in typical discharges of ADITYA tokamak, significant reduction in both magnetic and electrostatic fluctuations is observed leading to two distinct regimes of improved confinement with different characteristics. The important observation is that the magnetic fluctuations are reduced prior to that of electrostatic fluctuations. With the onset of bias first the magnetic fluctuations are suppressed due to substantial reduction in $m/n=3/1$ mode and

the H_α decreased with an increase in plasma confinement. After $\sim 4 - 8$ ms of the application of bias voltage, the electrode current falls sharply with the modest increase in the electrode voltage, indicating higher cross - field resistivity. Simultaneously, the electrostatic fluctuations are suppressed and confinement improves further. This state does not last long and magnetic fluctuations associated with $m / n = 2 / 1$ mode increases significantly leading to increase in H_α emission. However, the electrostatic fluctuations remains suppressed compared to their values before biasing till the end of the biasing pulse and plasma remains in the state of improved confinement due to reduction in transport related to the electrostatic fluctuations. Further investigation revealed that the possible cause of transition to the improved state might be the suppression of drift-Alfven waves due to bias, which exists before biasing.

5.7 References

- [5.1] T. L. Rhodes et al., *Nucl. Fusion* **33**, 1787 (1993)
- [5.2] G. Van Oost et al., *Plasma Phys. Control. Fusion* **45**, 621 (2003)
- [5.3] C. Silva et al., *Plasma Phys. Control. Fusion* **46**,163 (2004)
- [5.4] R. R. Weynants, *J. Plasma Fusion Res. SERIES* **4**, 3 (2001)
- [5.5] J. W. Connor and H. R. Wilson, *Plasma Phys. Control. Fusion*, **42**, R1–74 (2000)
- [5.6] K. C. Shaing and E.C. Jr Crume, *Phys. Rev. Lett.*, **63**, 2369 (1989)
- [5.7] P. H. Diamond and Y. B. Kim, *Phys. Fluids B* **3**, 1626 (1991)
- [5.8] H. Biglari, P. H. Diamond and P.W. Terry, *Phys. Fluids B* **2**, 1 (1990)
- [5.9] K. Toi, et al., *Phys. Rev. Lett.* **62**, 430 (1989)
- [5.10] Joydeep Ghosh et al., *Nucl. Fusion* **47**, 331 (2007)
- [5.11] C. Nascimento et al., *Nucl. Fusion* **47**, 1570 (2007)
- [5.12] H.W. Lu, et al., *European Physical Journal D* **66:213** (August 2012)
- [5.13] D. Biskamp, Natural current profiles in tokamaks, *Comments Plasma Phys. Controlled Fusion* **10**, 165 (1986)
- [5.14] B. B. Kadomtsev, *Comments Plasma Phys. Controlled Fusion* **11**, 153 (1987)
- [5.15] J. Y. Hsu and M. S. Chu, *Phys. Fluids* **30**, 1221 (1987)
- [5.16] T. S. Hahm and P. H. Diamond, *Phys. Fluids* **30**, 133 (1987)
- [5.17] C. M. Bishop, *Nucl. Fusion* **26**, 1063 (1986)
- [5.18] Z. O. Guimaraes-Filho et al., *Phys. Plasmas* **15**, 062501 (2008)

- [5.19] O. Anderson, W. R. Baker, A. Bratenahl, H. P. Furth, and W. B. Kunkel, *Appl. Phys.* **30**, 188 (1959)
- [5.20] K. Itoh and S.I. Itoh, *Transport and Structural Formation in Plasmas*, IOP Publishing Ltd, 1999
- [5.21] Weston M. Stacey, *Fusion Plasma Physics*, WILEY-VCH Verlag GmbH & Co. KGaA, Weinheim, 2005
- [5.22] S. I. Itoh and K. Itoh, *Phys. Rev. Lett.* **60**, 2276 (1988)
- [5.23] M. Tendler, *Plasma Phys. Control. Fusion* **39**, B371 (1997)
- [5.24] M. Tendler, *Plasma Fusion Res.* **5**, S1004 (2010)
- [5.25] K. C. Shaing, *Phys. Fluids B* **5**, 3841 (1993)
- [5.26] K. C. Shaing, *Phys. Rev. Lett.* **76**, 4364 (1996)
- [5.27] V. Rozhansky and M. Tendler, *Phys. Fluids B* **4**, 1877 (1992)
- [5.28] J. Cornelis et al., *Nucl. Fusion* **34**, 171 (1994)
- [5.29] F. Wagner et al., *Phys. Rev. Lett.* **49**, 1408 (1982)
- [5.30] R. R. Weynants et al., *Nucl. Fusion* **32**, 837 (1992)
- [5.31] B. Terreault et al., *Nucl. Fusion* **32**, 1181 (1992)
- [5.32] K. H. Burrell et al., *Phys. Rev. Lett.* **59**, 1432 (1987)
- [5.33] M. Kotschenreuther et al., *Phys. Plasmas* **2**, 2381 (1995)
- [5.34] V. Erckmann et al., *Phys. Rev. Lett.* **70**, 2086 (1993)
- [5.35] K. Toi et al., *Plasma Phys. Control. Fusion* **38**, 1289 (1996)
- [5.36] T. S. Hahm and K. H. Burrell, *Phys. Plasmas* **2**, 1648 (1995)
- [5.37] K. Itoh and S-I Itok, *Transport and Structural Formation in Plasmas*, Institute of Physics Publishing, 1999
- [5.38] R. Manchanda, *Phys. Plasmas* **17**, 072515 (2010)
- [5.39] P. K. Chattopadhyay et al., *Phys. Rev. Lett.* **81**, 3151 (1998)
- [5.40] A. B. Mikhailovskii and L. T. Rudakov, *JETP* **17**, 621 (1963)
- [5.41] E. D. Fredrickson and P. M. Bellan, *Phys. Fluids* **28**, 1866 (1985)
- [5.42] S. Vincena, *Phys. Plasmas* **13**, 064503 (2006)

Chapter 6

Conclusions and Future Outlook

6.1 Summary and conclusions

In summary, in this thesis we have successfully mitigated plasma disruptions in ADITYA tokamak using a biased electrode. Signatures of confinement improvement as observed in other tokamaks, also obtained using electrode biasing in ADITYA tokamak. Both the electrostatic (ES) and magnetic fluctuation suppression have been observed with electrode biasing. Observed occurrence of suppression of magnetic fluctuations prior to reduction in electrostatic fluctuations with biasing suggests an important role played by suppression of magnetic fluctuations in L to H transitions. The major conclusions of the thesis are as follows:

- Electrode assembly and biasing pulsed power supply were designed and installed in ADITYA tokamak to study physics of L-H transition and for disruption mitigation experiments. An especially designed electrode holding assembly was used to place the electrode inside the plasma with both its dimension and position inside the plasma can be controlled and varied. A single Langmuir probe array designed and installed to measure edge parameters like floating potential and electron density. For real time disruption avoidance experiments precursor MHD oscillations sensing circuit designed and developed. A magnetic probe array developed to measure changes in toroidal current density profile at the plasma edge.
- The signatures of improved confinement as well as successful mitigation of MHD induced disruption has been observed mainly at electrode-exposed length $L_{exp} \sim 20$ mm placed at $r_{elec} \sim 22$ cm by moving specially designed electrode-holding assembly in typical discharges of ADITYA tokamak.
- This thesis presents the first experimental demonstration of successful mitigation of H₂ gas puff induced plasma disruptions in ADITYA tokamak using a biased electrode at the

Chapter 6: Conclusions and Future Outlook

plasma edge by stabilizing MHD tearing modes ($m/n=2/1$ and $3/1$) through generation of large sheared poloidal flow near $q=3$ surface. Observations indicate that MHD tearing modes ($m/n=2/1$ and $3/1$) islands do not grow in presence of increased poloidal sheared flow and disruptions are avoided through prevention of mode locking. Disruption avoidance takes place when poloidal flow shear becomes equal or larger than magnetic shear. SVD analysis of magnetic fluctuations and tomographic results of SXR emissivity flux show that growth of all $m=3, 2, 1$ are affected by biasing as these are toroidal sidebands.

- Excitation and suppression of magnetic and ES fluctuations is studied during electrode biasing. Both the magnetic and ES fluctuations are suppressed during biasing, but not together. Importantly, magnetic fluctuation reduction occurred prior to suppression of electrostatic fluctuations. Soon after the biasing onset, the magnetic fluctuations reduced to $\tilde{B}_\theta/B_\theta \sim 0.1\%$ from its value $\tilde{B}_\theta/B_\theta \sim 0.3\%$ before biasing. After $t \sim 4-8$ ms of the biasing fluctuations increase to $\tilde{B}_\theta/B_\theta \geq 1\%$. On the latter time ES fluctuations suppressed simultaneously with the growth of magnetic fluctuations. Two regimes of improved confinement with distinct features were identified. In first regime low H_α , less MHD fluctuations were found due to suppression of Drift-Alfven modes. Tearing mode $m/n = 3/1$ suppression was found due to flattening of toroidal current density profile. No effect on $m/n = 2/1$ mode was observed in this regime. Second regime initiated by bifurcated electrode current. In this regime the ES fluctuations get suppressed and remained suppressed till the end of biasing voltage pulse whereas MHD fluctuations starts increasing again after sometime in this regime as the current profile steepens. The modes are mainly identified as $m/n = 2/1$ tearing mode in this regime. At the time of increased MHD activity in this regime, the H_α signal also increased as a result of enhanced particle recycling caused by increased transport due to enhanced $m=2$ mode.
- A leaky capacitor model of rotating plasma to explain rise time and magnitude of electrode voltage and electrode current was presented. It was found from this model that during transition to second confinement regime slow decrease in electrode current is due to slow rise in cross-field resistivity.

6.2 An outlook for future studies

Future works include mitigation of disruptions with a reciprocating electrode controlled by some precursor of disruption. Fixed electrodes cannot be put inside the LCFS of big tokamaks for long time, therefore, more systematic electrode position, electrode exposed length and biasing voltage scans along with reciprocating electrode system are envisaged for best optimisation of above three parameters in real time disruption avoidance. The effect of negative bias with electron emissive electrodes (e.g., LaB₆) on disruption event and other global parameters of ADITYA can be carried out.

Biasing experiments can be expanded in future towards better understanding of underlying physics with toroidal magnetic field of different magnitudes and with reversed field direction. Biasing experiments by inserting electrode from radial, bottom ports and electrodes with larger diameters can be done. Versatility of edge diagnostics such as direct measurement of toroidal and poloidal flows using radial and poloidal array of Mach probe or Gundstrup probe can be developed for these experiments.

In future disruption mitigation experiments can be carried out in ADITYA tokamak with divertor configuration. In our experiments we achieved disruption avoidance by generating poloidal flow shear larger than magnetic shear. It would be interesting to operate tokamak in configuration of low magnetic shear at the plasma edge and avoid deliberately induced disruptions. Low magnetic shear at the plasma edge can be generated by external current carrying coil.